MICROSCREENED ENDCAP HOLES AND BUFFER GAS PRESSURE TAILORING FOR QUADRUPOLE ION TRAP MASS SPECTROMETRY

By

DODGE L. BALUYA

A DISSERTATION PRESENTED TO THE GRADUATE SCHOOL
OF THE UNIVERSITY OF FLORIDA IN PARTIAL FULFILLMENT
OF THE REQUIREMENTS FOR THE DEGREE OF
DOCTOR OF PHILOSOPHY

UNIVERSITY OF FLORIDA

2009

To the ion trappist, young and old

ACKNOWLEDGMENTS

I am thankful for the meaningful learning experiences during my graduate career at the University of Florida, and the multitude of support from family, friends and colleagues. Without these important people, I could never have achieved what I have accomplished so far.

First, I would like to thank my advisor, Dr. Richard Yost, for taking me in his group, and guiding me throughout my stay here. He is a mentor I respect and admire for his pursuit of knowledge, for his generosity and patience, and for teaching me to become a better scientist and inspiring me to be a better person. He makes it seem so easy to do science, manage family matters, and do his "other" jobs at the same time. I would also like to thank the members of the Yost Group: the past members when I joined the group for showing me how to survive in the group and being patient when I was still learning, and the newer members with whom I have spent my time discussing about anything under the sun. I am grateful for their friendship and wish them all good luck in their careers and future endeavors.

I must also thank the support staff of the Chemistry Department (the Machine Shop: Joe, Todd, and Brian; the Electronics Shop: Steve and Larry; Analytical Staff: Jeanne and Julie; and the Chemistry Graduate Office: Lori and Ben) for the efforts they have put into their work. Without them, obtaining a graduate degree would have been close to impossible, and they are also nice and never let students down whenever they need help.

I would like to thank Dr. David Powell for allowing me to work in the mass spectrometry lab. Working as well as discussions with him allowed me to learn more about scientific life and other things beyond the scope of a research lab.

I would like to thank my friends here at UF, specifically the Pinoy UF group, who have been accommodating, far beyond what is required, to help me adapt to the way of living here in

Gainesville. Special mention goes to Cris, whom I had met way back when I was in the Philippines, as she suggested that I apply here for graduate school.

I would like to thank Jhoana, my wife and friend, for being my support, and for helping through the tough times of research, and celebrating the joys with me. I will return the favor when she is writing her dissertation.

I thank my loving parents, Papa and Mama, for allowing me to venture far from home and always supporting me in any undertaking I wanted to pursue. The life lessons I learned at home will always guide me.

Lastly, I would like to thank God. I thank Him for always guiding me and providing strength whenever I seem to run out.

TABLE OF CONTENTS

page

LIST OF TABLES

LIST OF FIGURES

Abstract of Dissertation Presented to the Graduate School
of the University of Florida in Partial Fulfillment of the
Requirements for the Degree of Doctor of Philosophy

MICROSCREENED ENDCAP HOLES AND BUFFER GAS PRESSURE TAILORING FOR QUADRUPOLE ION TRAP MASS SPECTROMETRY

By

Dodge Lo Baluya

May 2009

Chair: Richard A. Yost
Major: Chemistry

Field imperfections in the quadrupole ion trap (QIT) arise from the presence of holes in endcaps and from truncation of the hyperbolic electrodes. To reduce the nonlinear resonance effects, commercial 3-D QITs have a stretched axial configuration, which deviates from the theoretical z_0 by 11%. Furthermore, the use of buffer gas, which helps trap and cool injected ions by reducing ion kinetic energy, focuses the ions into the trap center and away from the field imperfections. However, the increase in the distance superimposes higher order fields and consequently causes nonlinear resonance effects. Previous simulation studies from our lab have shown that microscreening the endcap holes could reduce field imperfections in the vicinity of the holes.

Analysis of perfluorotributylamine (PFTBA) fragment ion *m/z* 69 without buffer gas and with stretched geometry showed that an extra peak at *m/z* 67 increased in intensity. Reducing the z_0 stretch to the theoretical value and with microscreened endcaps only reduced the "ghost" peak at *m/z* 67, but did not eliminate it. These combined results demonstrated that the compensation for stretching the trap may need to be optimized for use with microscreening methods. Among the microscreened endcap experiments without buffer gas, the reduced endcap spacing of 7.34 mm achieved the best overall performance in terms of reducing the ghost peak at *m/z* 67,

although with some unexpected results. Furthermore, nonlinear resonances, which caused these ghost peaks to appear, were identified.

In addition, the potential for buffer gas pressure tailoring in quadrupole ion trap operation was investigated. The use of buffer gas during ion injection has beneficial effects, but in other events of the mass scan function, having gas inside the QIT can be disadvantageous. During the mass isolation and ejection events, fragile ions can collide with buffer gas molecules, causing fragmentation and degrading mass resolution. Currently, commercially available QITs maintain a constant buffer gas pressure (around 1 mTorr) that is a compromise. Here a multi-pulsed valve system is developed that delivers buffer gas only at points of the scan where it is needed. Results on evaluation of the gas profile output are presented as well as an application for the system.

CHAPTER 1
INTRODUCTION

Background and Significance

Overview

The quadrupole ion trap (QIT) in a commercial mass spectrometer is based on the solutions to the Mathieu differential, which analytically calculate the masses. However, QIT designs with theoretical configuration have problematic mass shifts, which give rise to errors in the mass analysis of specific compounds. The modifications made by Finnigan (i.e., stretching the geometry) were effective solutions in correcting for these mass shifts and thus, making the QIT a successful mass spectrometer; however, it was a global solution for a local problem of the field imperfection contributed by the endcap holes. Previous simulation studies in the Yost laboratory have found an alternative solution, microscreening the endcap holes that would help preserve the linearity of the quadrupolar field. Hence, the motion of ions trapped in the near ideal quadrupolar field would be characterized more closely by the Mathieu equation. One focus of the research presented here is to evaluate experimentally microscreening endcap holes. A second focus was on tailoring buffer gas pressure within the ion trap using pulsed valves.

In order to understand the basis of the research presented, it is important to review the fundamental concepts as well as the history of the QIT. The next section gives a preparatory understanding of ion trapping theory, aimed for the novice reader as well as a review of helpful concepts for the adept mass spectrometrist.

History of the Quadrupole Ion Trap

The QIT along with the quadrupolar mass filter was developed by Paul and Steinwedel in 1960 [1]. An illustration of the QIT from this patent is shown in Figure 1-1. They proposed that in a purely quadrupolar field, a charged particle or an ion can be stored within the confines of the

electrodes as long as its motion is stable. The ion motion in the trap is well known to be characterized by applying the Mathieu equation. By manipulating the parameters in the equation, one can determine experimental parameters to selectively store ions of interest with certain mass-to-charge ratio (*m/z*) by making the trajectories of ions stable in the x, y and z planes or alternatively r and z in cylindrical coordinates. The ions that have unstable trajectories will either be ejected from the trap or hit the walls of the electrodes.

After the ion trap was developed, there were only a few people who experimented with the concept. Among them were Wuerker [2] who worked on storing charged microparticles, and Dawson and Whetten [3,4] who investigated on the use of the quadrupole ion trap to discriminate between ions of different *m/z* ratios. During this era, the main mode of operation was to selectively store ions of a single *m/z* ratio, similar to the operation of the quadrupole mass filter. Mather et al. used the ion trap as a chemical ionization source for the sector instruments [5]. Lawson and coworkers employed a quadrupole mass filter for mass analysis of ejected ions from the trap [6]. Still, the ion trap did not gain popularity until 1984, when Finnigan introduced it commercially as an inexpensive mass spectrometer coupled to a gas chromatograph [7]. For practical reasons, the trap was truncated to a manageable size and holes were added to the end caps for the purpose of getting electrons into the trap for internal electron ionization and getting ions out of the trap to a detector. The use of a buffer gas (usually helium) at a relatively higher pressure than typical vacuum in mass spectrometry was added to make the trap work because of its effect on intensity and mass resolution [8] Instead of selectively storing ions as was its predecessors' mode of operation, this mass spectrometer utilized a mass-selective instability scan, which consisted of storing all ions and then ejecting them in sequential order. This was done by linearly ramping the amplitude of the RF voltage applied to the ring electrode [7].

Another significant modification to the trap was the stretched geometry of the commercial trap, which Finnigan held as a trade secret. It was only divulged to the public in 1992 [9] when several groups, particularly Traldi et al. [10] found some anomalies in their experiments, which they attributed to nonlinear resonances.

Over the twenty years since the introduction of the commercial GC/MS ion trap, studies involving the QIT have increased in number. Coupled with advancement in ion sources and vacuum technology, what started as a novelty instrument for physicists to study ions evolved into an analytical tool for various modern applications. The list starts from a detector for gas chromatography and eventually liquid chromatography, to being used in more complex applications such as peptide sequencing, high-throughput metabolomics and drug discovery studies, and even mass spectrometric imaging [11-16].

A notable development in the QIT field is the introduction of the 2-D linear ion trap (LIT), which has a geometry more like the quadrupole mass filter than the traditional 3-D quadrupole ion trap geometry [17]. While it offers advantages such as improved sensitivity and MS^n performance when compared to the 3-D ion trap, the fundamental theory behind ion trapping and detection is still based on the 3-D model, and the modifications for manufacturing a practical 2-D QIT such as stretched geometry are carried over.

Quadrupole Ion Trap Mass Spectrometer

A traditional 3-D ion trap consists of three electrodes, two identical endcap electrodes with hyperbolic surfaces, entrance and exit holes in the center of each and a hyperbolic ring electrode with a radius, r_0, between the two endcaps (Figure 1-2). The distance between the apex of the entrance endcap to the exit endcap is $2z_0$. A quadrupolar field is created by applying a radio frequency (RF) voltage to the ring electrode while the two endcaps are held at ground. This generated field can trap entering ions.

To be able to describe the motion of an ion confined in a quadrupole ion trap, the Mathieu equation (Equation 1-1) is applied.

$$\frac{d^2u}{d\xi^2} + (a_u - 2q_u \cos 2\xi)u = 0 \qquad (1\text{-}1)$$

where u = r, z describes the ion position in the radial (r) and axial (z) dimensions. The parameter ξ is a dimensionless parameter equal to Ωt/2, where Ω is frequency and t is time. Solving for the trapping parameters a_u and q_u will lead to the following solution equations (1-2) and (1-3): [18].

$$a_z = -2a_r = -\frac{16\,e\,U}{m(r_0^2 + 2z_0^2)\Omega^2} \qquad (1\text{-}2)$$

$$q_z = -2q_r = \frac{8\,e\,V}{m(r_0^2 + 2z_0^2)\Omega^2} \qquad (1\text{-}3)$$

where e is the charge of an electron (1.602 x 10^{-19} C), U is the DC potential component, V is the amplitude of the RF potential component from 0 to peak and Ω is the angular frequency of the applied RF. The r_0 refers to the radius of the hyperbolic ring electrode and z_0 is the distance from the trap center to the endcap. q_u is directly proportional to the RF amplitude component (V) and a_u is proportional to the DC component (U). Setting these experimental conditions to appropriate values determines whether the trajectories of injected ions are stable for successful trapping.

Mathieu Stability Diagram

QIT operation involves the stability (or instability) of the ion trajectory within the field. It is assumed that the motion of an ion in a pure quadrupolar field is not coupled between the r and z directions. The solution parameters, a_u and q_u, in which the ions are stable in both dimensions, can be mapped to produce the well-known Mathieu stability diagram (Figure 1-3). The diagram is depicted in a_z and q_z values for simplification purposes, as using equations 1-2 and 1-3, would give the equivalent values in the r dimension. The iso-beta lines, β_z and β_r, are on the stability

diagram and are related to the frequency of ion motion in the r and z directions. This new stability parameter is a complex function of a_z and q_z, and can be used to delineate the stability boundaries at $\beta_z = 0$ and $\beta_z = 1$ [18]. The $\beta_z = 1$ stability boundary intersects with the q axis at $q_z = 0.908$. The fundamental secular frequencies are given by $\omega = \frac{1}{2}\beta\,\Omega$. Thus, the ions at the stability edges $\beta_z = 0$ have $\omega = 0$ (moving in one direction, never turning around) and at $\beta_z = 1$, $\omega = \frac{1}{2}\,\Omega$, half the drive frequency, where the motion is unbounded (increases in amplitude). In either case the ions are unstable and leave the trap. Most commercial traps do not apply a DC component (U) to the ring electrode thus all the ions fall on the $a_z = 0$ line. The position of the ions within the stability region is thus moved simply by changing the RF amplitude.

In the Mathieu stability diagram, trapped ions within the quadrupolar field are arranged from the highest to the lowest *m/z* along the $a_z = 0$ line, because the value qz is inversely proportional to *m/z* (equation 1-3). The amplitude of the RF voltage determines the lowest *m/z* that can be held within the ion trap (i.e., the lowest *m/z* ion will be to the left of the $q_z = 0.908$). This corresponds to a low mass cut-off (LMCO), which is expressed in terms of *m/z* for simplicity. The ions with an *m/z* below the LMCO will not have a stable trajectory and consequently be lost. Technically, there is no high mass cut-off but considering equation 1-3, high *m/z* ions will be clustered at low q_z values (i.e., close ion space) and the ions will be inevitably lost due to space charging or a shallow potential well, which exists at low qz values.

The parameter q_z is useful in relating ion injection and ejection for a particular *m/z* and determining the position of an ion (in terms of q_z value) on the stability diagram during a scan event. Knowing the LMCO and the q_z of ejection, the q_z position of any *m/z* can be determined by using equation 1-4.

$$m_1 q_1 = m_2 q_2 \tag{1-4}$$

Equation 1-4 was obtained with the assumptions that the other factors in equation 1-3 were kept constant. For example, if the LMCO is *m/z* 69 and the q_z ejection = 0.908, *m/z* 69 is at q_z = 0.908 and *m/z* 502 would be at q_z = 0.125.

Buffer Gas

As mentioned previously, the commercial QIT is operated with buffer gas of ~ 1 mTorr. During the development of the QIT as a GC detector, the buffer gas that filled the ion trap was carrier gas from the GC column output. Using only one small vacuum pump reduced the price and thereby increase the commercial viability of the instrument, but meant that the system would operate under higher pressure than typical vacuum conditions for other mass analyzers. Serendipitously, the improvement in resolution and signal intensity with the presence of buffer gas was significant and since that time, the QIT has been almost always operated in this manner [19]. Further details on the effects of buffer gas are provided in Chapter 3.

Instrumentation

All of the experiments presented in this dissertation were performed with a custom built QIT, which was constructed at the University of Florida. Thus, a detailed account of this instrument is included in this chapter. This QIT consisted of a large vacuum manifold that allowed for easy modifications for varying experiments. The QIT electronics and electrodes were from the commercially available GCQ (ThermoFinnigan, San Jose, CA), which is a GC/MS QIT instrument.

The custom built QIT nicknamed SweetP is constructed with a cast aluminum manifold, which is separated into three chambers (Figure 1-4). A glass cover was used as a top for the manifold. Each chamber is evacuated with its own turbomolecular pump, making it differentially pumped. This vacuum technique allowed the use of a high pressure ion source and prevented it from interfering with the performance of the low pressure mass analyzer. The first chamber held

the GCQ ion source and lenses. The second chamber contained a bent octopole ion guide, which directs ions from the ion source to the trap while minimizing the transfer of neutrals. The third chamber housed the ion trap electrodes, the conversion dynode and the electron multiplier.

Ion Source and Ion Optics

The ion source used was the GCQ ion source, which is mounted to the baffle wall dividing the first and second chambers (Figure 1-5). Though the ion source is capable of both electron ionization (EI) and chemical ionization (CI), the experiments used only EI. The ion volume, which is the center of the source, has three holes on the side of the cylinder. The two opposing 0.090" holes were designed as an inlet for GC effluent. A heated transfer line went through one hole and calibration gas through the other. Through these holes, analytes were introduced for ionization. The smallest hole, 0.0015" aperture, served as the inlet for the electron beam from the filament, which is located directly above the ion volume. The filament, along with the reflector, directed electrons towards the ion volume. It was held at a default value of -70 V relative to the ion volume. Thus, the kinetic energy of the electrons produced will be 70 eV, and the flow of electrons is controlled by measuring the filament emission current. The default value for the current was 250 μA.

A heated source block is placed around the ion volume and filament assembly. Through this block, the ion source temperature can be controlled from 50 to 225 °C. For the experiments, the ion source was maintained at 200 °C, as was the heated transfer line, to minimize condensation of sample analytes on the ion source region and to prevent variation in ionization efficiency. Initially, this instrument was connected to a GC, but the experiments reported here did not require chromatography, thus the heated transfer line was sealed off. A Pfeiffer-Balzers TPH 240 turbomolecular pump was installed for the ion trap chamber and the pressure was

monitored by a Granville-Philips ion gauge. Depending on the experimental conditions, the base pressure was 2 x 10^{-7} Torr without any sample being introduced.

Located in front of the ion volume were three electrostatic lenses composed of stainless steel and insulated with hard-anodized aluminum spacers. These ion lenses served to extract, focus and gate ions from the ion volume and into the octopole ion guide. The heaters from the source block are extended to heat these ion lenses. The potentials for the lenses can be set from -130 V to +130 V and were tuned to give the optimal peak signal intensity of a sample analyte ion under buffer gas conditions. Since the QIT is a pulsed mass analysis instrument, there is a need to inject the ions into the trap at specific scan function portions (i.e. ionization). The third lens (the last lens before the octopole ion guide) is the gate lens, which has a potential that is switched back and forth between two values, +100 V for the closed state and -100 V for the open state (for positive mode). Only during the open state were the ions are allowed to pass into the octopole ion guide.

The octopole ion guide is installed in the second (middle) chamber. Its length is 9" and it has an r_0 of 0.11". It also has a 10º bend in the center to keep neutral compounds from entering into the trap. These neutral compounds may cause ion/molecule reactions inside the trap and interfere with mass analysis. A Thermo TSQ 45 lens power supply is used to set the amplitude of the octopole RF potential. Values of 200-500 $V_{0\text{-}p}$ for the amplitude, and 2.475 MHz for the frequency were used to transmit the entire *m/z* range that can be analyzed by SweetP. The octopole potential is offset from the ion source by +/- 30V, which is also controlled by the TSQ 45 lens power supply. This chamber is pumped by a Pfeiffer Balzers TPH 170 turbomolecular pump and the pressure is not monitored.

Ion Trap and Detector Chamber

The third chamber held the ion trap electrodes along with the conversion dynode and electron multiplier. There are three stainless steel electrodes for the 3-D QIT: a hyperbolic ring electrode and two endcap electrodes (Figure 1-6). The ring electrode has an $r_0 = 7.07$ mm. Silicon nitride ring spacers were used to separate the electrodes to secure the electrode positions and to serve as electrical insulators. Each spacer has a width of 13.65 mm to give an equivalent distance of $z_0 = 7.85$ mm. The holes in each endcap are 1.5 mm in diameter. The three electrodes are secured to the baffle wall by two non-conducting posts passing through the endcaps and held by a spring washer and nut on each post. Analyte ions enter the mass analyzer through the entrance endcap electrode, which is seated next to the end of the octopole ion guide.

Electrical feedthroughs are connected through the manifold to link the electrodes to the supply of respective potentials. An RF voltage at a frequency of 1.03 MHz is applied to the ring electrode via a ceramic-insulated feedthrough with a spring-loaded pin; the RF amplitude has a range of 0 -8.5 $kV_{0\text{-}p}$. With these available RF values, the instrument has an upper mass limit of *m/z* 1000, which is sufficient for the range of compounds amenable to GC analysis. Resonant ejection is used during mass analysis by applying a supplementary (alternating current) AC waveform with a frequency of 476.375 kHz that corresponds to a q_z ejection at 0.901643, which is below the stability boundary. This method of ejection was done to enhance resolution of the mass peaks [20].

By default, a DC trap offset of -10 V is applied to the ion trap electrodes with respect to the ion source to determine the kinetic energy of ions when entering the mass analyzer. This value was kept constant throughout the experiments unless otherwise noted. An exit lens is attached outside of the exit endcap electrode. The purpose of this lens was to isolate the ion trap from the strong potential field emitted by the dynode. It was set at ground potential, which was the default value.

The detector for the instrument is composed of a conversion dynode and a DeTech continuous dynode electron multiplier, which are both positioned off-axis from the ion trap. For positive ions, the dynode is set at -15 kV. Ions ejected from the trap are accelerated towards the dynode and emit secondary ions and electrons. The multiplier, which is set at -1.8 kV, receives the secondary emission and converts it to current with enough gain for measurement. This signal is received and processed by the microprocessor on the GCQ electronics board and recorded by the instrument computer as a mass spectrum.

The trap chamber has a Pfeiffer Balzers TPH 240 turbomolecular pump attached, with the chamber pressure monitored by a Granville-Philips ion gauge. Similar to the commercial analogue, helium is delivered directly into the ion trap through a hole in the endcap. The helium flow is controlled by having a head pressure of 5 psi behind a 6" fused silica capillary with an i.d. of 0.050 mm, keeping the He pressure at 1 mTorr inside the ion trap. The typical pressure for this chamber with the buffer gas normally leaked into the system was 2.5×10^{-6} Torr.

The SweetP QIT uses electronic boards that were taken from the GCQ QIT. For compatibility reasons, GCQ software from Thermo Finnigan was used to control the ion trap operation. A development kit that enabled experienced users to modify the software was also supplied. Using a Visual Basic interface, the instrument source code can be changed to add features that are not available in the commercial version. This allows parameters such as adding zoom scan and altering the q_z ejection to be changed by programming.

The instrument calibration is routinely done before the start of every experiment presented here. Diagnostics were also checked daily to maintain the RF frequency of the trap, specifically whenever ion trap configurations were changed. Calibration was performed using the GCQ Tune software, with perfluorotributylamine (PFTBA) in EI positive mode.

Scan Function

The scan function is a representation of the sequence of events that take place to obtain a mass spectrum. To perform a mass spectrometric analysis, the sample has to be ionized and the analyte ions must be guided into the trap, cooled and then ejected for detection. This series of steps involves the critical timing of various potentials to the lenses, QIT electrodes and electron multiplier. The scan function is embedded in the software that controls the QIT instrument; some values can be changed by the user. Figure 1-7 shows a typical scan function for the quadrupole ion trap. The steps are arbitrarily classified into 4 major categories: pre-injection, injection, post-injection and detection events. Each step has a particular time period, which may differ from scan to scan, depending on the user settings. Values for typical scan event duration times are shown in Table 1-1.

The pre-injection event initializes the electrode potentials to ensure the same starting values on each scan. Particularly, the gate lens, as well as the multiplier, is turned off to prevent ions from being injected into the trap and being detected erroneously. This step is important when the user needs to do certain functions (e.g. triggering a pulsed valve) prior to ionization, thus, any commands related to that can be inserted in this step. The duration for pre-injection event is usually set at 1 ms (Table 1-1).

The injection event involves turning on the filament and the gate lens to inject subsequent ions into the trap. The duration of this scan function portion depends on whether the user is using automatic gain control (AGC) or fixed ionization method. AGC is used to prevent the ion trap from overfilling with ions, in order to avoid space charging [21]. The AGC method adjusts the injection time by pre-sampling with a fixed injection time and fast scan out, comparing the resulting current with a preset target value and adjusting the injection time based on the difference. The default maximum injection time is set at 25 ms. The post-injection event involves

the cooling phase, which comes immediately after the end of injection. This event serves to give time for the kinetically energetic ions to cool down by colliding with buffer gas inside the trap, increasing the chances of trapping. The commercial setting fixes the post- injection event duration at a default constant value of 3 ms. For the experiments, the development kit allow the user to change this value.

During the detection event, the trapped ions are ejected sequentiallyin order of increasing *m/z* from the trap for detection. The trapped ions begin at a low q_z, then are moved to the q_z ejection for detection by ramping up the RF amplitude. The multiplier is also warmed up by placing a voltage on it and allowing it to stabilize for a short time. SweetP QIT uses resonant ejection, which applies an auxiliary waveform across the endcaps to eject ions at a q_z value below the q_z = 0.908 stability edge . Using resonant ejection during detection gives better mass resolution and sensitivity [22]. The chosen q_z ejection value for the research instrument is q_z = 0.901643.

The RF amplitude value is controlled by a digital-to-analog converter (DAC), which in turn is calibrated to a range of mass assignments. To ensure the stability of the RF amplitude ramp, a number of backsteps (6 by default) is subtracted from the starting DAC value that is assigned for the LMCO ion to allow the RF potential to stabilize before the start of the LMCO ion ejection.

Study Overview

The purpose of this research was to evaluate novel modifications in ion trap operation that would improve performance. Chapter 2 presents a novel solution to the field imperfections local to the endcap holes. Another solution, which is microscreening of endcap holes, is compared to the current solution, which is increased endcap-to-endcap spacing. This chapter also reports practical method for such experimentation without having the burden of manufacturing

numerous sets of electrodes. Chapter 3 describes a novel system for delivery of buffer gas to the ion trap chamber. This chapter describes a multi-valve system design to tailor the buffer gas pressure to deliver buffer gas only when it is required. Performance of this system is compared to that of the traditional constant-pressure mode. Chapter 4 presents conclusions about the research conducted and offers future perspectives on the use of these systems in conjunction with quadrupole ion traps.

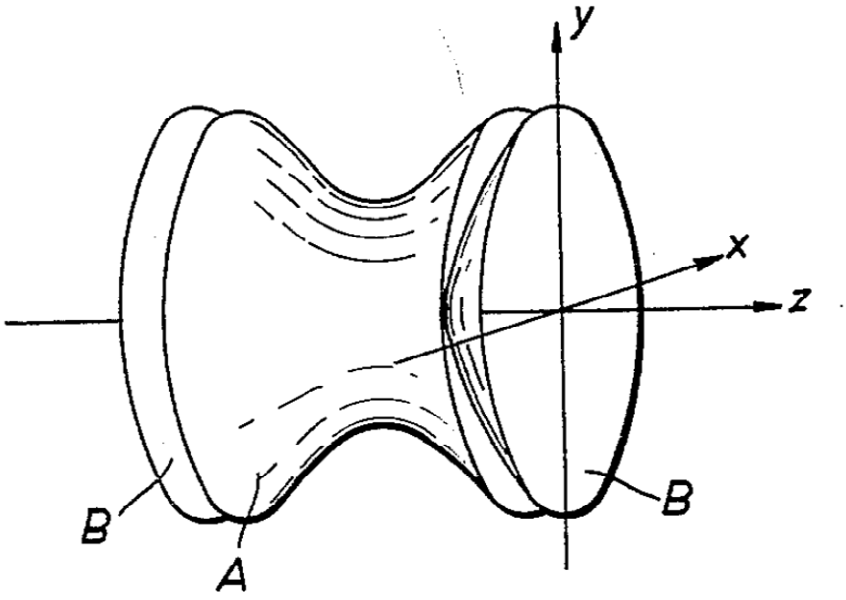

Figure 1-1. The 3-D quadrupole ion trap illustration from the patent, which also described the quadrupole mass filter [1]. The center ring electrode (A) is in between two matching endcap electrodes (B) along the z-axis.

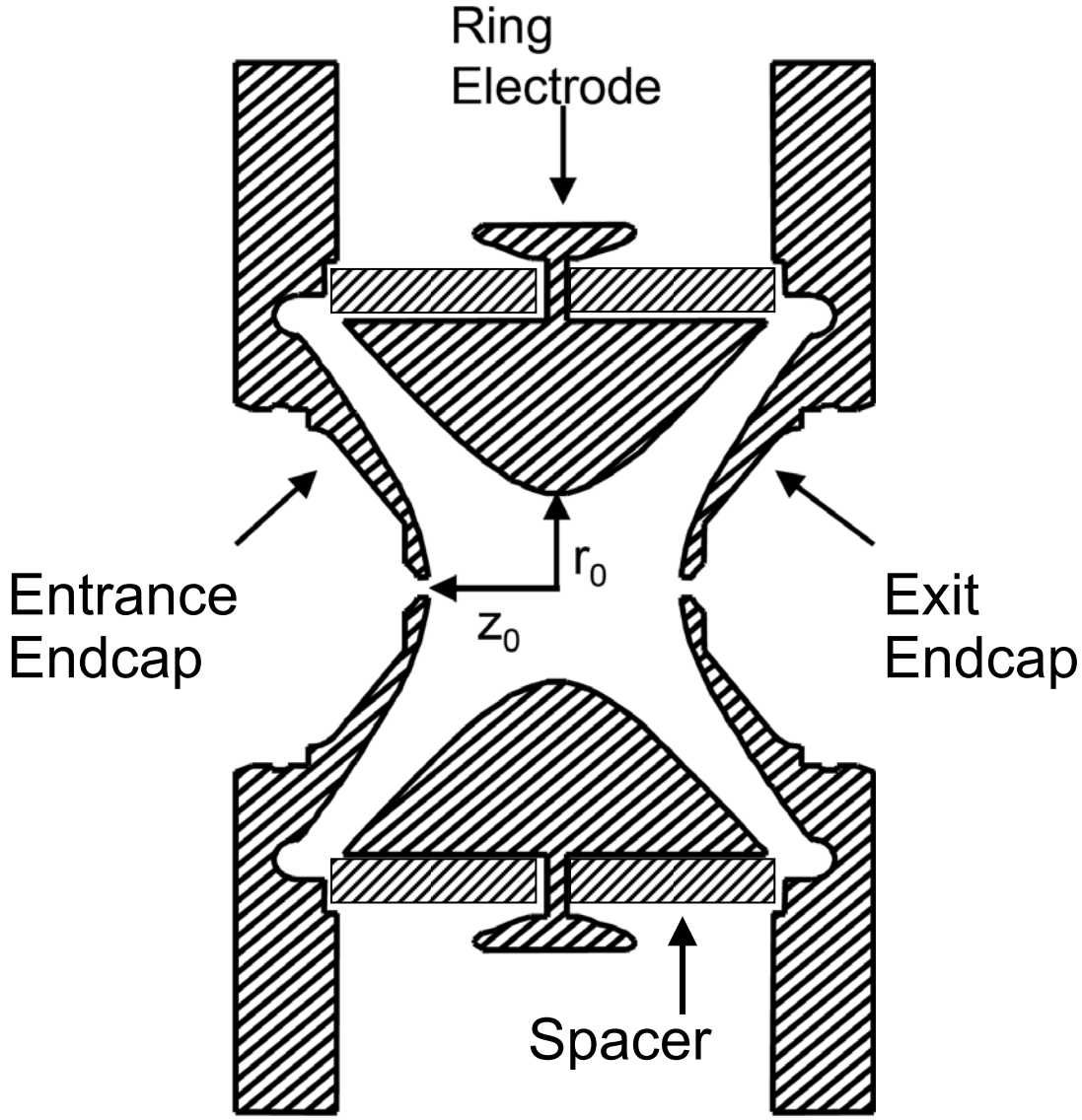

Figure 1-2. Cross sectional view of the QIT, showing the three electrodes and their assembly. The r_0 dimension is defined as the inner radius of the ring electrode and the z_0 dimension is the distance from the trap center to the endcap. Adapted from Murphy [23].

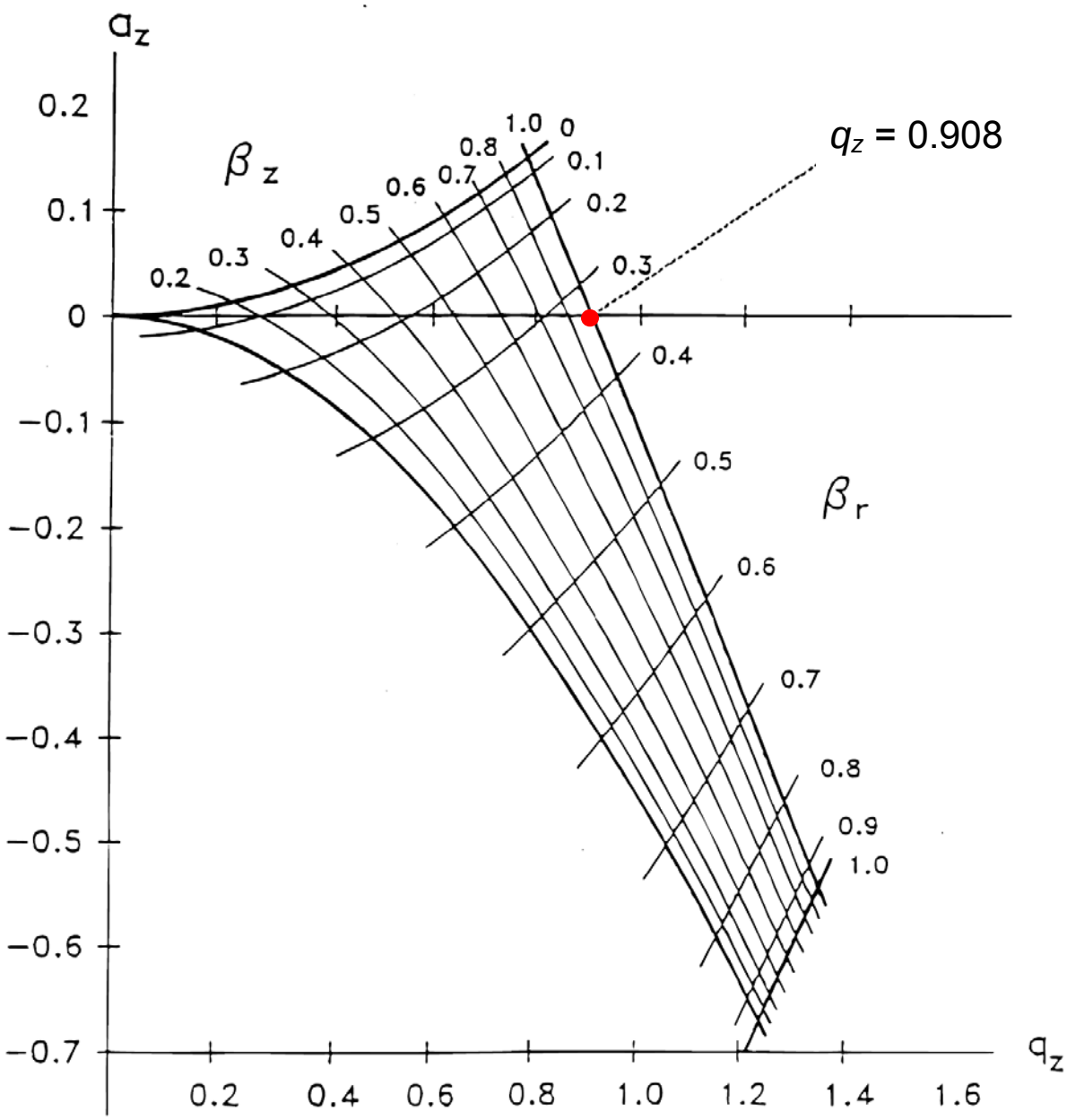

Figure 1-3. The Mathieu stability diagram plotted in a and q space. The iso-β_r and the iso-β_z lines are depicted. The $\beta_z = 1$ boundary intersects the q_z axis at $q_z = 0.908$, marked by the red dot. Adapted from March [18].

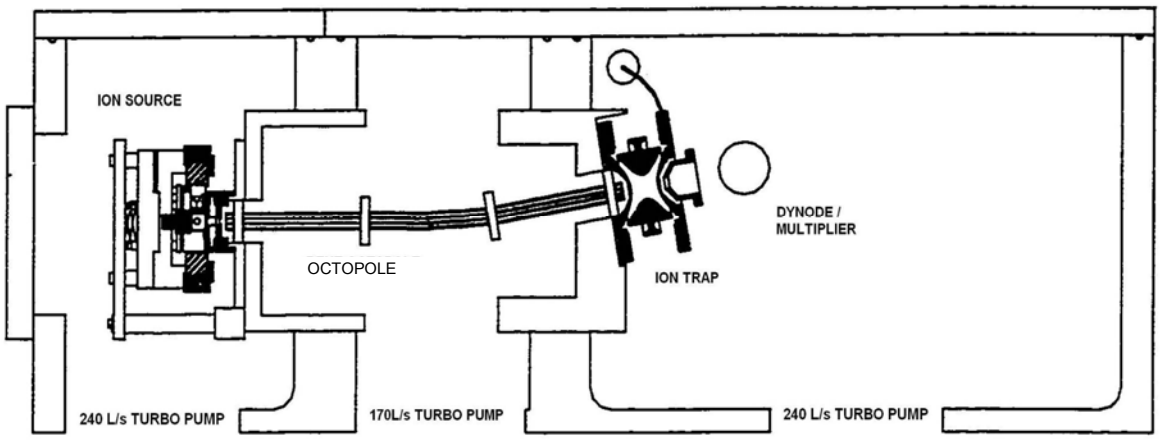

Figure 1-4. Research instrument SweetP. Side view. Shown are the three chambers separated by baffle walls for differential pumping. Adapted from Murphy [23].

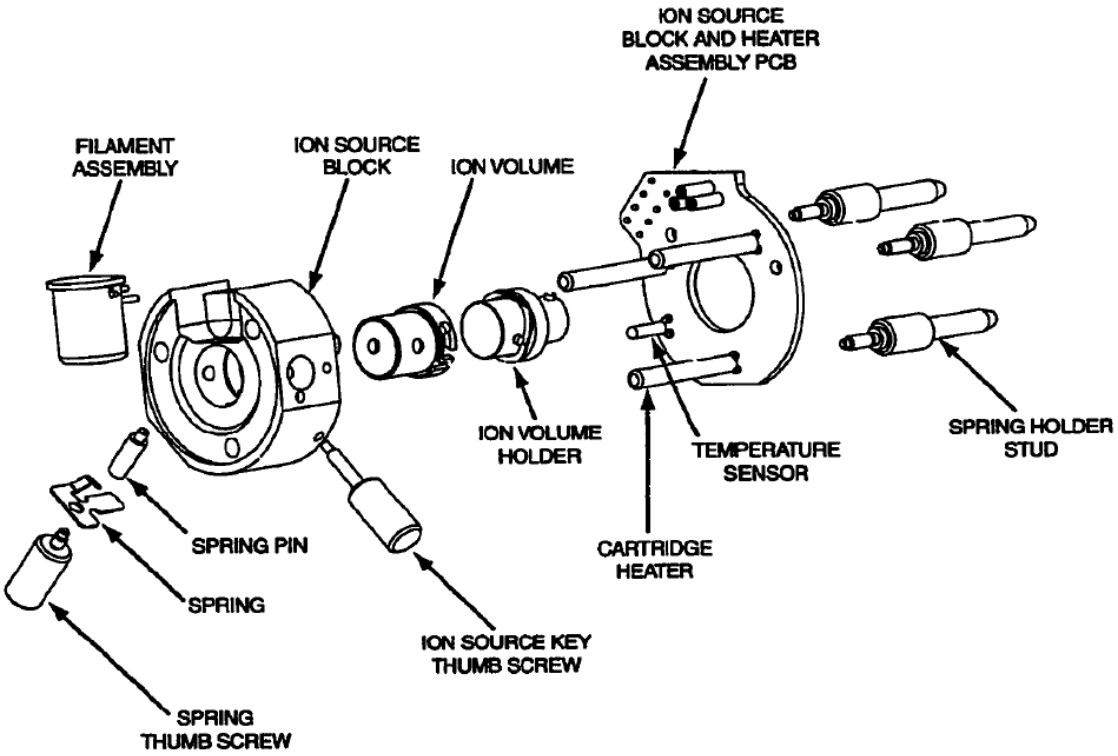

Figure 1-5. Layout of the GCQ ion source with the main parts shown. No modifications were made when it was integrated into the custom built QIT instrument. Adapted from the GCQ instrument hardware manual.

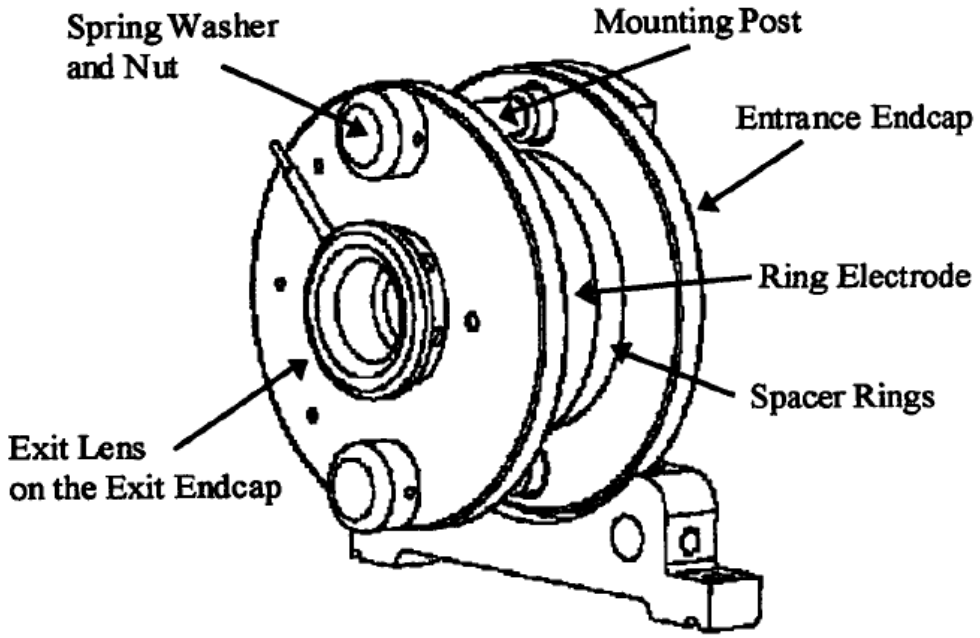

Figure 1-6. The GCQ ion trap electrodes mounted on a bracket. For SweetP, the electrodes are attached to the baffle wall that separates the second and the third chamber. Adapted from the GCQ instrument hardware manual.

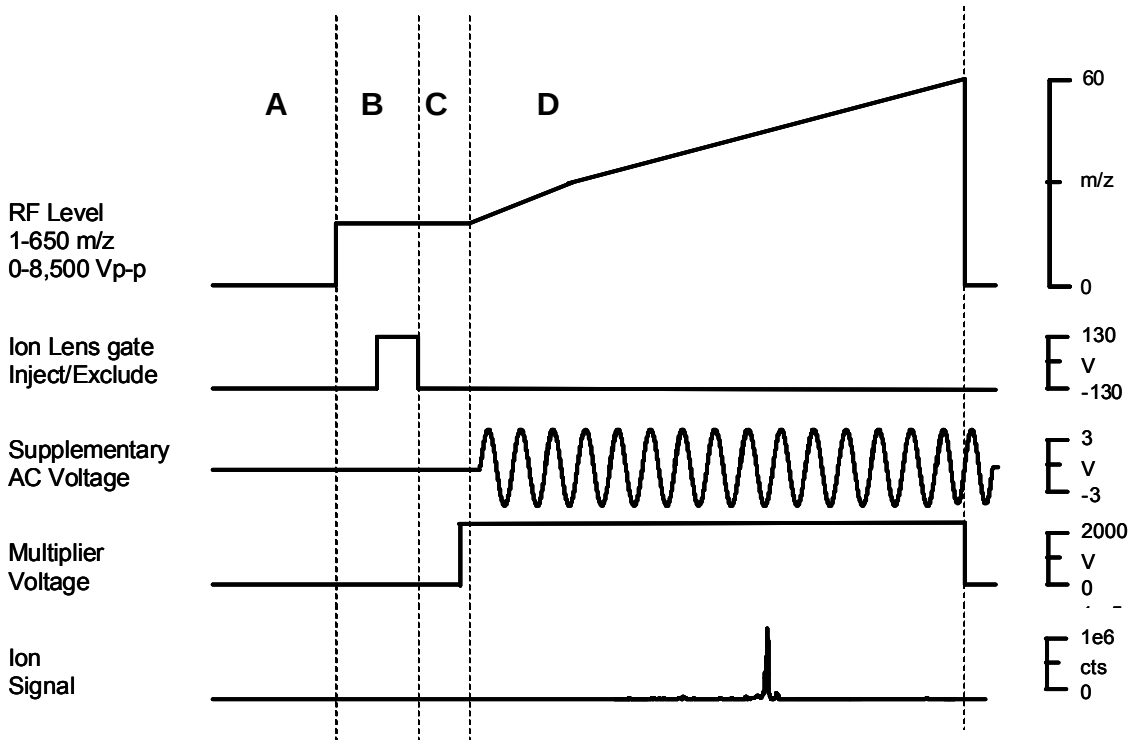

Figure 1-7. Typical scan function for the QIT, which is categorized into four divisions: A) pre-injection, B) injection C) post-injection and D) detection event. Also shown are the potentials associated with each step. The traces are not to scale. Adapted from Yates [24].

Table 1-1. Typical scan event times for the research instrument SweetP

Scan event	Duration (ms)	Notes
Pre-injection	1	
Injection	25	With AGC, varies
Post-injection	3	
Ramp time	1	
Multiplier warmup	2	
Backsteps	1.08	
Scan time	108	*m/z* 50-650, 0.180 ms/*m/z*
Post scan time	1	

CHAPTER 2
MICROSCREENED ENDCAP HOLES

Introduction

As mentioned in the first chapter, successful commercialization of the ion trap was dependent on modifications of the ion trap configuration to improve mass spectrometric performance. The first of these modifications was the change to the "stretched" configuration, [9]. wherein z_0 was increased by 0.78 mm , and the second was the use of He buffer gas, [7]. which reduces the kinetic energy of ions with collisions (further details on buffer gas effects is found in Chapter 3).The stretched geometry was an empirical solution made by Finnigan to compensate for problematic mass shifts of certain compounds (e.g. nitrobenzene) [9,19,25]. However, this stretch introduces superpositions of positive higher-order multipole fields, creating a non-ideal field within the QIT [26]. It is inconsistent to have chemical shifts in the trap with theoretical geometry and purely linear fields, while chemical shifts are removed in the trap with stretched geometry. Thus one must conclude that there are existing higher order fields in the theoretical geometry ion trap to begin with, where stretching the z_0 is needed to compensate for the effects of these existing higher order fields.

The attributes in the design of a practical ion trap that are identified [26]. as the sources of higher-order fields are: 1) truncation of the trap electrodes and 2) presence of holes in the endcaps. Truncation of the trap is required to limit the size of the device and to avoid a voltage arc between the RF ring and grounded endcap electrodes as they approach each other asymptotically (the maximum RF voltage can be achieved in the GCQ is 8500 $V_{0\text{-}p}$). It was understood that stretching the geometry was implemented to negate the effects of higher order fields caused by truncation, but calculations suggested that the contribution does not warrant the degree of increase in the spacing of the endcaps [27]. Another major factor to be considered as a

source of negative higher order fields is the presence of endcap holes. The RF field penetrates out of the endcap holes and affects ions during injection as they approach the ion trap, thus reducing injection efficiency [28]. Also during cooling and detection, areas near the endcap holes have a weakened RF trapping field; thus, ions that have a large axial excursion from the trap center would be affected as well as during ejection. Generally after being collisionally cooled by the buffer gas, trapped ions reside near the center of the trap where they experience an almost pure quadrupolar field. Stretching the endcap spacing further places the ions further from the areas with field imperfections, thus improving the performance. However, this stretch superimposes higher order fields within all of the QIT; hence, stretching the trap can be viewed as a global solution to a local problem (field imperfections in the vicinity of the holes). This non-ideal field causes nonlinear resonances and unexpected ion ejections that complicates the mass spectrum [29,30]. Note that 2-D linear ion traps (LIT) [17].are also stretched in one dimension to counteract the effects of the slits in two of the rods, also have the problem of superimposed higher order fields.

As an alternative to increasing the endcap spacing, other researchers have modified the hyperbolic angle, which also adds higher order fields; the resulting nonlinear resonances are used to enhance ion ejection [31].

Nonlinear Resonance Effects

Some notable investigations about nonlinear resonances include the works of Dawson and Whetten where they observed peak splitting and peak shape distortions that were potentially caused by unstable ion trajectories due to resonances in the ion trap [32]. Within a perfect field, ions would have stable trajectories and be limited in amplitude. They applied the theory of nonlinear resonances in a quadrupolar field to the three dimensional ion traps to determine the resonance locations in the Mathieu stability diagram. Based on their numerical simulation

experiments, they concluded that those errors in electrode shape, spacing, or harmonics in the RF field can cause these resonances. Beaty reported his work on the effects of truncation of the ring and end cap electrodes on trap performance [33]. His results showed that it is possible to have truncated electrodes with the harmonic character of the trap still preserved.

Wang and coworkers postulated a general condition for nonlinear resonances caused by superposition of weak multipole fields on the quadrupolar field [34]. They classified nonlinear resonances as coupling (difference and sum) resonances and non-coupling (r- and z-) resonances. They also added that the main contributors of nonlinear resonances were the low-order multipole fields (hexapole and octopole), since the magnitude of multipole fields decreases dramatically with increasing order. Resonance conditions can be expressed by trapping parameters, β_r and β_z, which can be translated back to a_z and q_z, and the frequency of the RF voltage placed on the ring electrode.

Several groups have tried to map the resonance lines in the Mathieu stability diagram. Shown in Figure 2-1, Eades et al [35,36]. and Alheit et al. [37]. have mapped "black canyons" connoting inefficient storage of ions at specific a_z and q_z values. These corresponded to $\beta_z = 2/3$ (hexapolar q_z =0.78 at $a_z = 0$), $\beta_z = 1/2$ (octopolar q_z =0.64 at $a_z = 0$), and $\beta_z = 1/3$ (dodecapolar q_z =0.45 at $a_z = 0$). Mo et al. reported that some ions were ejected before reaching the $\beta_z = 1$ boundary when the RF voltage is ramping through a q_z value corresponding to a nonlinear resonance on the stability diagram [38]. For example, the CF_3^+ *m/z* 69 fragment ion of perfluorotributylamine formed under electron ionization can be partially located at *m/z* 60-61 (ghost peak) because of the hexapolar resonance $\beta_z = 2/3$. Kocher et al. affirmed that under space charged conditions and with nonlinear resonances, ghost peaks can even occur at higher *m/z* values when using extended mode, ejecting at β_z=1/3 (q_z =0.45) [39].

Currently, the QIT in a commercial mass spectrometer is operated under the premise that it utilizes an ideal quadrupolar field to trap the ions, using the solutions to the Mathieu differential equation to analytically calculate the masses. The modifications made by Finnigan (i.e. stretching the geometry) were effective solutions in making the quadrupole ion trap a successful mass spectrometer, but it was a global solution for a local problem of field imperfection near the end cap holes. Previous simulation studies in the Yost laboratory [40]. have found a replacement solution that in the end would preserve the linearity of the quadrupolar field. Hence the motion of ions trapped in the closer to ideal quadrupolar field can be characterized more closely by the Mathieu equation. The goal of this research was to evaluate the local solution that would repair the problem at the end cap holes.

Simulation Studies

Before modifications can be made to the ion trap electrodes to reduce the field imperfections local to the endcap holes, it is prudent to do computer modeling simulations to map the field strength profile around the area and establish some fundamental views. The electric (RF) field gradient was used as the primary criterion during the evaluation. The experimental design was started with SIMION version 7.0 (SIS, Ringoes, NJ), and was continued with version 8.0 for the computer simulations [40]. Models of the Finnigan GCQ QIT using ideal and stretched geometry were created. Voltages were set for the ring and endcap electrodes, reproducing typical MS parameters and electro-potential contours. The RF electric field was plotted near the endcap of ion traps with both stretched and theoretical geometries and with different hole modifications. Results were exported to an ASCII file and Excel (Microsoft, Redmond, WA) was used for graphing.

Figure 2-2A shows the three hole modifications used for the computer simulations, along with the standard (STD, one hole) design and ideal (no hole) design. These SIMION studies used

cylindrical symmetry along the z axis to work within the computer resources' limits and to minimize computation lag time; simulated mesh designs were limited to concentric circles corresponding to the concentric rings of holes. Both endcap apertures were modified to be the same. The voltage between ring and endcap electrodes was set to 8500 V, the maximum $V_{0\text{-}p}$ for GCQ QIT and electric field data (resolution) was taken at every 0.05 mm.

To evaluate the effect of the holes on the RF field gradient, the electric field (in V/mm) was plotted vs. the distance from the center of the trap (normalized so that the endcap is at 100%). The electric field for the theoretical geometry trap is plotted for the endcap electrode with the standard hole and the ideal (no hole), shown in Figure 2-3. As both electric field strengths were compared from the distance of 0% to 69% away from the trap center, the electric field deviation of the STD hole was less than 1%. As the distance increases further, the electric field with the STD hole deviates significantly such that at 99.3% distance, the field fell to 43% less than that of the ideal (no hole). The RF field gradient is distorted in the vicinity of the hole, allowing the field to leak out.

In Figure 2-4, several hole designs were chosen (ideal, STD hole and three mesh types) and plotted their electric field strength as affected by distance from the trap center with stretched geometry QIT (z_0 = 7.85 mm). The illustrations of the meshes are found in Figure 2-2A. Mesh 1 has a hole diameter of 1.5 mm and consisted of three concentric rings that are 0.05 mm thick and spaced 0.15 mm apart. For mesh 2, the hole diameter was 1.5 mm and consisted of 5 concentric rings that are 0.001 mm thick and spaced 0.15 mm apart. The depths of these meshes were 0.5 mm. Mesh 3 has a smaller hole, 1.4 mm diameter and consisted of three concentric rings that are 0.05 mm thick and 0.15 mm apart. For this mesh, the depth was 0.1 mm.

Comparing the ideal (no hole) with the STD hole design, there was an improvement when using the stretched geometry in preserving the field strength, with the field strength deviation less than 1% from 0-79% distance from trap center. Using a mesh design, the electric field was significantly improved, producing an electric field profile much closer to that of the ideal (no hole) design. In this case, the most significant improvement was observed with mesh 2 design.

The electric field was also evaluated by plotting the field at displacement of 0.05 mm (99.3% trap center distance) above the outermost electrode surface vs the off axis (Figure 2-5) for the ideal (no hole), STD hole and three mesh designs, all for the stretched geometry trap. Again, with the STD hole design, it is observed that the field dropped significantly to 43% less than that of the ideal (no hole). With the use of any of the mesh designs, the field strength profile is brought closer to the ideal profile. The wavelike patterns of the meshes' electric field were due to the presence of the concentric ring electrodes inside the hole, rising when approaching towards and dropping when retreating from an electrode. It should be noted also that the last data point (at 99.3% normalized distance from trap center) from Figure 2-3 are the same corresponding data that is found at offaxis distance = 0 mm. These results are in agreement with the work of Plass and coworkers where it was found that the field potential leaks out near the end cap holes, thereby, weakening the field [26]. With the field deviating from the ideal, ions with large amplitude oscillations in the z-direction will be affected and will not behave as predicted by the Mathieu equation.

Experimental Section

Design and Construction of Microscreened Endcap Holes

The mesh designs used for simulations consisted of concentric circles floating in space to form the mesh; those designs were dictated by the cylindrical geometry employed in the simulation. This type of design is physically impossible to manufacture; thus a different

approach was required. An array of small individual holes arranged in concentric rings is the closest approximate to the simulation designs. Another factor to consider is the manner of constructing the endcaps with meshes. The ideal method for the construction would be to machine endcap electrodes by the same procedure as the commercial standard electrodes are manufactured, but with multiple small holes could be laser cut instead of machine-drilled to prevent distortion of the hyperbolic surface. Several sets of electrodes could be machined to permit various combinations of size and number of holes to be evaluated. A more efficient approach would be to modify single set of modified endcaps with interchangeable microscreened inserts for the holes. For the studies reported here, a set of standard GCQ endcaps (Thermo, San Jose, CA) was modified. This approach was selected as the least resource-intensive that allowed for the investigation of the impact of endcap hole modifications non-linear resonances in the ion trap.

The specifications and design of the interchangeable mesh insert is shown on Figure 2-6A. It consists of three pieces with stainless steel as the material of choice. The top piece (frame) keeps the mesh from falling into the trap with the knife edge shoulder. Its outer frame (the surface exposed to the inside of the trap) was machined to have a similar profile to that of the hyperbolic surface of the endcap electrode, which was calculated to be 7° at 4 mm from the center of the electrode. The middle piece is the selected mesh sandwiched between the top piece and the bottom piece (chock). The curved edge of the chock touching the mesh will push the mesh outwards towards the trap, making it conform to the juncture of the frame and chock. This procedure will compensate for the depth that is inherent in putting a top piece over the mesh. As shown in Figure 2-6B, The three-piece unit was inserted into a 4 mm diameter hole machined into the center of the endcap (where the original 1.5 mm diameter hole is in the standard endcap).

Microscreens: Pattern and Size

There are several commercially available meshes made with different materials and methods. Stainless steel was the material of choice since it is unreactive, durable, and does not easily distort when machined. Perforated mesh was preferred because the surface is smoother than that of wire mesh. A sample mesh product (70 μm thick) from VACCO (South El Monte, CA), shown in Figure 2-6C, a mesh manufacturing company, was obtained; and two designs on this sample were selected for the microscreen patterns. A third design consisting of one 1.5 mm diameter hole (the same diameter as the standard endcap electrode), was made as a control to determine whether the junction of the endcap and the microscreen insert design significantly affects performance compared to the standard endcap.

Evaluation of the Microscreened Endcap Holes

For the choice of analytes, commercially available perfluorotributylamine (PFTBA, CAS# 311- 89-7) was selected because it forms stable and well known fragment ions under electron ionization. PFTBA was leaked into the ion source via a needle valve and an electronically controlled shut-off valve. It was ionized using electron ionization at 70 eV. The chemical structure and a list of various fragment ions of PFTBA and their exact *m/z* value is shown in Figure 2-7. Automatic gain control (AGC) was turned off in all of these cases except when noted. Each mass spectrum is an average of 100 scans. The instrument was mass calibrated with PFTBA using the standard GCQ software under normal operating buffer gas pressure. The RF frequency was 1030 kHz and the amplitude range was from 0-8.5 $kV_{0\text{-}p}$. Resonant ejection at q_z=0.901643 (β_z=0.92499, frequency= 476.374 kHz) was used. The QIT was always retuned and calibrated with buffer gas for every change in trap configuration.

Without collisional cooling, ions would tend to have larger trajectories from the trap center and would be more affected by the field perturbations close to the endcap holes. In this manner, ghost peaks will be more evident at nonlinear resonance positions for experiments without buffer gas. Thus, experiments were done with and without the presence of buffer gas. With buffer gas leaked in, the optimal pressure was 2.6×10^{-6} Torr (uncorrected); after the He flow was shut-off, the pressure was 2.0×10^{-7} Torr (uncorrected). Pressures in the source and trap chambers were measured with Granville-Philips ion gauges. Comparison among the different designs of microscreened holes and the standard electrode was carried out by monitoring the PFTBA fragment ion at *m/z* 69. The performance of each design was evaluated in terms of identification of the nonlinear resonances causing the prevalent ghost peaks, number and intensity of ghost peaks, as well as mass resolution and intensity of the real peaks.

Different z_0 Spacing

The effects of varying z_0 spacing with the use of microscreened holes were investigated. If microscreening the endcap holes removed all the field imperfections, then the ideal spacing would be the theoretical geometry. Upon review of the simulation results, however, the field perturbations were only minimized instead of removed, since small holes were still present and electrodes are still truncated. Currently, the commercial GCQ ion trap has a spacing of 7.85 mm from the center of the trap to the endcaps, which is defined to a 11% stretch from the theoretical spacing of 7.07 mm. These two spacings and two other distances in between were tested by using modified spacing rings with the standard and modified electrodes.

Results and Discussion

Several materials were considered for the mesh. Given the dimensions required for the holes in the mesh (≤ 0.5 mm), it would be difficult to fabricate them by classical machining approach. However, manufactured mesh produced by electroforming and photochemical etching

is commercially available. The material has to be conductive to allow the endcap potential to be maintained. Physical attributes such as malleability and resistance to heat expansion were also considered.

The shadow masks that are used inside a television were initially considered. The material commonly used for these masks is Invar, an Fe-Ni alloy that is excellent in resisting heat expansion. The shadow mask has a flat smooth surface with perforated holes, as opposed to wire mesh, which has an irregular surface inherent to the design. Upon examining the shadow mask, the mesh was found to be too pliable and that the holes in the mesh easily got deformed, thus posing a problem later when cutting disks to use. Another issue with this kind of mesh was that different sizes and patterns for the holes were not readily available.

A second candidate was transmission electron microscopy (TEM) grids that are used to hold samples for electron microscopy. Common materials for this type of mesh are copper, molybdenum, nickel, gold, and titanium. Different patterns and sizes for the holes are also readily available. However, the thickness of the TEM grids was less than 50 μm and posed a problem for cutting out disks.

Lastly, companies offering perforating services and vending perforated products were considered. A sample of mesh was obtained from VACCO, a company that has the capability of perforating materials with the use of photochemical etching (Figure 2-6B). Their stainless steel mesh products can withstand the requirements of machining. The mesh sample was examined under a microscope with a millimeter ruler to measure the size and spacing of the holes (Figure 2-8). Figure 2-8A to E shows the mesh samples examined under an optical microscope. Notice the holes were uniform made and had a smooth surface. Different patterns such as hexagonal or

squared shaped holes (not shown) were also available. Figure 2-8F shows the hole (1.5 mm diameter) of a standard endcap.

Mesh E from Figure 2-8E was installed into the modified endcap, as shown in Figure 2-9B, for microscreening; 3.8 mm diameter piece of the mesh was mounted in the chock and frame design in Figure 2-6A. The outer diameter of the insert was 4 mm and the inner diameter of the chock with the exposed microscreened holes was 2 mm. The hole area of the STD hole is 1.7 mm^2 and the mesh E open area was calculated to be 1.2 mm^2. It is important that the insert is flush with the endcap electrode surface.

Analysis of PFTBA

Initial test with the mesh inserts consisted of using the one hole insert design shown in Figure 2-9D. Under buffer gas conditions and stretched geometry, the performance of the one hole design was similar to the STD hole design. It was concluded that the field imperfections created by the junction of the inserts and endcap electrode were minimal compared to the field imperfection contributed by the hole.

Figure 2-10A shows the comparison of PFTBA fragment ion *m/z* 69 spectra with buffer gas used, using a stretched geometry (z_0 = 7.85 mm) and STD hole design; in this mass range, the spectrum includes the *m/z* 68.9 ion (CF_3^+, accurate mass 68.995) and the $^{13}CF_3^+$ peak at *m/z* 69.9 (at 1.1% relative abundance). With helium buffer gas and stretched endcap spacing, QITs can be operated without significant nonlinear resonance effects. The absolute intensity for this peak was $4.8x10^6$ counts The trap chamber pressure reading was around $2.0x10^{-6}$ Torr (uncorrected) with buffer gas introduced; when the buffer gas supply to the trap was shut off, the chamber pressure dropped to $2.0x10^{-7}$ Torr and a drastic reduction in ion signal intensity was observed due to inefficient trapping and cooling of the ions (Figure 2-9B). Without buffer gas, peaks at *m/z* 64.5 and 66.9 appeared, and the peak at *m/z* 66.9 was higher that the peak at *m/z*

68.9. There was also a need to increase the ionization time from 1 to 10 ms to observe the *m/z* 69 peak with an intensity of 6.9×10^5 counts. As there is no possible fragmentation pathway for a loss of 2 from *m/z* 69 (CF_3^+), it was concluded that the peak at *m/z* 66.9 (nominally *m/z* 67) was a "ghost" peak of the *m/z* 69 (CF_3^+) fragment ion. Another method to test this conclusion would be to prolong the cooling time. If the intensity of the "ghost" peak decreased, it would suggest that cooling the ions towards the center of the ion trap simply reduced the effect of field imperfections. On the other hand, if the intensity of the "ghost" peak increases, it would be an indication of an ion-molecule reaction. The intensity decreased as the cooling time was increased from 3 ms to 100 ms, further supporting the conclusion that that peak at *m/z* 67 was a ghost peak of the ion at *m/z* 69.

Since the *m/z* 69 peak was resonantly ejected at $q_z = 0.901643$, the other peaks can be assigned q_z values relative to the main peak, and $q_r = -1/2q_z$ values. β_z and β_r are defined by a continued fraction expression [18]., thus a custom program that was written in Visual Basic by Finnigan engineers was used to calculate β_z and β_r from the q_z and q_r values. The calculated β_z and β_r values were compared to reported nonlinear resonance [41]. The peak at *m/z* 67 has a q_z value of 0.875, corresponding to $\beta_z = 0.83046$ and $\beta_r = 0.33310$; thus corresponds to a hexapolar nonlinear resonance with $\beta_z + 1/2\beta_r = 1$. As shown in Figure 2-10C, reducing the endcap spacing to theoretical dimensions ($z_0 = 7.07$ mm) without repairing the imperfection caused by the endcap holes showed extra ghost peaks in the spectrum even with the use of buffer gas. In the absence of buffer gas, the theoretical spacing yielded several relatively abundant ghost peaks (*m/z* 60.3, 61.7,64.5 and 66.9), with low absolute intensities (*m/z* 68.9 peak at 9.5×10^5 counts). Comparing the spectra without buffer gas in figures 2-10B and 2-10D, it is shown that the ratio

of the *m/z* 67 ghost peak to the real peak at *m/z* 69 was reduced with the theoretical compared to the stretched configuration, but other ghost peaks appear.

Data from experiments with mesh E for microscreening and theoretical endcap spacing are shown in Figure 2-11. With buffer gas, the mass spectrum obtained using microscreened endcaps was similar compared to with using standard endcaps (Figure 2-11A; the intensity for *m/z* 68.9 peak was $9.3x10^5$ counts. Without buffer gas, the intensity was lowered by two orders of magnitude for *m/z* 68.9 peak ($1.1x10^3$ counts) and various ghost peaks appeared (peaks at *m/z* 59.9, 64.8, 66.0, and 67.2). A notable feature of this mass spectra was the ratio of ghost peak at *m/z* 67 (found at *m/z* 67.2) to the real peak at *m/z* 68.8 was lower than that of using standard endcaps. Another observation is the large peak at *m/z* 59.9, which was not previously predominant with the other endcap configuration. This peak was concluded to be caused by the mesh insert after interchanging for several times.

Endcaps with another mesh (type D, Figure 2-8D) were constructed and evaluated for performance, shown in Figure 2-12. The main difference between mesh D and mesh E is the 2x larger diameter hole and the less open area available for the passage of ions. The open area for this mesh with 0.6 mm diameter holes was calculated to be 0.985 mm^2. After tuning and calibration, it was concluded that the mass spectra shown in Figure 2-12B and C, have similar intensities with slight ly improved resolution when compared to the mass spectra taken using mesh type E (Figure 2-10), with and without buffer gas.

Different z_0 Spacing

Plots of absolute ion intensities (log) and normalized intensities as a function of endcap spacing using endcaps with the STD hole design are shown in Figure 2-13. The data in figures 2-13A and B were taken with buffer gas while the data in figures C and D were taken without buffer gas. The intensities in Figure 2-13B and D are relative to *m/z* 68.9 = 100. The peaks at *m/z*

60.3 and 60.8 are the same peak, as well as for *m/z* 64.7 and 64.5 peaks, just shifted due to a combination of factors, such as space charging and mass calibration. It should be also noted that the listed masses were an average of *m/z* peaks that were identified to be the same among the different trap configuration. For example, mass spectra with the trap configurations of z_0 = 7.07, 7.34, 7.59 and 7.85 mm and without buffer gas have peaks at *m/z* 60.3, 60.1, 60.3 and 60.4 respectively. The *m/z* assignments were averaged to a value of *m/z* 60.3.

With helium buffer gas (Figure 2-13A and B), the "ghost" peaks are lower in intensity by at least 2 orders of magnitude compared to *m/z* 68.9, regardless of endcap spacing. After shutting off the buffer gas supply, however, the conventional stretched configuration at z_0 = 7.85 mm has the ghost peak at *m/z* 66.9 of greater intensity than the *m/z* 68.9 peak. Returning to theoretical geometry (z_0 = 7.07 mm) the ghost peak intensity at *m/z* 68.9was lower but still present. The lowest peak intensity at *m/z* 68.9was achieved by reducing the stretch to z_0 = 7.34 mm, but with the side effect of a new ghost peak at *m/z* 60.3. This *m/z* 60.3 peak had a q_z = 0.786, which corresponded to hexapolar resonance line at β_z = 2/3 (Table 2-1).

The mass assignments (at a_z = 0) for the major intensity peaks found and their corresponding qz and calculated resonance equations are listed in table 2-1. Using the βz and βr values to obtain the equation and comparing with reported resonance equations by Wang and Franzen [27]., the peaks were described as follows: *m/z* 66.9 and 60.3 peaks were caused by resonance with a hexapolar field and *m/z* 64.5 by a dodecapolar field. The hexapolar resonance effect with βz = 2/3 have been always experimentally observed [10,35,36].; however, observation for the hexapolar resonance with βz +1/2βr =1 have been limited [41]. The peak at *m/z* 66.0 was not successfully identified with a resonance equation. The cause may be due to

splitting of the peak at *m/z* 66.9 especially at low pressures with inelastic collisions, which was reported by Plass [26].

Absolute ion intensities (log) and normalized intensities vs axial distance were also graphed for data taken using microscreened endcaps with mesh E (Figure 2-14). Same as in Figure 2-13, the data in figures 2-14A and B were taken with buffer gas while the data in figures C and D were taken without buffer gas. The intensities in Figure 2-14B and D are also normalized to *m/z* 68.9 = 100. The peaks at *m/z* 67.1 and 66.9 from these figures are the same peak. The peak at *m/z* 60.3 from Figure 2-13 is identified as the same peak as *m/z* 60.1 peak in Figure 2-14. Comparing data taken with buffer gas between figures 2-13B and 2-14B, the relative intensity of the ghost peak at the best spacing for microscreened (7.07 mm) is significantly lesser than for the standard single hole endcap at its best spacing (7.85 mm). Without buffer gas, the relative intensity of the *m/z* 66.9 peak is consistently smaller at all geometries. Unfortunately, the less intense ghost peaks at lower *m/z* are increased.

Upon removal of the buffer gas, the best overall performance (lowest abundance for all ghost peaks) was achieved when using the z_0 = 7.34 mm stretch for both standard and microscreened endcap. This may be due to the field imperfections caused by the repeated replacement of microscreened holes.

Conclusions

The experimental evaluation of microscreening the endcap holes have been presented. Using mesh inserts was a practical method of evaluating the solution of repairing the field imperfection, local to the vicinity of the endcap holes. With the use of buffer gas, ghost peak intensities were significantly lower than that of the real peak, for any of the trap configurations. On experiments without buffer gas, the reduced endcap spacing of 7.34 mm achieved the best performance in terms of reducing the ghost peak at *m/z* 66.9 for both standard (one hole) and

microscreened endcaps. However, field imperfections contributed by the microscreened endcaps were also encountered, as peaks not present with standard endcaps appeared with microscreened endcaps.

The practical solution employed by Finnigan from a commercial standpoint is enough for most applications. For some applications, however, the use of buffer gas is a problem (e.g. space exploration where carrying He is unappealing, or in cases where ion-molecule reactions with impurities such as water in the buffer gas are problematic.) In such cases, using the QIT with the $z_0 = 7.85$ mm spacing would be problematic as the spectra it produces will be complicated with ghost peaks due to nonlinear resonance.

Another significance of this research is that it should also apply to the 2-D LIT. The X-rods, where the slits are located and the ions are ejected, were also stretched by 0.75 mm; the same way as the endcaps to compensate for the field imperfection in the vicinity of the slits [17]. It would be beneficial to know if microscreening would have more favorable effects in 2-D LIT, judging that the aperture slits spans across the center rods. The slits are 0.25 mm wide, which is significantly smaller that that of the 3-D trap. An idea for microscreening would be to separate the slits into smaller segments.

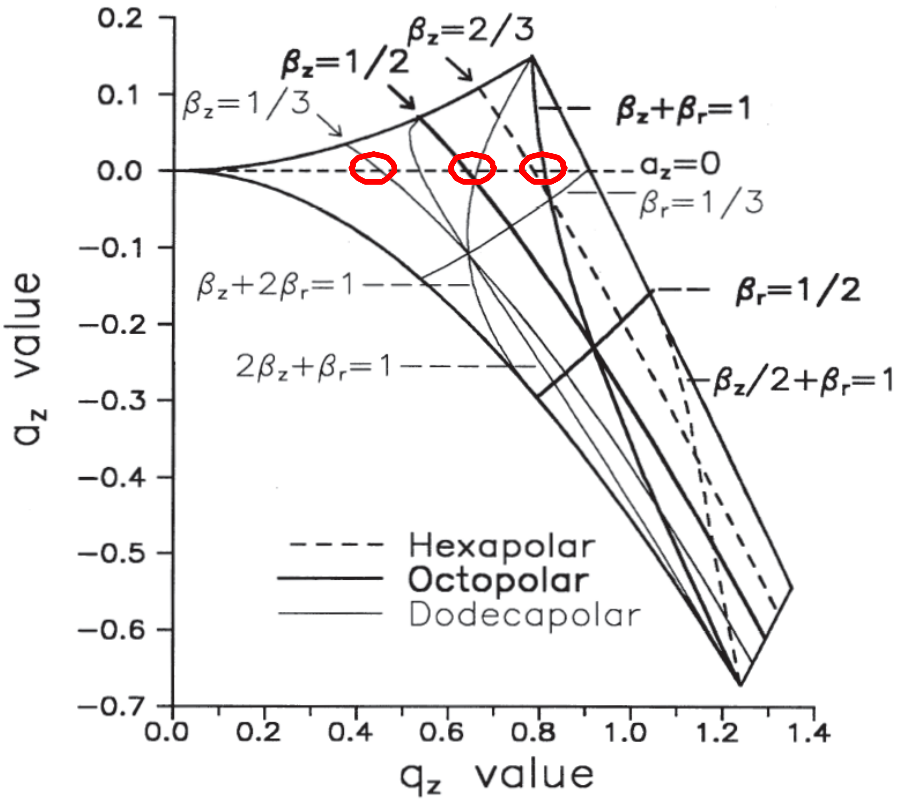

Higher order field	Resonance Equation	q_z value
Hexapolar	$\beta_z = 2/3$	0.785
	$\beta_z + \beta_r/2 = 1$	0.876
Octopolar	$\beta_z=1/2$	0.639
	$\beta_z + \beta_r = 1$	0.811
Dodecapolar	$\beta_z=1/3$	0.448

Figure 2-1. Previously reported nonlinear resonances. The red circles indicate the resonances caused by higher order fields in the Mathieu stability diagram along the $a_z = 0$ line. Adapted from Eades [36].

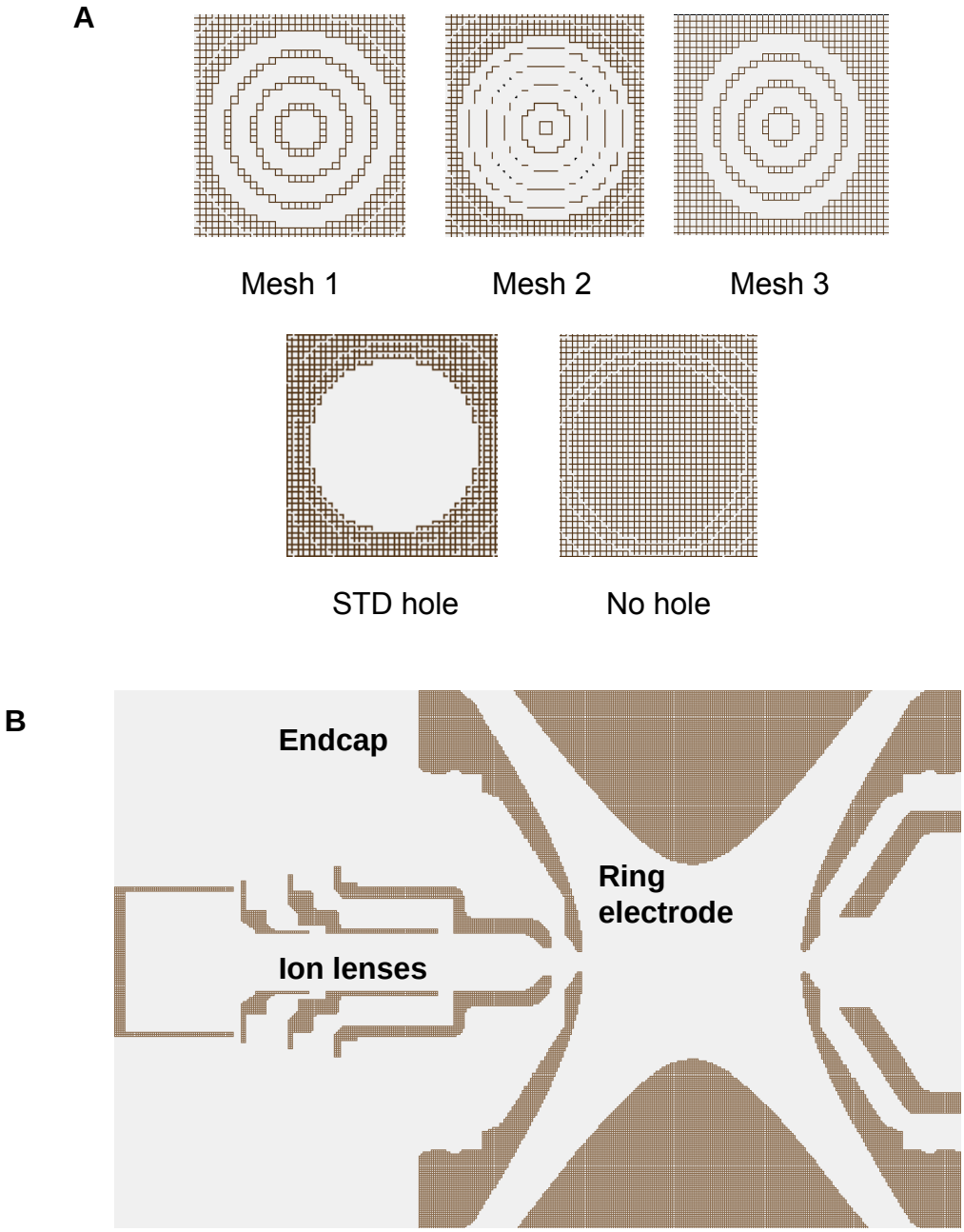

Figure 2-2. SIMION drawings of GCQ and endcap hole types. A) Hole modifications used for simulation in SIMION 8.0 B) A SIMION construct of GCQ QIT electrodes and ion lenses. Shown here is the stretched geometry and STD hole endcaps.

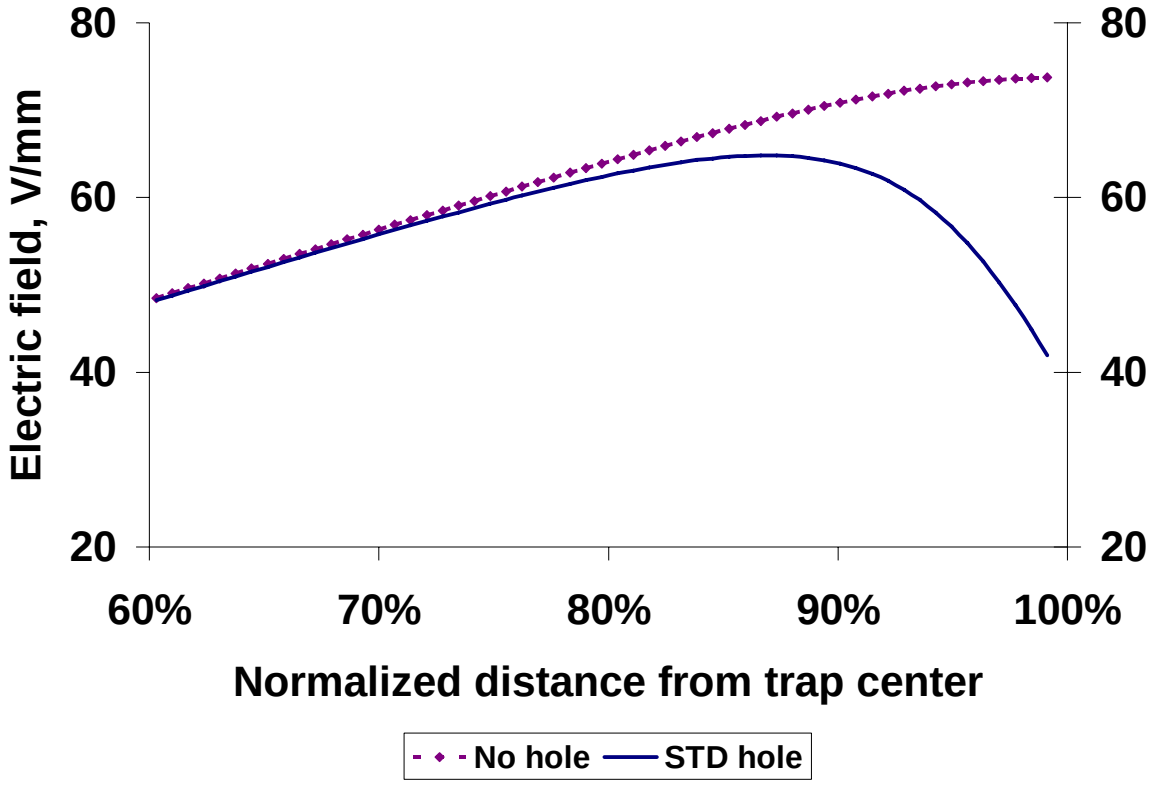

Figure 2-3. Plot of the electric field strength vs distance from the trap for theoretical (unstretched) geometry QIT. The field strength for the no hole (ideal) and the STD hole designs were compared. From the 0% to 69% away from the trap center, the field strength deviation of the STD hole was less than 1%. At 99.3%, the field fell to 43% less than that of the ideal (no hole).

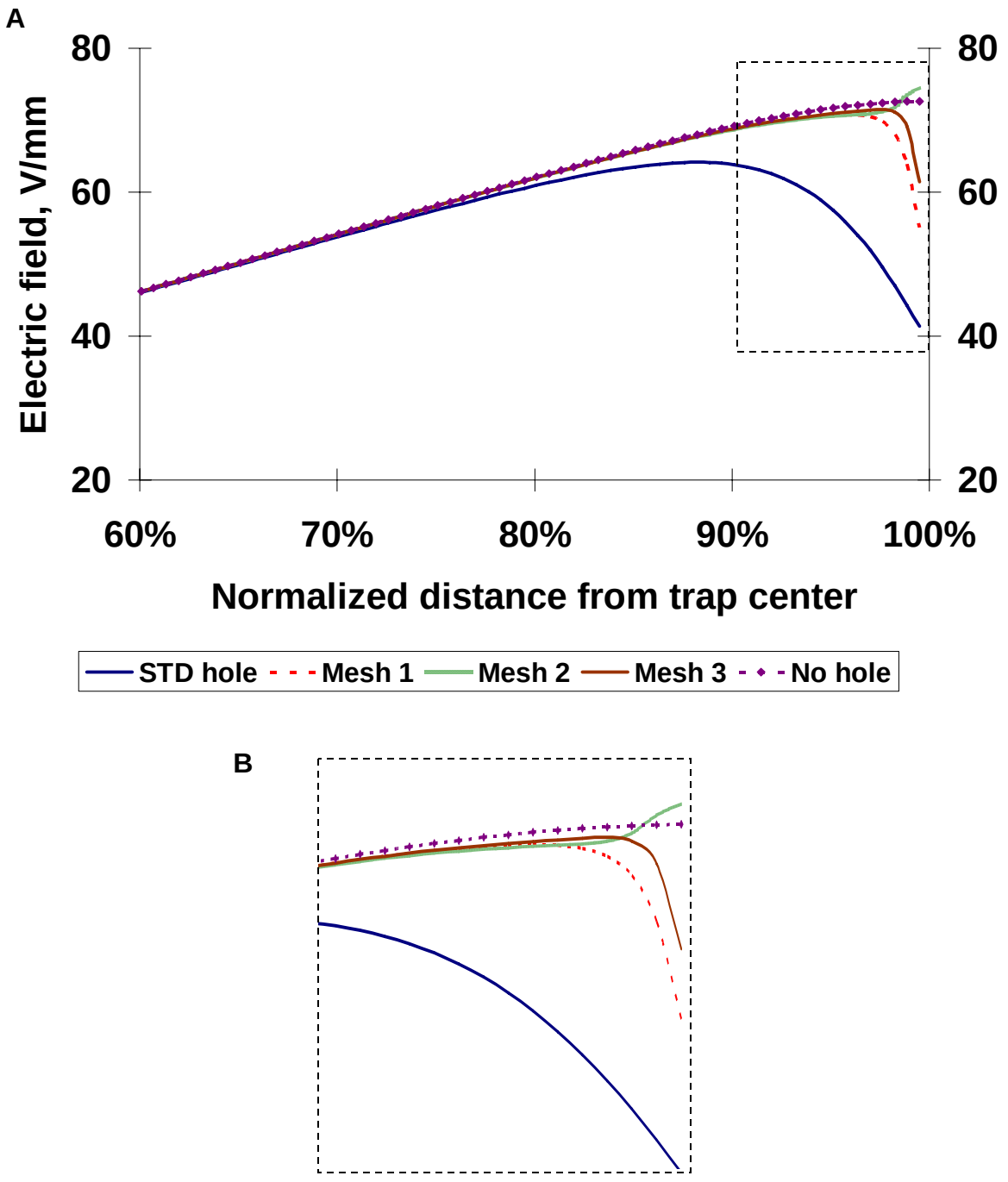

Figure 2-4. Plot of the electric field strength vs distance from the trap for the stretched geometry QIT (z_0 = 7.85 mm).with a close up of the plot (B), boxed in Figure A, to give better details on the electric field. Comparing the ideal (no hole) with the STD hole design, there was an improvement when using the stretched geometry in preserving the field strength, with the field strength deviation less than 1% from 0-79% distance from trap center. Using a mesh design, the electric field was significantly improved, bringing the field profile closer to the ideal(no hole) profile. In this case, the most significant improvement was observed with mesh 2 design.

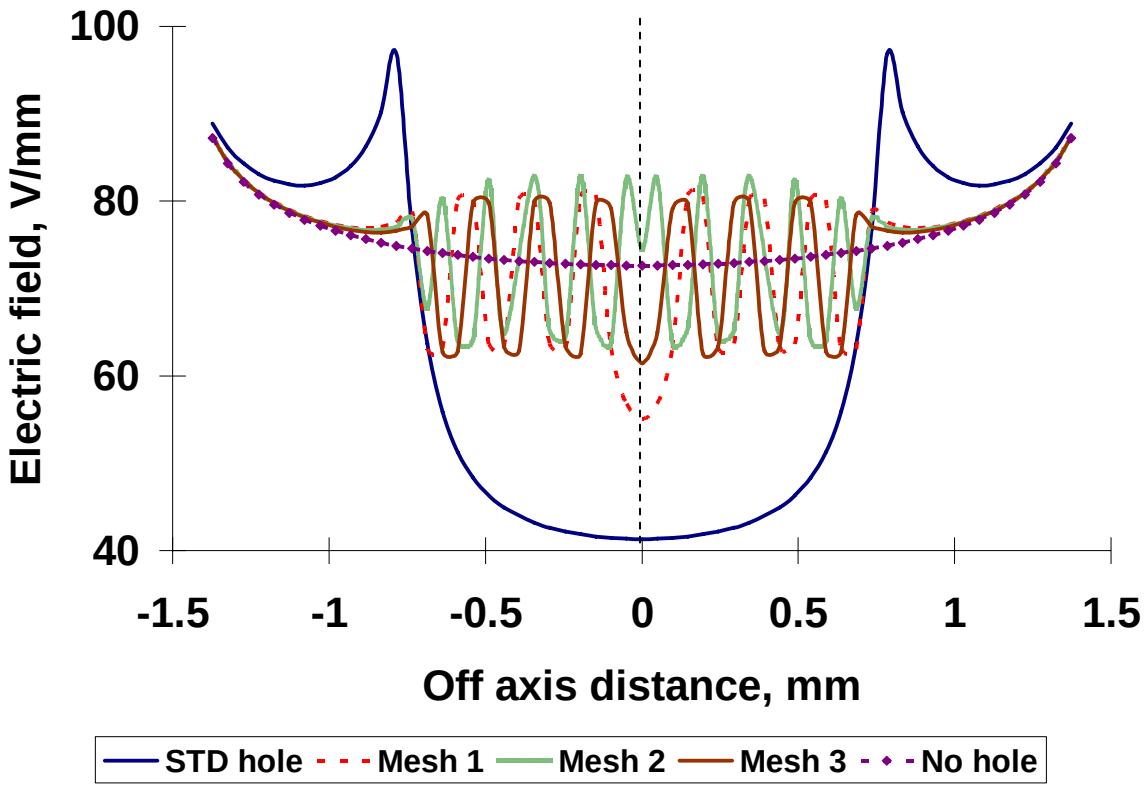

Figure 2-5. Plot of the electric field strength vs off axis distance (displacement across the hole) for the stretched geometry QIT of 0.05 mm (99.3% trap center distance) above the outermost point of the electrode.

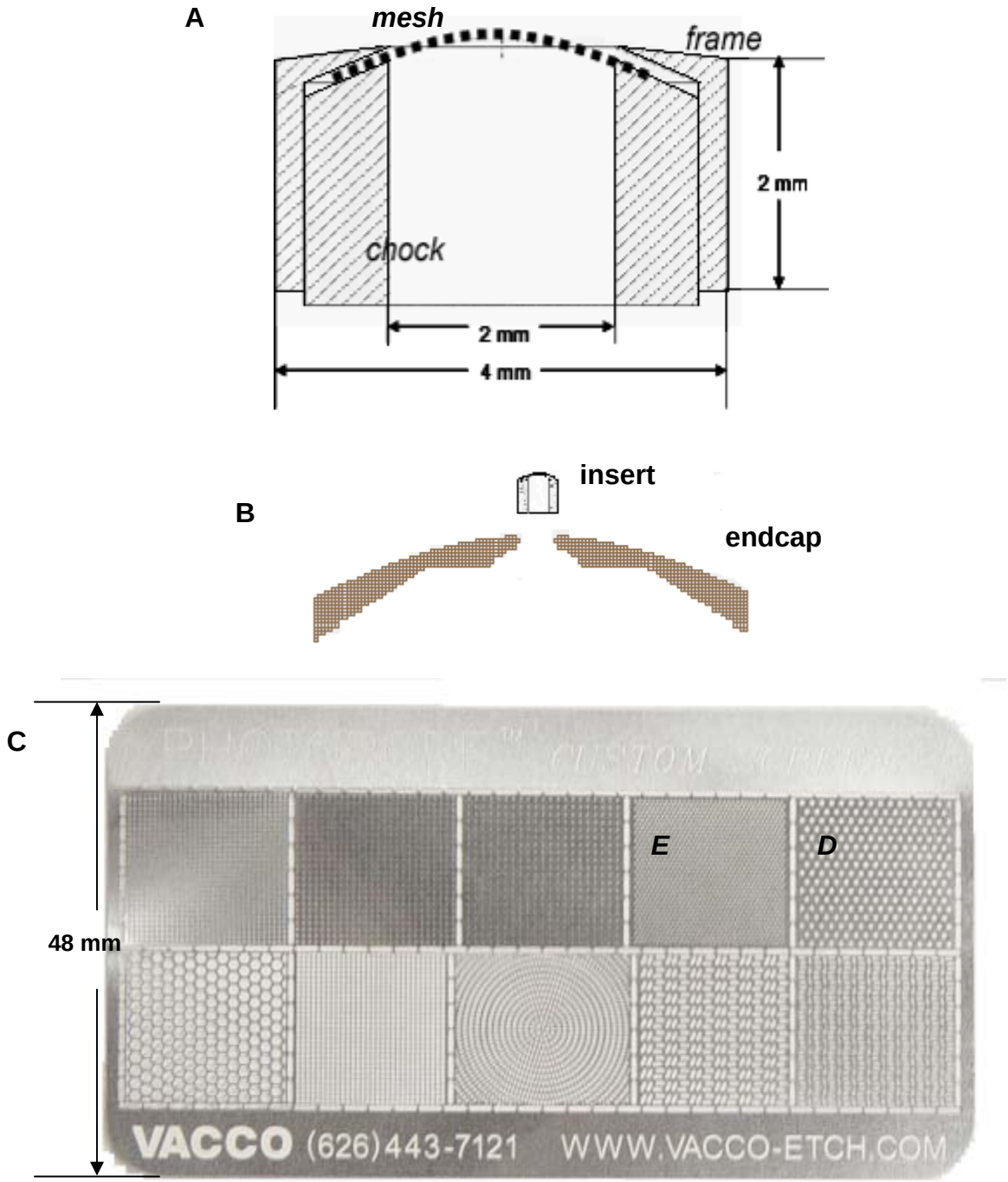

Figure 2-6. Mesh insert design, parts and materials. A) Interchangeable mesh insert design for microscreening the endcap hole. A special tool was used to cut 3 mm disks of the mesh. B) The insert is installed in the endcap hole that was drilled to size. The drawing is unscaled for emphasis. C) A commercially available sample mesh acquired from VACCO. Photochemical etching was used to create the holes for these sizes. Mesh types labeled D and E were chosen for the investigation

A

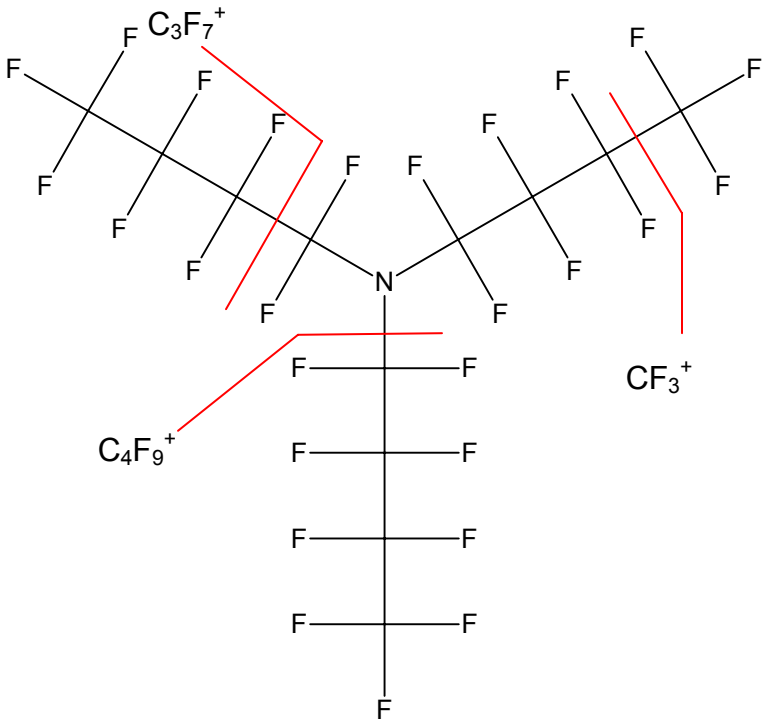

B

Chemical Formula	Exact Mass, Da
CF_3^+	68.995
$C_2F_4^+$	99.994
$C_2F_5^+$	118.992
$C_3F_5^+$	130.992
$C_3F_7^+$	168.989
$C_4F_9^+$	218.986
$C_5F_{10}N^+$	263.987
$C_8F_{16}N^+$	413.978
$C_9F_{20}N^+$	501.971
$C_{12}F_{24}N^+$	613.965
$C_{12}F_{26}N^+$	651.962

Figure 2-7. The PFTBA calibrant compound. A) Structure of perfluorotributylamine PFTBA, $(C_4F_9)_3N$, with fragment cleavages. B) Fragment ions of PFTBA and their exact masses [23].

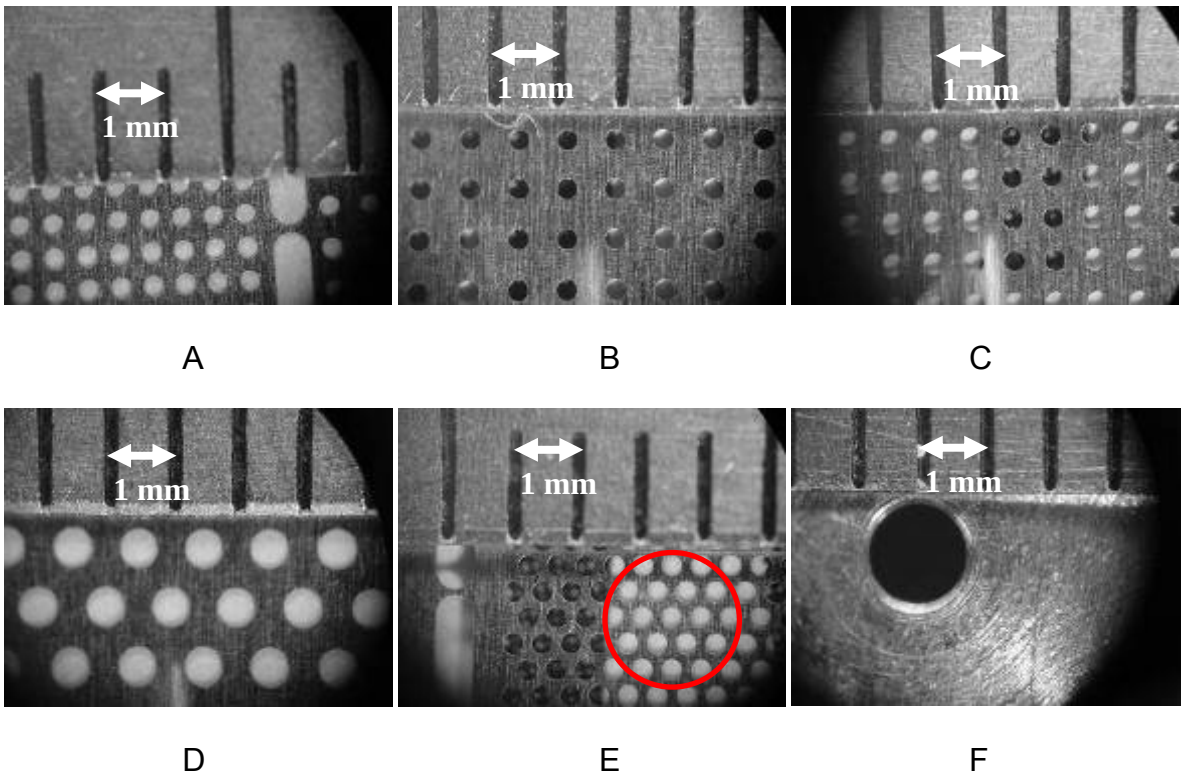

Figure 2-8. Mesh samples from Figure 2-6C under a microscope. Meshes with irregular-shaped holes were not considered. A) square spacing of 0.2 mm, hole size is 0.3 mm. B) square spacing of 0.5 mm, hole size is 0.3 mm. C) square spacing of 0.3 mm, hole size is 0.3 mm. D) hexagonal spacing of 0.4 mm, hole size is 0.6 mm. E) hexagonal spacing of 0.2 mm, hole size is 0.3 mm. The circle outline shows the 2 mm exposed area after mesh installation on the insert F) standard endcap, hole size is 1.5 mm.

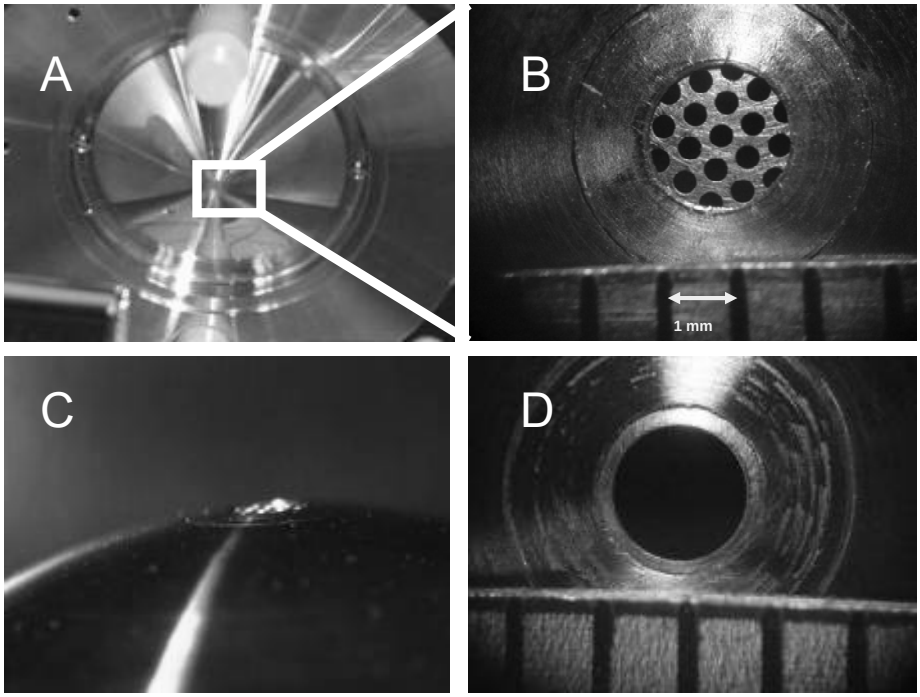

Figure 2-9. Photographs of mesh inserts. A) Mesh E installed on the modified end cap electrode. B) An endcap electrode with the microscreened holes. C) Horizontal view of the same microscreened holes. D) An insert with a 1.5 mm diameter hole (same hole size as the STD hole endcap).

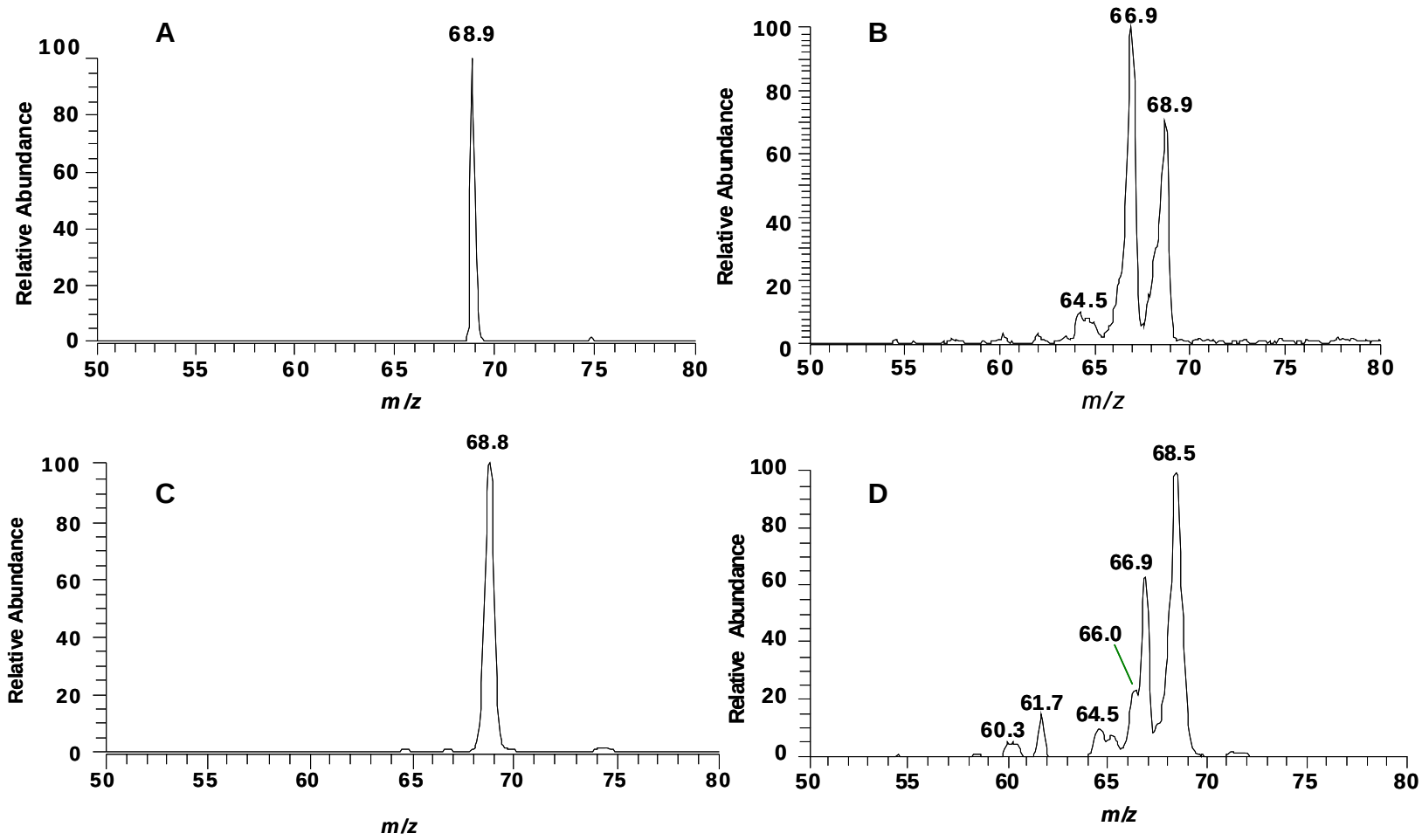

Figure 2-10. Comparison of the mass spectra of *m/z* 69 (CF_3^+), a fragment ion of PFTBA, with the standard one-hole endcap in 2 different geometries with and without the use of buffer gas. A) Stretched endcap spacing (z_0 = 7.85 mm) with buffer gas. B) Stretched endcap spacing without buffer gas. C) Theoretical endcap spacing (z_0 = 7.07 mm) with buffer gas D) Theoretical endcap spacing without buffer gas.

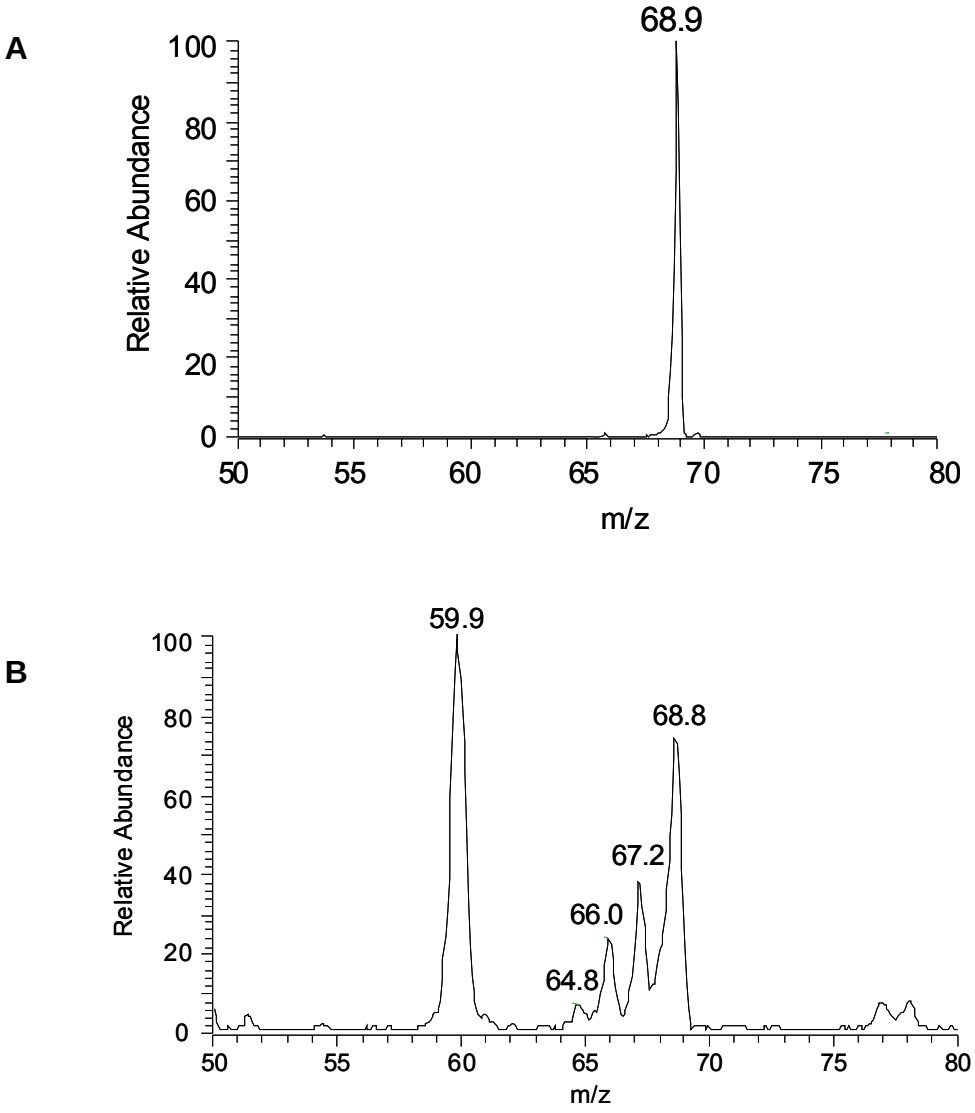

Figure 2-11. Mass spectra of PFTBA fragment ion CF_3^+ with microscreened insert (Mesh E) and theoretical geometry (z_0 = 7.07 mm). A) Experiment with buffer gas. B) Same sample after shutting off the buffer gas supply.

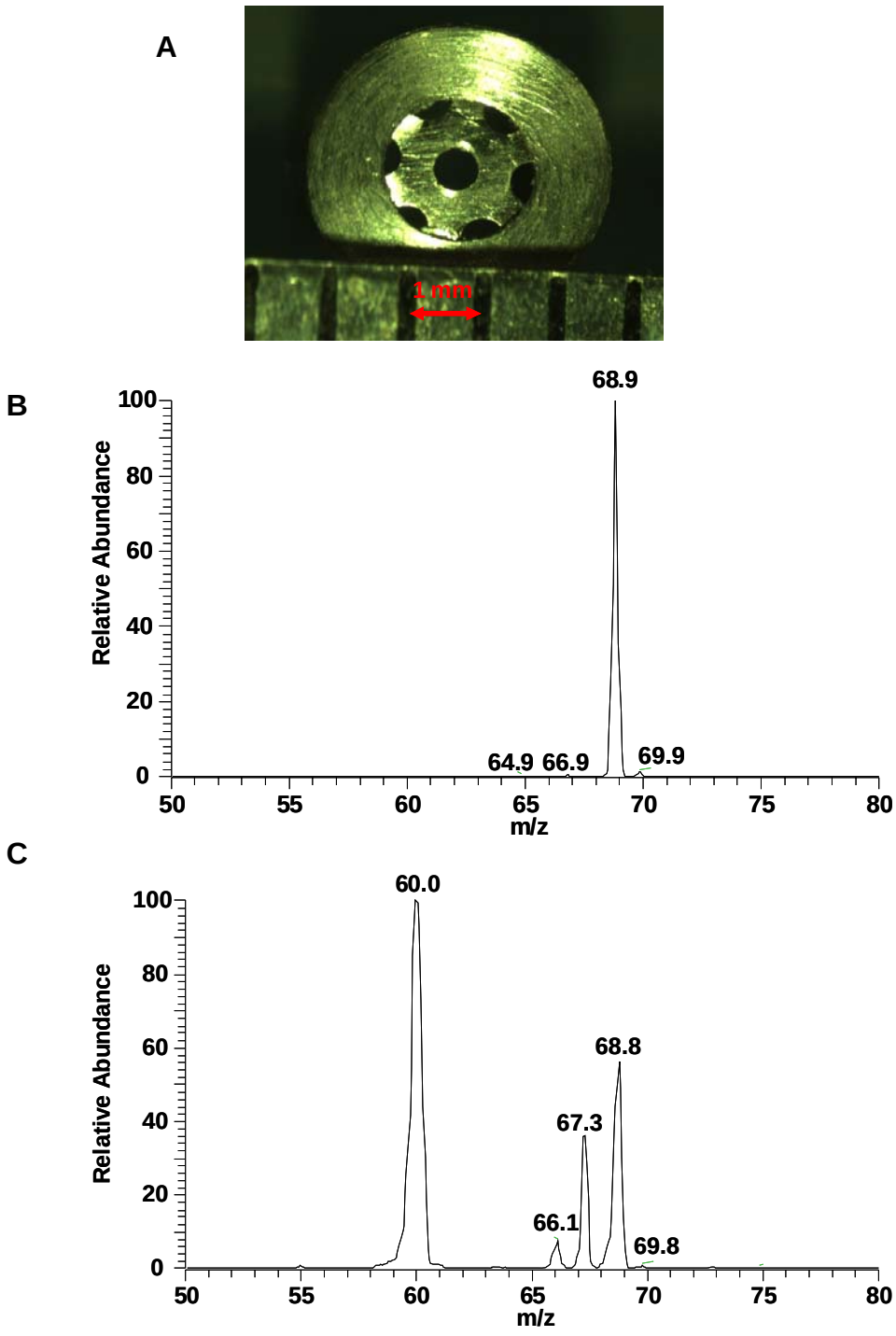

Figure 2-12. Microscreened hole (Mesh D) and results. A) The mesh insert with Mesh type D from Figure 2-8D. B) Mass spectra of PFTBA fragment ion CF_3^+ with microscreened insert (Mesh D) and theoretical geometry (z_0 = 7.07 mm). A) Experiment with buffer gas. B) Same sample after shutting off the buffer gas supply.

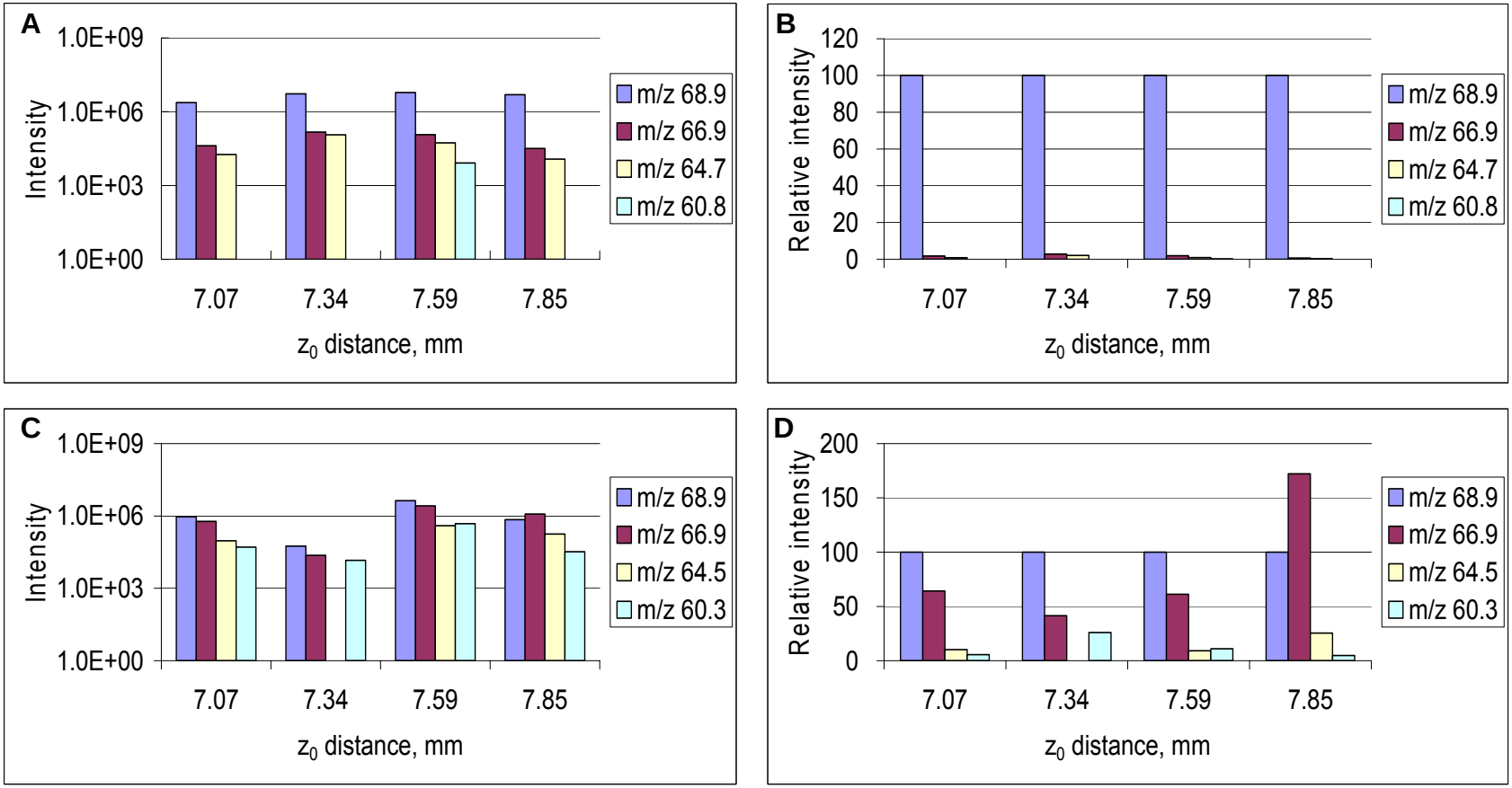

Figure 2-13. Plots of absolute ion intensities (log) and normalized intensities vs. axial distance and using standard endcaps (STD hole design) for the PFTBA fragment at *m/z* 69 and its ghost peaks. The intensities in B and D are relative to *m/z* 68.9 = 100. The peaks at *m/z* 60.3 and 60.8 are the same peak, as well as for *m/z* 64.7 and 64.5 peaks, just shifted. Plots A and B are data taken with buffer gas while plots C and D are without buffer gas.

Table 2-1.Major peaks found and their corresponding *m/z*.

m/z	q_z	q_r	β_z	β_r	Resonance equation	Higher order field
68.9	0.90164	-0.45082	0.92499	0.33310		
66.9	0.87547	-0.43774	0.83036	0.32254	$\beta_z + 1/2\beta_r = 1$	Hexapolar
66.0	0.86369	-0.43184	0.79901	0.31781	Undetermined	Undetermined
64.5	0.84406	-0.42203	0.75917	0.30997	$1/2\beta_z + 2\beta_r = 1$	Dodecapolar
60.3	0.78910	-0.39445	0.67284	0.28822	$\beta_z = 2/3$	Hexapolar

List of mass assignments for the major peaks found and their corresponding q_z and calculated resonance equations [34,41]

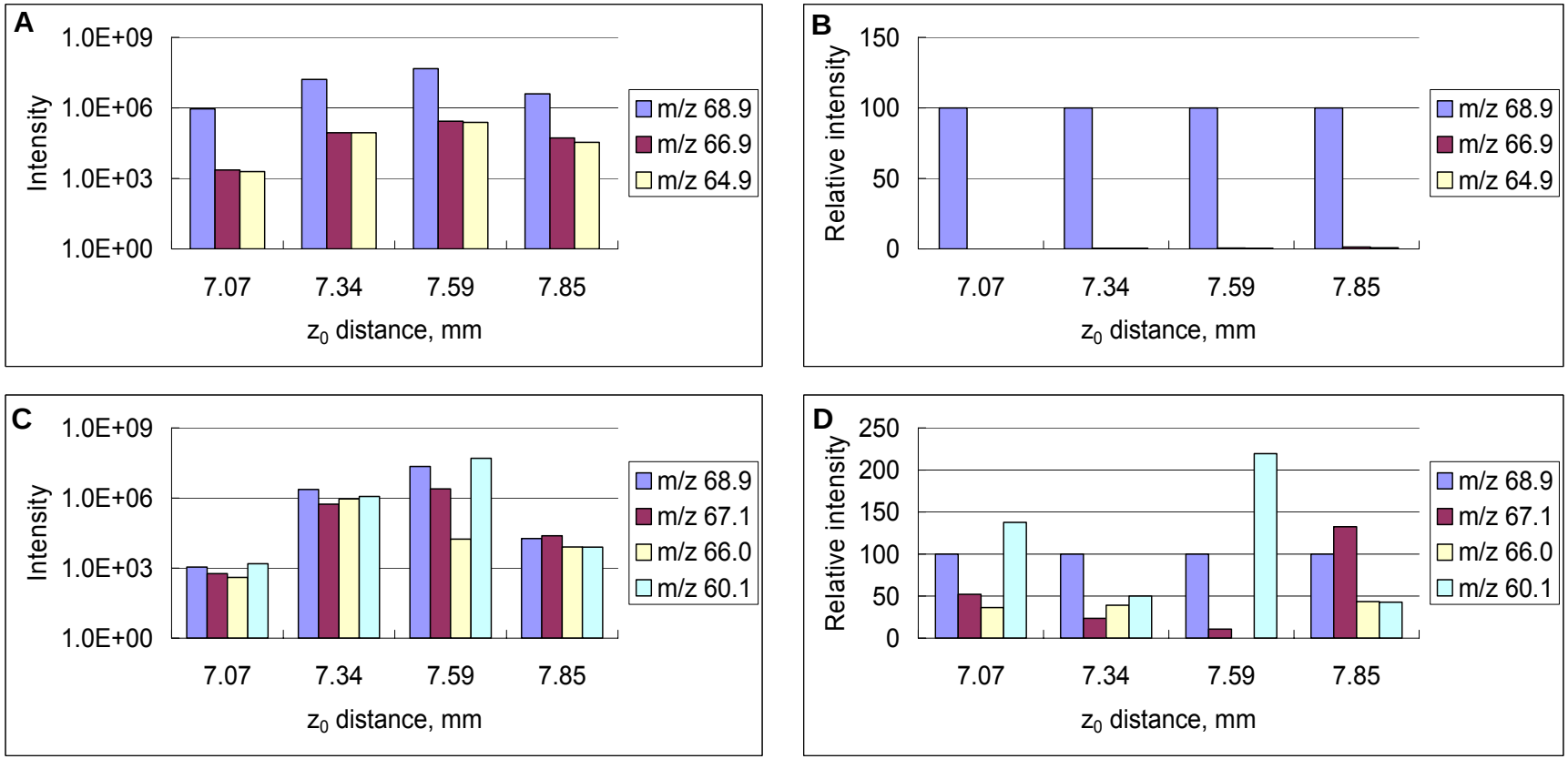

Figure 2-14. Plots of absolute ion intensities (log) and normalized intensities vs axial distance and using microscreened endcaps (Mesh E) for the PFTBA fragment at *m/z* 69 and its ghost peaks. The intensities in B and D are relative to *m/z* 68.9 = 100. Plots A and B are data taken with buffer gas while plots C and D are without buffer gas. The peaks at *m/z* 66.9 and 67.1 were identified as the same peak.

CHAPTER 3
BUFFER GAS PRESSURE TAILORING

Overview

Buffer gas in QITs cools injected ions by reducing the ions' kinetic energy, thereby enhancing trapping efficiency, and serves as the collision gas for CID in tandem mass spectrometry. However, during other events of the analytical scan, having gas inside the QIT can be disadvantageous. During the mass isolation and ejection events, fragile ions can collide with buffer gas molecules with enough kinetic energy to cause fragmentation and degrade mass resolution. Currently, commercially available QITs maintain a constant buffer gas pressure of ~1 mTorr, a compromise between efficient cooling and limiting possible fragmentation of ions.

Previous research has shown significant improvement of mass spectrometric analysis when pulsed buffer gas introduction techniques have been employed, [42-45]. but all these studies have employed single gas pulses from a single pulsed valve. This pulsed technique, however, is not used commercially due to the added costs and complexity of operation. Furthermore, precise control of buffer gas pressure cannot be achieved by a single valve alone. This chapter explores the potential of using multiple pulsed valves to tailor the buffer gas pressure during each segment of the MS scan function.

Role of Buffer Gas in Ion Trap Operation

Original Discovery

In the 1950s when Paul and Steinwedel invented the quadrupole ion trap and the quadrupole mass filter [1], the use of buffer gas was not even considered in their design. It was only in 1984, when the quadrupole ion trap was initially presented as a commercial detector for GC, that the use of buffer gas was introduced. The presence of 1 mTorr of helium in the trap was not by design, but rather the result of GC carrier gas introduced (along with the compounds

eluting from the GC column) directly into the trap with limited vacuum pumping (a 60 L/s turbo pump) to minimize the size and price of the instrument. The ability of this lightweight gas (helium or hydrogen) to enhance mass resolution and sensitivity was (unexpectedly) observed, as shown in Figure 3-1 [7,8]. At that time, the reasons behind the improvement had not been fully explained, but it was suspected that the buffer gas had a major effect on ion injection and trapping [19].

Ion Injection and Trapping Efficiency: Role of Buffer Gas

Buffer gas plays a key role in trapping ions, especially those which are created externally and injected into the trap. Before the importance of using buffer gas was established, ions were created within the cavity of the ion trap. This ion-generation technique did not allow for the flexibility of coupling ionization sources such as electrospray ionization (ESI) or matrix-assisted laser desorption ionization (MALDI). On the other hand, externally creating ions away from the ion trap prevents or reduces ion-molecule reactions inside the trap. With neutral (sample) molecules being introduced outside (rather than within) the ion trap volume, the population of neutrals inside the trap can be minimized, thereby reducing ion-molecule reactions during trapping and mass analysis steps. Several groups have looked into the fundamentals of trapping externally created ions; the general finding in those studies was that reduction of the kinetic energy of injected ions was necessary for trapping [46-49]. This kinetic energy, which is needed in order for the ions to penetrate the trap RF field, is also sufficient enough to allow them to escape. A number of collisions with a low-molecular weight gas can reduce the kinetic energy. Within a short period after ion injection, the displacement of ions collapses to the trap center. The center is where field imperfections are at a minimum, thus diminishing ion losses due to nonlinear resonances [26].

On the other hand, having a pressure of buffer gas that is too high can be detrimental to ion trap performance. The real problem as shown in Figure 3-1A, is the loss of resolution due to collisional broadening of the peak (in time) during the mass-selective instability ejection. A tight packet of ions (of a particular *m/z*) being ejected toward the detector can experience collisions, delaying the ejection time and resulting in peak broadening [50].

Another reason for peak broadening is ion fragility, which has been previously reported to be a cause of mass shifts [23,51-53]. As the name suggests, fragile ions tend to dissociate easily into fragment ions. Ion fragility becomes more problematic in ion trap mass spectrometry during resonant ejection, when the fragile ions approach the border of the stability diagram. The ions gain kinetic energy, experience more energetic collisions with the buffer gas, and if fragile, can dissociate into fragment ions prior to ejection. The fragment ions are already beyond the border of the stability diagram and thus will be ejected earlier than the fragile parent ion. The resulting effect on the mass spectrum is peak fronting or mass shift to lower apparent mass, which is intensified with the increase in the resonance voltage amplitude [53]. Ion fragility can also lead to ion losses during mass isolation for MS/MS.

Studies using gases other than helium as a buffer gas have been conducted. The addition of small amounts of heavy target gases (neon, argon, krypton or xenon) to the helium buffer gas improves trapping efficiency of cesium iodide cluster ions of high mass-to-charge ratio as well as improving performance in collision-induced dissociation [54]. Other researchers have attempted to replace helium entirely with air or argon as a buffer gas. The use of heavier gases was found to improve sensitivity and collision-induced dissociation efficiency at the expense of mass resolution [55].

Collision-Induced Dissociation: Role of Buffer Gas

Another aspect of QIT MS that highlights the importance of buffer gas is tandem MS, wherein structures of ions can be further elucidated by fragmentation using collision-induced dissociation [56]. The technique involves isolation of mass-selected ions after ionization, and resonant excitation of those ions via the application of a supplementary sinusoidal potential across the endcaps. This potential, which is called the resonant excitation or tickle voltage, has a frequency that is tuned to the selected ion's fundamental secular frequency. The amplitude of the tickle voltage is small enough just to move the ions away from the trap center but not to be ejected. In this way the ions acquire kinetic energy from the RF drive potential and collide with neutral buffer gas. The resulting collisions, if energetic enough, produce fragment ions, which are trapped and then analyzed in the detection step. Effective fragmentation requires both the use of a buffer gas and application of the tickle voltage, as shown in Figure 3-2. Since it is straightforward to optimize the tickle voltage, there have been a few attempts to optimize the buffer gas pressure for higher CID efficiency. Furthermore, the optimum pressure for CID is limited to a few mTorr because higher pressures during other events in the scan function can compromise mass resolution and sensitivity [23].

Another disadvantage of higher buffer gas pressures for CID is lower internal energy deposition, which becomes a problem for CID experiments of larger m/z ions of biomolecules [50]. Higher m/z ions typically require greater energy deposition to induce fragmentation, which is difficult to achieve at higher pressures. Increased buffer gas pressure lowers the distance of travel before a collision can occur, thereby lowering the number of energetic collisions. While it is practical to use the existing buffer gas as the CID gas, some studies have shown advantages of using gases heavier than helium for more effective fragmentation [43]. Typically, CID is carried out at q_z values between 0.2 and 0.6 for high fragmentation efficiency [54,56].

Fragmentation of higher mass ions, such as a peptide ions, is often performed at lower q_z values in order to trap the parent ions and observe lower *m/z* fragment ions, but at the expense of lower excitation energy. A study showed that peptide ion CID fragmentation efficiency was increased when heavy gases, such as argon and xenon, were introduced via a pulsed valve during CID [43]. It was also noted that the use of a pulsed valve for CID gas delivery was important to avoid negative impact of heavy gases as buffer gas during other periods in the ion trap scan function.

Reagent Gas: Use of Pulsed Valves

Applications for reagent gases introduced directly into the ion trap for targeted ion-molecule reactions have been reported; these applications take advantages of the QIT's ability to isolate analyte ions and serve as a reaction chamber for gas-phase reactions [57,58]. Pulsed introduction of reagent gas into a QIT was reported by Emary as a method for enhancing control over reactions occurring inside the trap [45]. Unwanted ions can be removed by using mass-isolation techniques, but elimination of neutral molecules required a different approach. Neutrals can only be eliminated by the pumping action of the high vacuum pump. In their investigation to locate the positions of carbon-carbon double bonds in alkenes, ionized alkenes were isolated prior to injecting neutral reagents. In this way, ion-molecule reactions were more controlled and therefore, reduced product ion complexity [59]. Another application is the differentiation of enantiomers within the QIT by mass-selecting chiral reactant ions and generating Diels-Alder reaction products [60]. Although it was reported to be inconclusive of enhanced chiral selectivity, the importance of having reproducible means of injecting neutral reagents into the trap was pointed out as well as consideration for increased pressure in the QIT.

For all of the different roles of gases in the ion trap, a common theme is that different events in the scan function would require different pressure (or even different gases). The continuous introduction of gases, particularly buffer gas, is a compromise between the

requirements of trapping and detection. Moving to a more dynamic approach would permit optimization of the pressures for the individual events in the scan function. The tailoring of buffer gas pressure is proposed to maximize the efficiency of each event in the analytical scan.

Pressure Tailoring Concept

A typical scan function for obtaining a full mass spectrum with the ion trap mass spectrometer, also known as the timing diagram, has been described in Chapter 1. As shown in Figure 3-3, the simplified scan function includes 4 events: pre-injection , injection , post-injection , and detection events. The major timed components are also listed. Another timed parameter, buffer gas pressure, has been added to the scan function in this Figure. This proposed parameter can be treated like a potential that can be turned "on" and "off". It can be anticipated that the time constant for the buffer gas pressure will be longer for than an electric potential, as the rate of pressure changes will be limited by "impedances" such as limited conductance into and out of the ion trap, limited pumping speed and response time for opening and closing the pulsed valve.

When ions are created externally and then injected into the trap, they must be injected with enough kinetic energy to penetrate the RF field within the QIT. Once inside the trap, however, the ions need to be slowed down in order for them to be successfully trapped. During ion injection, therefore, the presence of buffer gas inside the QIT is critical to effectively reduce the ions' axial and radial motion by collisional cooling; thus the buffer gas must be turned "on" for this event, as shown in Figure 3-3. At the post-injection event, buffer gas is turned "off" and a delay time is added to pump away the buffer gas before detection. In the detection event where the ions are sequentially ejected from the QIT, buffer gas presence is not needed and can even be detrimental to the analysis because collisions with gas molecules can promote fragmentation of fragile ions during mass-selective ejection, affecting mass resolution and mass assignment

[51]. Thus, it is kept turned off until the next scan. Clearly, there are potential advantages to having buffer gas present during some portions of the scan function and absent during others.

A typical MS/MS with CID scan function has the same events as the full MS scan function, plus additional events for mass isolation and CID after ion injection and cooling. Thus, the buffer gas pressure parameter could be adjusted accordingly (Figure 3-4). The post-injection event (C) for the MS/MS CID scan function has three steps in addition to cooling the injected ions, (C_1): isolation (C_2) and excitation (C_3) of precursor ions for fragmentation, and then (C_4) cooling the fragment ions before scanning them out for detection. For collision-induced dissociation and cooling (C_3 and C_4), the buffer gas pressure is raised then lowered prior to detection.

Previous studies in our laboratory have investigated the effects of pulsed introduction of buffer gas on ion storage and detection efficiencies in a QIT [44]. These studies determined strategic points within the scan function where the presence of buffer gas is important, and monitored the effects on ion signal intensity as the presence and pressure of buffer gas were varied. These previous experiments have all been performed on ion trap systems using internal ionization. They demonstrated that a higher ion signal can be obtained by using the pulsed introduction of buffer gas as compared to operation at a constant pressure. However, with a single pulsed valve, control of the pressure and pulse duration is limited to the supply pressure applied to the pulsed valve and the valve open time. There are several limitations to this approach, as discussed below.

First, the amount of gas that can be delivered will be limited by the supply flow. The valve has only two states, open and closed, wherein only two levels of buffer gas flow can be achieved. Secondly, the amount of gas delivered is not proportional to the valve open time, because of the

pressure build-up during the times when the valve is closed. As a result, the longer the valve is opened, the higher the apex of the gas pulse instead of having a longer gas pulse of the same height [61].

The gas pressure profile from the pulsed valve has similarities to a sinusoidal peak, and in concept could be combined with other peaks to produce another gas profile. This method is similar to combining multiple sinusoidal waveforms to form a square wave. Figure 3-5 illustrates this concept, using two pulsed gas profiles from different sources of varying supply pressures, which are then combined to produce a new profile. For example, valve 1 outputs a single gas pulse (Figure 3-5A) while valve 2 is opened twice to produce a gas profile that has two smaller peaks, one before and one after the first peak with a particular interval between (Figure 3-5B). Summing both valves' profiles will produce a new profile (Figure 3-5C) that is only attainable by combination of two valves. The dotted lines in Figure 3-5C shows the outline of the intended gas profile. The various combinations can provide the means to tailor the buffer gas pressure with more flexibility than employing just a single valve.

Experimental Section

The quadrupole ion trap used for this study was a research-grade QIT (nicknamed SweetP) with a customized differentially pumped vacuum chamber and controlled with Finnigan GCQ electronics, as shown in Figure 3-6. For clarity, Figure 3-6 shows only one valve installed. A second valve was installed in the same manner. The pulsed valves used were 3-Way High Performance Series 9 from General Valve (Fairfield, NJ) with an orifice of 0.060". The pulsed valve has three connections: a common input to which the gas supply is connected, and two outputs between which the valve switches during open and closed states.

There were two different connections to the common (C_{in}) input arranged during the course of the research. The first pulsed valve's common input was connected to the same supply as the

continuous helium buffer gas supply. Shutoff valves leading to the continuous and the first pulsed valve lines were installed to select the supplies without venting. For example, during instrument calibration and tuning, a continuous supply of helium is needed. This supply passes through a 1/16" i.d. stainless steel tubing and is inserted into the vacuum chamber through a 1/8" bored-through Swagelok (Solon, OH) O-seal connector. This supply input flow was regulated using a pressure regulator valve (Porter Instruments Company, Hartfield, PA) connected to a capillary restrictor. The second valve's C_{in} was connected to a helium gas tank with 1/8" i.d. stainless steel tubing and with a Granville-Philips (Boulder, CO) Series 203 variable leak valvel; the He supply pressure was controlled with a Matheson (Montgomeryville, PA) 2-stage pressure regulator on the cylinder.

The normally closed (NC) outputs for the pulsed valves were also connected to the ion traps with different configurations. As shown in Figure 3-6B, the continuous buffer gas supply is typically connected through the outer edge of an endcap where there is a 1/16" hole leading to one side of the hyperbolic surface. Thus, the first valve was connected in the same way, but using a 2.5" x 1/8" i.d. Teflon tube with a stainless steel adapter. The second valve's NC was connected to the ion trap using a 2.5" x 1/4" i.d. Teflon tube, which is anchored by a PEEK adapter (1/8" i.d.) and mounted in a hole bored into a Delrin endcap spacer. This later configuration was also implemented on the first valve during the multi-pulse experiments.

Unless specified otherwise, both valves' normally-open (NO) outputs were connected together and coupled to an Alcatel mechanical pump with 1/8" i.d. stainless steel tubing passing through a welded 1/4" bored-through connector on the flange on the vacuum chamber; the flow rate to the pump was regulated by a Granville-Philips variable leak valve. In this manner, the amount of buffer gas could be controlled by varying the setting on the variable leak valve.

The Custom Tune software (Thermo, San Jose, CA) was used to allow software control of the transistor-transistor logic (TTL) signal generated by the GCQ processor. This TTL signal, taken from the GCQ main board U68 pin#, was sent to the trigger input of an SRS Model DS345 (Sunnyvale, CA) function generator, in which a customized waveform allowed for setting the multiplier warm-up time (2 ms) and ramp time (1 ms), ion/detect time was calculated to be 10.3 ms. To help the reader understand better, the ion/detect event could be treated similar to a sampling window that is used when measuring waveform signals, and ion/detect time is the sampling resolution. The concept is that the gas pulse has the same temporal profile for each repetition, and since it is periodic, by shifting t_{delay} sequentially across the gas profile one can sample the pulsed gas profile by monitoring the product of the charge-exchange reaction, in this case, the N_2^+ ion at *m/z* 28 (Figure 3-7B). The series of data were then extracted from the files and plotted in Excel for the reconstruction of the gas profile. Post scan times were lengthened to 1000 ms to ensure no carry over of pulsed gas between scans.

Pulsed Helium Buffer Gas Effects

In this series of experiments, evaluation of the ability of the pulsed valve system to create different gas profiles for use of helium as buffer gas was carried out. The PFTBA fragment ion, CF_3^+ at *m/z* 69, was selected due to its stability and its ready formation in EI. The effects of the pulsed He buffer gas on the intensity of injected CF_3^+ ions (without He, the ions are not efficiently trapped; see Figure 3-1B) was monitored. Another target was to create new gas profiles from synchronized operation of the two pulsed valves. Individual valve gas profiles, as well as combined gas profiles, were monitored similar to the Ar^+/N_2 charge-exchange experimental method.

For these experiments, two pulsed valves were used with two different helium gas supplies. The first valve's supply was from a helium gas tank controlled by a pressure regulator

(Porter Instruments Company, Hartfield, PA) followed by a 6" long fused silica capillary (0.050 mm i.d.). The second valve's supply was from another helium tank via a Granville Philips variable leak valve (GP). Both valves' NC outputs were connected to the ion trap via 2.5" x 1/4" i.d. Teflon tubing through holes drilled in the endcap spacers with PEEK adapters. Both valves' NO outputs were connected together inside the vacuum chamber using 1/8" copper tubing and a Tee union, and then connected to a mechanical pump outside the vacuum chamber via another Granville Philips variable leak valve (GL).

Each valve had its own triggering circuit, composed of an SRS function generator that was coupled with a custom-built amplifier. This arrangement was used to that each valve could be operated independently, in terms of timing and pulse width. The general settings for the function generators were as follows: mode = arbitrary/burst mode with point value format, amplitude = 10 V peak to peak, frequency = 10 kHz, trigger mode =positive in (triggers on the rising edge). With these settings, pulse widths in increments of 0.1 ms with an amplitude of 5 $V_{0\text{-}p}$ could be created (data point values 1000 is equivalent to 5 V).

Pressure Effects on Fragile Ions

The benefit of using buffer gas pressure tailoring is most evident in the analysis of fragile ions. N-butylbenzene (*m/z* 134) has been reported to produce fragile ions [51,53]. It was purchased from Sigma Aldrich (St. Louis, MO) and was chosen to monitor the behavior of fragile ions in terms of both intensity and mass shifts when using pulsed helium buffer gas. Static pressure effects were investigated by increasing the head pressure of the static buffer gas supply. For the pulsed valve experiment, the first valve was used with helium supply (2.5 psi head pressure, from the continuous buffer gas supply) and the peak signal intensity and mass shift were monitored.

Results and Discussion

An important aspect of using the pulsed valve system was to evaluate the valve performance in terms of its ability to produce a gas peak. A single scan time for the ion trap MS from the pre-ionization to post-scan events is around 150 ms from *m/z* 50-650 scan range, as observed in the SweetP QIT. The events where gas is required (ion injection and cooling) typically have durations from 1-25 ms. On the other hand, the duration of the events where gas is not needed (ion ejection and detection) is approximately 100 ms. From these times, the ideal gas pulse width is seen to be approximately 10-30 ms FWHM (matching the maximum ion injection time) in order to be used practically in MS experiments. For example, in detecting a typical chromatographic peak with a peak width of 1 s, having a 150 ms scan duration would give 6 data points across the peak. Increasing the scan duration would lower the number of data points and thus result in a loss of resolution for the chromatographic peak.

Optimization of the Gas Pulse Profile

The Ar/N_2 charge-exchange reaction was used for the experiments to characterize the output of a single pulsed valve. Initial configuration of the pulsed valve was with the NO output capped with an SS plug, thus converting the 3-way into a 2-way pulsed valve. The NC output was connected to the trap via the same entrance used for the static buffer gas, i.e. through one of the endcaps. The continuous helium gas supply line leading to the ion trap was split with a tee union and connected with shut-off valves, which enabled it to be connected to the pulsed valve and to the ion trap at the same time. With the shut-off valve configuration, the continuous supply and pulsed supply could be used independently, while sharing the same source. Initially, a nitrogen gas tank was connected as the source, but even with the lowest setting on the pressure regulator(0.5 psi), neither ion signal for N_2^+ nor Ar^+ was obtained, leading to the conclusion that nitrogen gas at least at the pressures used was not a suitable buffer gas. As noted previously, N_2

and other more massive buffer gases are not commonly used with QITs. To overcome this problem, residual nitrogen (< 0.01%) in the helium gas supply was monitored instead. The advantage of using residual N_2 in the helium buffer gas was it provided a low-mass buffer gas (He) plus the target charge-exchange gas (N_2). This may have also allowed a lower pressure of N_2 in the trap when compared with using pure N_2, even at the lowest head pressure setting.

Mass spectra for the residual N_2^+ ion were obtained and the peak width of the pulsed gas as affected by the head pressure of the pulsed valve is shown in Figure 3-8A. As the Figure showed, control of the head pressure only did not reduce the peakwidth significantly, with the average FWHM peakwidths at > 100 ms. The absolute intensities for the 5, 2.5 and 1.5 psi peaks at 100% peak height were $3.1x10^6$, $2.5x10^6$ and $3.4x10^6$ counts, respectively.

The next setup that was attempted to shorten the peakwidth was to unplug the NO output and let the gas supplied to the valve during the closed valve states be discarded into the vacuum chamber (the right hand chamber in Figure 3-6). This setup was designed to reduce the pressure behind the poppet of the pulsed valve. However, the continuous leak of He from the NO output raised the overall trap chamber pressure to > $1x10^{-5}$ Torr. Therefore, the gas supply connection was changed to helium gas supply with a variable leak valve in front of the fused silica restriction (head pressure set to 2.5 psi) for finer control of the supply pressure.

Data for this experimental setup are shown in Figure 3-8B. Having the NO output uncapped did not allow the pulse valve to build up enough backing pressure, thus explaining the slower rise times (70 ms to reach 100% ion intensity as compared to 10 ms from the previous setup) of the gas pulse. Another reason for the slower rise time was the impedance brought about by the small diameter orifice used by the continuous supply to put buffer gas inside the trap (Figure 3-6B). It was also noted that the signal intensity for the pulsed N_2^+ was only 1.5x higher

than the baseline signal of N_2^+ (from the N2 from the NO output into the chamber). The setting on the variable leak valve could not be increased too high as it would raise the overall trap chamber pressure too high, which would pose a problem for the turbo pumps. It was concluded from these initial experiments that as a compromise, a restriction between the NO output and a vacuum source would provide for better control of the gas pressure behind the valve.

The following changes were therefore made to the valve setup: 1) connecting the gas supply to the valve C_{in} inlet via a variable leak valve with no capillary restrictor in between, 2) connecting the NO valve output via another leak valve to a mechanical pump instead of dumping into the vacuum chamber, and 3) increasing the conductance of the connecting tubing between the valve and the ion trap. The previous tubing (2.5"x1/8" i.d. that was connected to a 1/16" hole through the endcap (refer to Figure 3-6B for the location) was replaced with Teflon tubing that was 2.5" long with an i.d. of 1/4". As shown in Figure 3-6B, a hole was drilled into the one of endcap spacers and a PEEK tube with screw threads was attached to the hole in order to accommodate the larger diameter tube. Using a larger diameter tube should increase the conductance of the pulsed gas inlet and thereby decrease the rise times. Figure 3-8C shows the data with the preliminary settings of this setup. The parameter GP is the setting for the inflow leak valve and GL is the setting for the outflow leak valve. Notice that with less supply flow and more leak flow (GP 30, GL 100) the pulse profile signal did not rise much from the baseline signal. On the other hand, decreasing the outflow restriction improves the pulse profile rise time. After evaluating several combinations for both settings, it was concluded that the smallest pulse width achieved was ~100 ms FWHM, with GP setting of 40 and GL setting of 200.

Until the gas pulse profile can be reduced to around 10 ms, which is the average cooling time and excitation time for CID, the pulsed valve system can only be used for limited research

applications. The ion trap scan function can be adjusted to accommodate time intervals suited for the current gas pulse width, but scan times will be longer by 500 ms more, which is not practical for applications such as LC-MS or GC-MS experiments where faster scan rates are needed to get better chromatographic data. Nevertheless, the current setup permits proof-of-principle demonstration of pressure tailoring.

Multi-Pulse Experiments

Experiments were performed to investigate the reproducibility of the gas pulses within 100 ms and determine if the gas pulses from a valve could be added. The experimental setup was similar to that of the single pulse experiment; multiple pulses from the same valve were used in the scan function. Signal intensity of the PFTBA fragment ion at *m/z* 69 was monitored versus delay time, as this will show the intensity as a function of the amount of pulsed gas. As shown in Figure 3-9, the function generator was configured to produce two pulses, with the second pulse 70 ms after the first one. Experimental data from a single pulse experiment were used to create a projected two-pulse profile and plotted to compare with the experimental data for two pulses. It can be concluded from the agreement between these two plots that two pulses for a single valve provide the pressure one would expect. The next step in the development was to implement control of two independent pulsed valves.

The results from the two-valve experiment are shown in Figure 3-10. The two pulsed valves were triggered simultaneously or with 100 ms delay between them. The CF_3^+ ion profile was measured in separate experiments for each valve; those profiles were summed to generate the projected profile to compare the data when both valves were triggered. The trigger pulse from the MS was connected to two function generators. The first valve's supply head pressure was set to 2.5 psi. For the second valve's supply settings were set to GP= 40 and GL=200 with a head pressure of 10 psi. The delay time for opening each pulsed valve was adjusted with its

function generator. Each data point in the profile was an average of 30 scans. Post scan time was reduced from 1000 ms to 500 ms to speed up data gathering.

For the data in Figure 3-10A, both valves were triggered at time 0 ms. The profiles for each valve are plotted as well as the projected profile (sum of the CF_3^+ ions of two valves) for comparison. The intensity for the experimental data was ~25% lower than the projected profile. This is readily explained by recalling the effect of buffer gas pressure on ion intensity shown in Figure 3-1B. At lower buffer gas pressures, the signal intensity increases approximately linearly with increasing buffer gas pressure. However, at higher pressures, the increase in the signal intensity drops and eventually the signal reaches a maximum.

In Figure 3-10B, a delay of 100 ms was set for the 1st valve relative to the timing of the 2nd valve. Again individual profiles for each valve as well as the projected profile were plotted with the experimental profile. The experimental profile has good agreement with the projected profile. With the delay of 100 ms, most of the gas from the 2nd valve was already pumped away and thus, the pressure contributed by both valves remains in the linear range for ion intensity in Figure 3-1B.

Pressure Effects on Fragile Ions

For this study, the M+ ion of n-butylbenzene (*m/z* 134) was chosen as a model since it has been studied previously and classified as a fragile ion [51]. The SweetP QIT was set to the commercial configuration (standard endcaps and z_0 = 7.85 mm) and calibrated using PFTBA under normal buffer gas conditions. The analyte was put into a 1/8" i.d.x 3" long glass tube and the vapor headspace was admitted into the ion source via a Granville-Philips Series 203 variable leak valve to yield ion gauge pressures of $5x10^{-6}$ to $1x10^{-5}$ Torr. All data points in the graphs were averaged from 100 scans.

Zoom scan mode [62]was used to take the mass spectra. Zoom scan is defined as a method of taking mass spectral data with slower mass scan rates, thus having more data points defining the mass peaks, resulting in higher mass resolution.. The normal mass scan rate of the GCQ is 0.180 ms/ amu, whereas in the zoom scan mode, the scan rate is slowed down ten times to 1.8 ms/amu. The zoom scan method is not an inherent function in the GCQ tune software, but the Custom Tune software has advanced feature controls to change the mass scan rates. Furthermore, the mass assignments in the spectra needed to be calibrated after the data were taken, as the default mass calibration was done with different conditions.

Figure 3-11A shows the effects of variation of helium buffer static gas pressure on signal intensity and shift of mass assignment of the n-butylbenzene M^+ ion. As shown in Figure 3-1A, the signal intensity increases as more buffer gas is available in the QIT for higher trapping efficiency. But it was also observed that at higher pressures of buffer gas, the mass assignment shifted downward as collisions with buffer gas led to increased dissociation of the fragile ion and thus earlier ejection of fragment ions. The mass spectrum of n-butylbenzene is shown with its major fragment ion at *m/z* 91 in Figure 3-11B. In this case, the mass shift is slightly toward the left, as buffer gas pressure was at adequate levels.

Figure 3-12 shows the effect of pulsed buffer gas during the detection event in the scan function. Cooling time is defined as the length of time after ion injection and before the RF amplitude is ramped for detection. Post scan time is defined as the length of time after the end of the RF amplitude ramp before the start of the next scan function. In these experiments, the first pulsed valve was used and operated with a pulse width of 1.9 ms. The helium head pressure behind the valve was set to 2.5 psi. Each data point was an average of 30 scans. The ion injection time was fixed to 1 ms.

The conditions for the data in Figure 3-12A were set to have buffer gas present during both the ion injection and the detection event in the scan function. The cooling time was set to 1 ms and the post scan time was set to 1000 ms to ensure that the pulsed gas for each scan did not carry over to the next scan. It was observed that the *m/z* 134 ion intensity profile followed the pulse gas profile; in contrast, the mass shift decreased at longer delay times as the amount of buffer gas during detection event decreased. In Figure 3-12B, the cooling time was set to 1000 ms, which allowed the buffer gas that was introduced during injection to be pumped away before starting the detection event. Results showed that there was minimal mass shift of the n-butylbenzene ion, even at the highest buffer gas level (indicated by the signal intensity profile).

These findings confirm that the buffer gas is needed during ion injection in order to efficiently trap injected ions, while the presence of buffer gas during ion detection can affect analysis of fragile ions and cause mass shifts. Implementing a pulsed valve system allows the gas pressure to be tailored for different events in the scan function. Unfortunately, the current pulsed valve system does not provide a narrow enough buffer gas pulse to tailor the pressure without adding delays in the scan function.

Summary and Conclusions

The potential of tailoring buffer gas pressure with the use of multiple pulsed valves has been demonstrated. Buffer gas, when introduced at the right point in the scan function, can enhance the trapping of injected ions, as well as increasing the fragmentation efficiency for CID and MS/MS. With tailored buffer gas pressure, the possibility of using increased pressure during trapping and CID events without the detrimental effects of buffer gas during detection can be achieved. The effects are highlighted in the analyses of fragile ions.

The gas pulse was profiled by a technique using the QIT as a pressure gauge. Even though the pulse can be reproduced and tailored, the narrowest gas peak width achieved was 100 ms

FWHM, five times the ideal peak width of 20 ms. Thus, applications for the current setup are limited. The scan function can be lengthened to accommodate the wide buffer gas pulse, but scan rates will be decreased below practical speeds for GC/MS and LC/MS. Nevertheless, improved ion trap performance with pulsed buffer gas tailoring may justify the added complexity in QIT operation.

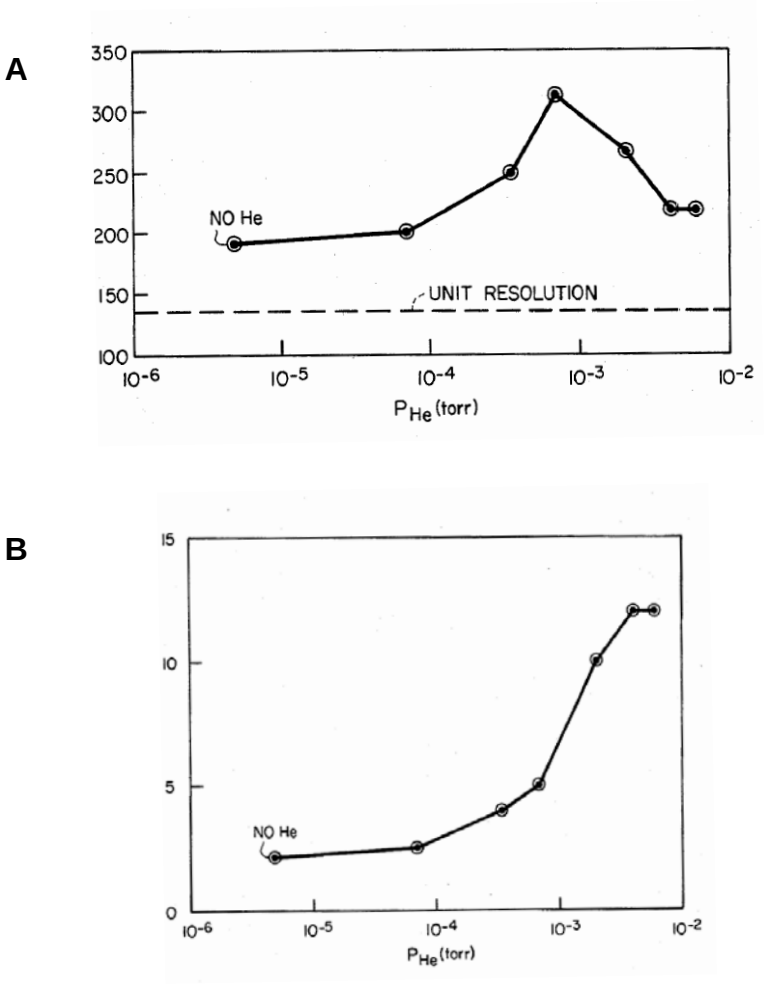

Figure 3-1. Pressure effects on signal intensity and mass resolution in the quadrupole ion trap. A) Resolution vs pressure was plotted. Optimum resolution was achieved at ~1 mTorr. B) Signal intensity vs pressure was plotted. Intensity increases with buffer gas pressure. Adapted from Stafford [7].

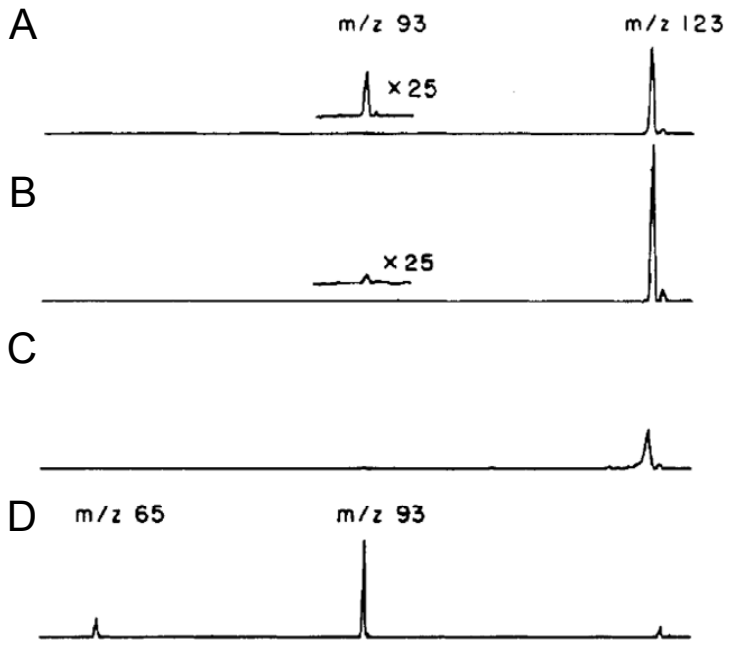

Figure 3-2. Mass spectra showing the effect of buffer gas and resonant excitation on CID of the M^+ ion of nitrobenzene (*m/z* 123). A) Without helium and no resonant excitation. B) With helium and no resonant excitation. C) Without helium and with resonant excitation. D) With helium and resonant excitation. Adapted from Louris [56].

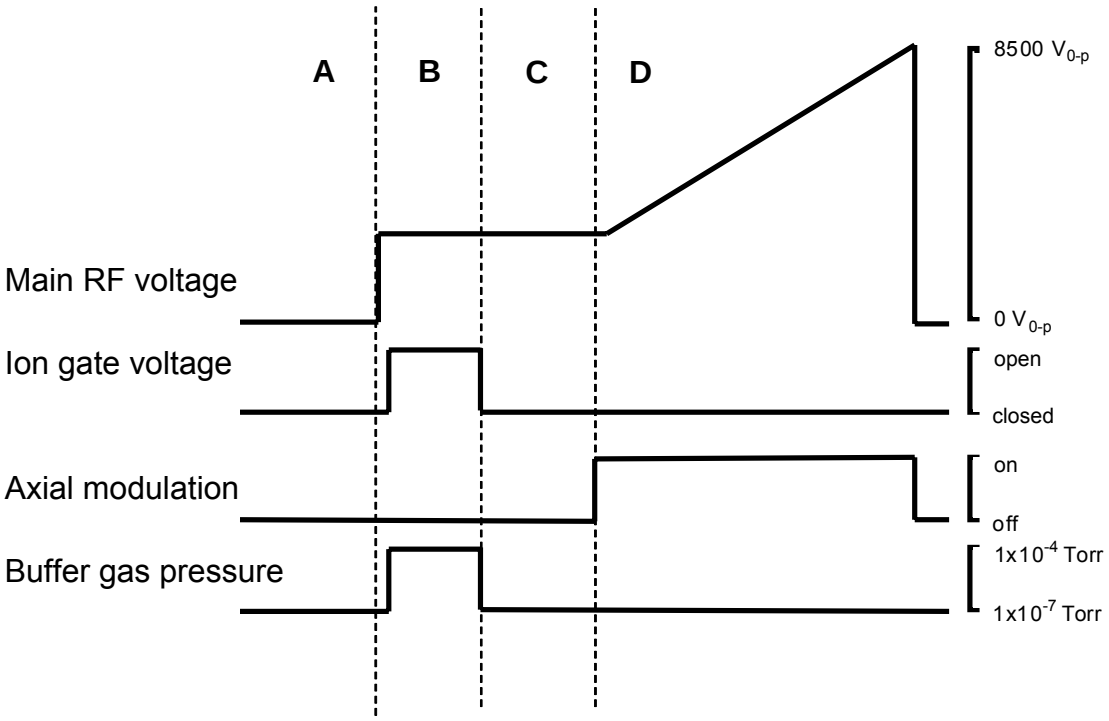

Figure 3-3. Simplified QIT scan function for a full scan MS using the mass selective instability technique with the proposed buffer gas pressure tailoring scheme. It can be divided into 4 general events A) pre-injection, B) injection C) post-injection and D) detection. This scan function includes the concept that the buffer gas pressure could be added as another parameter varied during the scan function, rather than kept constant, as is typically done. Buffer gas pressure scales are approximate values based on the minimum and maximum level readings for the SweetP QIT. In this scan function, buffer gas pressure is increased only during ion injection.

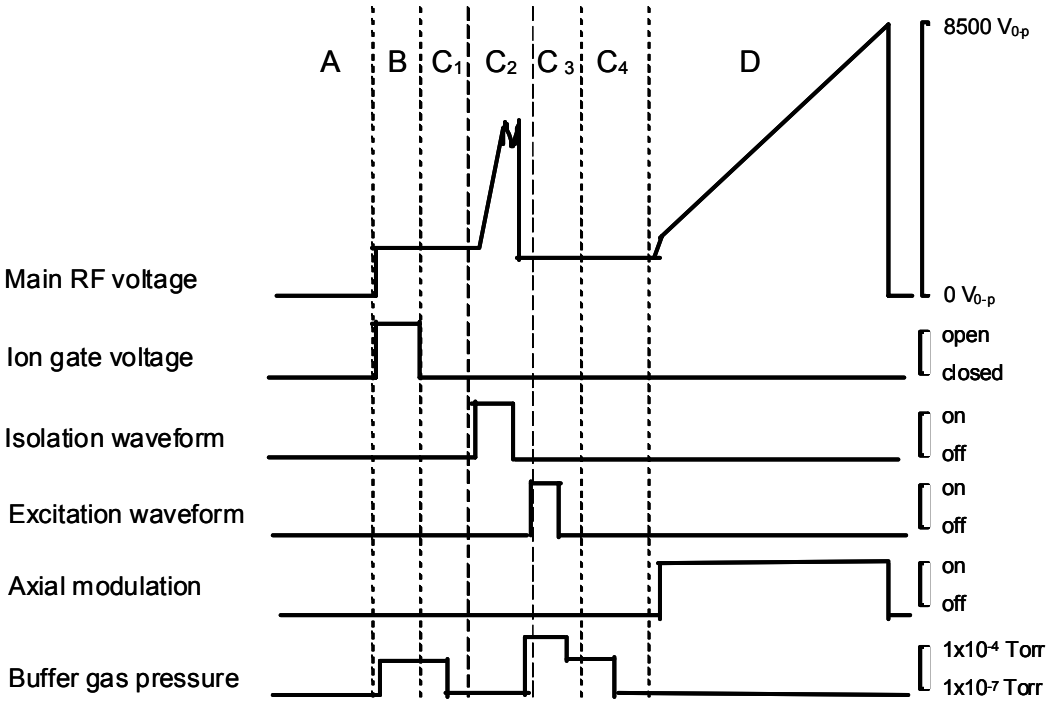

Figure 3-4. Simplified QIT scan function for MS/MS scan with CID. Similar to the full MS scan, it is divided into 4 general events but with some changes: A) pre-injection , B) injection C) CID version of post-injection (cooling C_1, isolation C_2, excitation C_3, and cooling C_4) and D) detection. This scan function shows the proposed variation of buffer gas pressure during different portions of the scan function. Buffer gas pressure scales are approximate values based on the minimum and maximum level readings for the SweetP QIT.

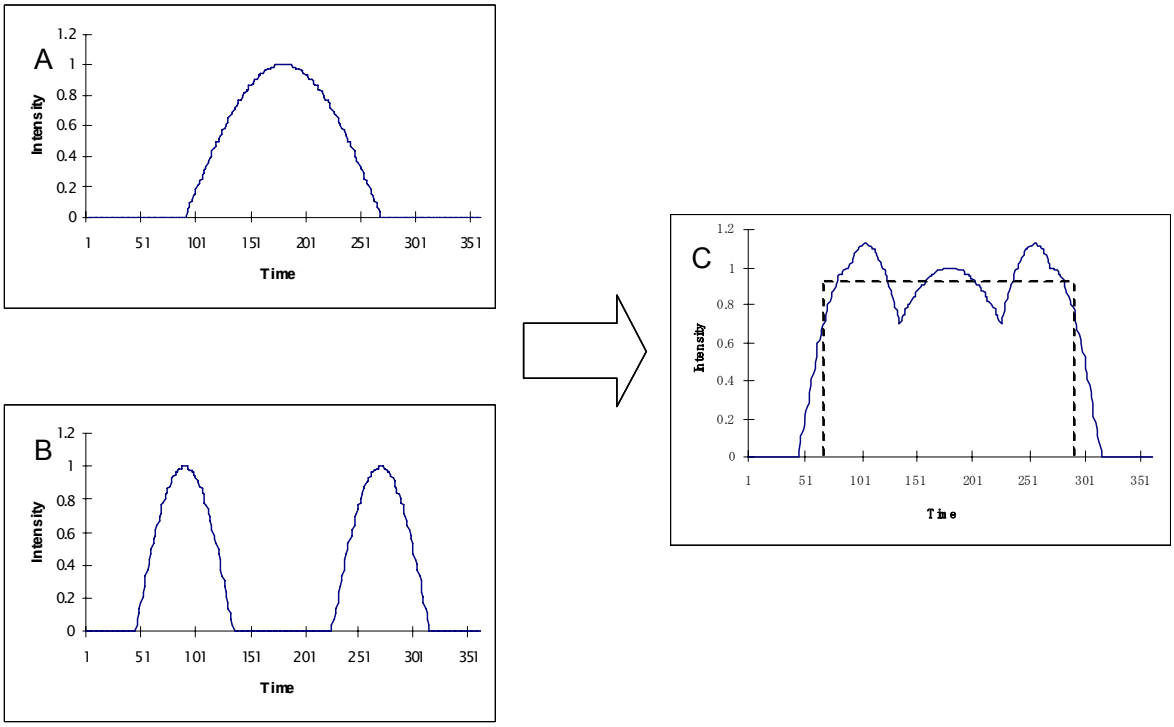

Figure 3-5. Simulated profile of using two pulsed valves with varying gas pulse patterns to generate a "square" gas pulse profile. Similar to constructing a square wave from sine waves, timed gas pulses from A and B can be combined to form C, a new gas pulse profile. An overlay of the desired square pulse profile is shown (dashed line).

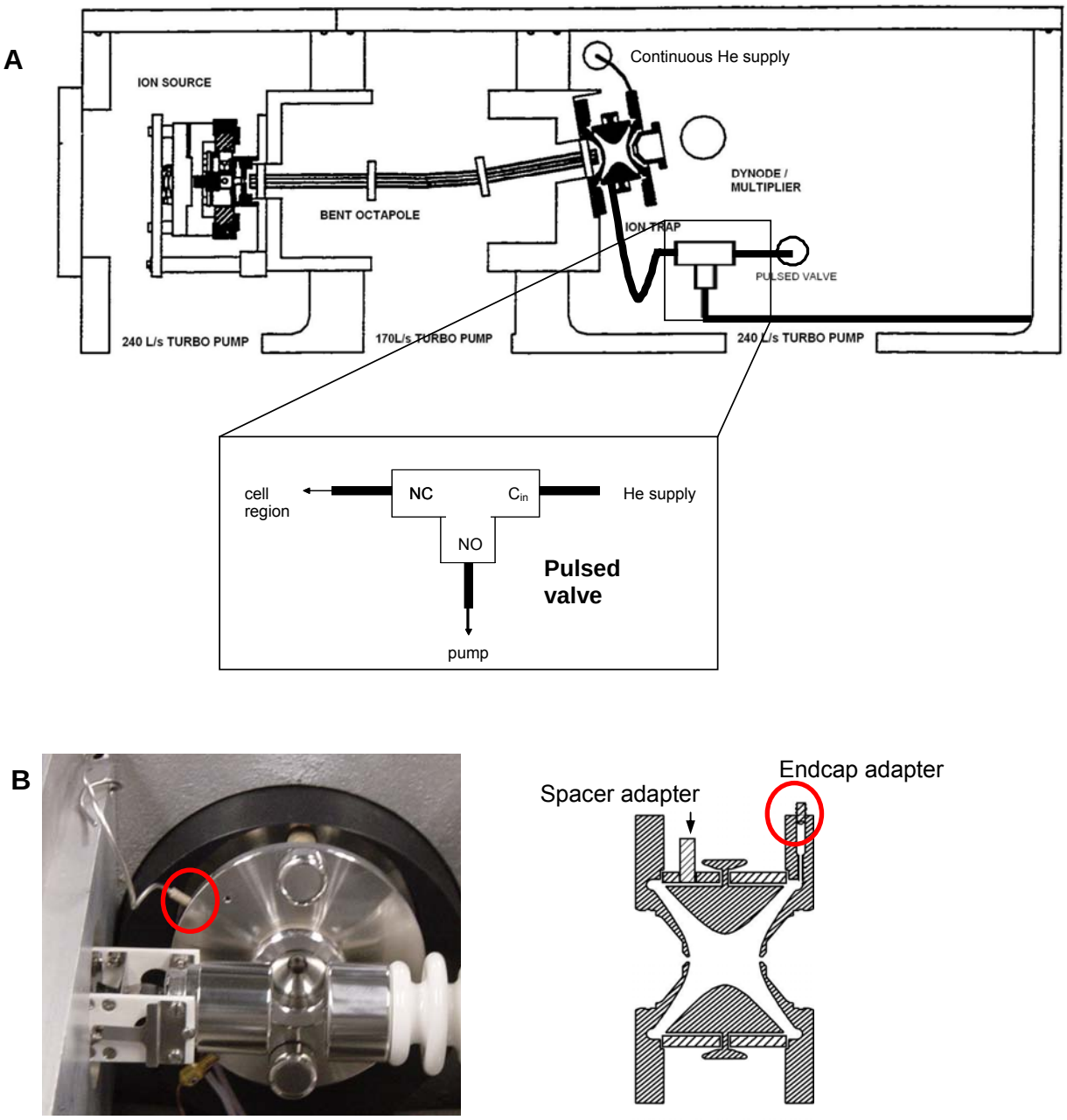

Figure 3-6. Pulsed valve placement in the QIT. A) Diagram of a 3-way pulsed valve placement inside the vacuum chamber of the SweetP QIT. The normally closed (NC) output was connected to the QIT with Teflon tubing (2.5"x 1/4" i.d.) that passed through a hole drilled in one of the nonconductive spacers between the trap electrodes. The normally open (NO) output was connected to a mechanical pump via a variable leak valve. The common (C_{in}) input was connected to a helium gas supply via another variable leak valve. The head pressure on the helium supply was controlled by a pressure regulator. B) Picture(and cross section view) of the trap showing the continuous supply line connected to the side of the endcap (in circle).

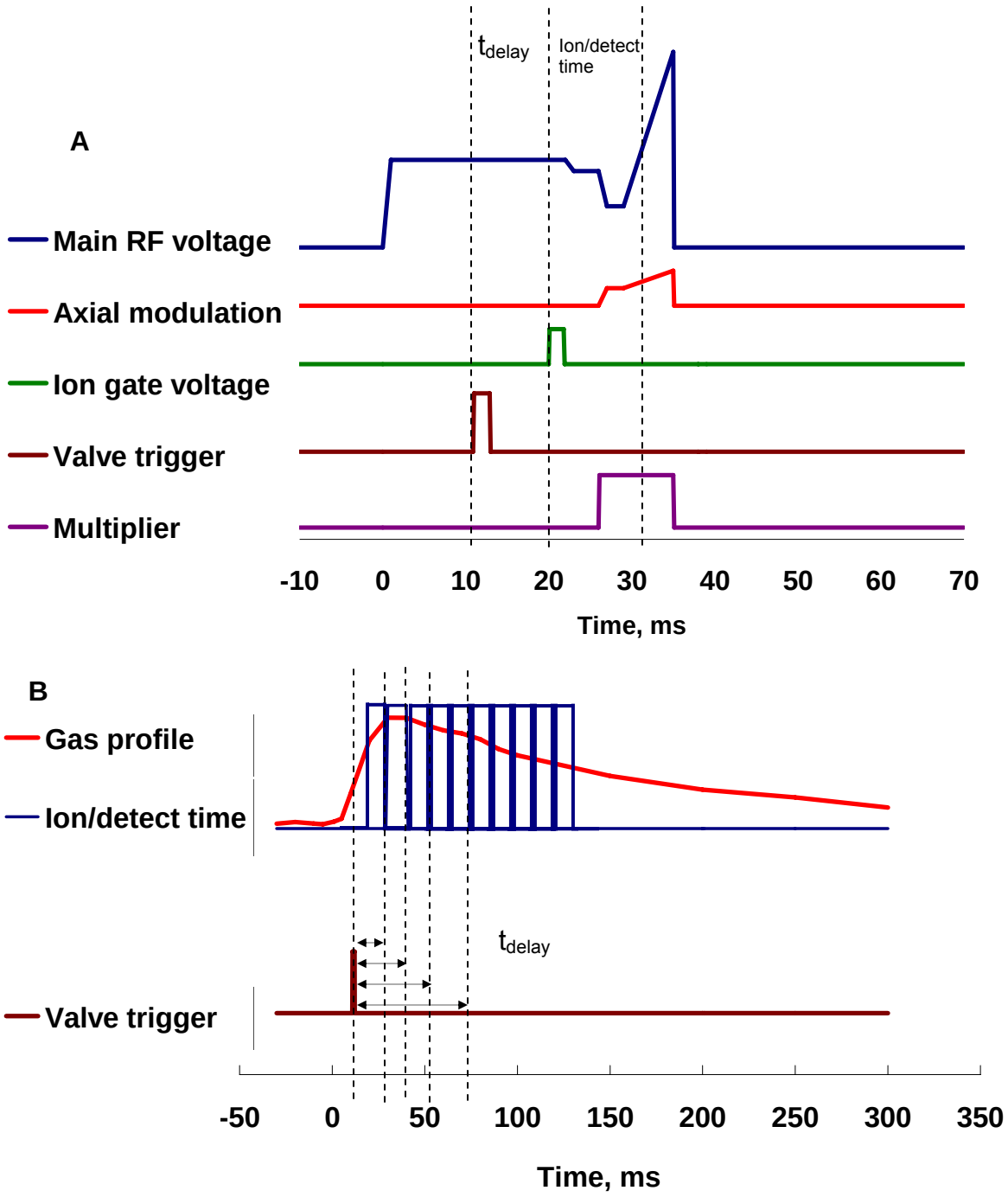

Figure 3-7. Diagrams showing how the t_{delay} is inserted into the scan function and its operation. A) A scan function that shows the timing of opening the valve for ion molecule reactions between Ar^+ ions and N_2 introduced via a pulsed valve. Using 24 VDC to drive the pulsed valve, the minimum pulse time to open the valve was 1.9 ms. As shown on the diagram, t_{delay} was set at 10 ms. B) N_2^+ signal intensity as a function of pressure. This can be interpreted as a neutral gas profile (in red) with a series of ion/detect times overlayed on the profile. This shows how the gas profile is sampled across its peak by shifting t_{delay} sequentially.

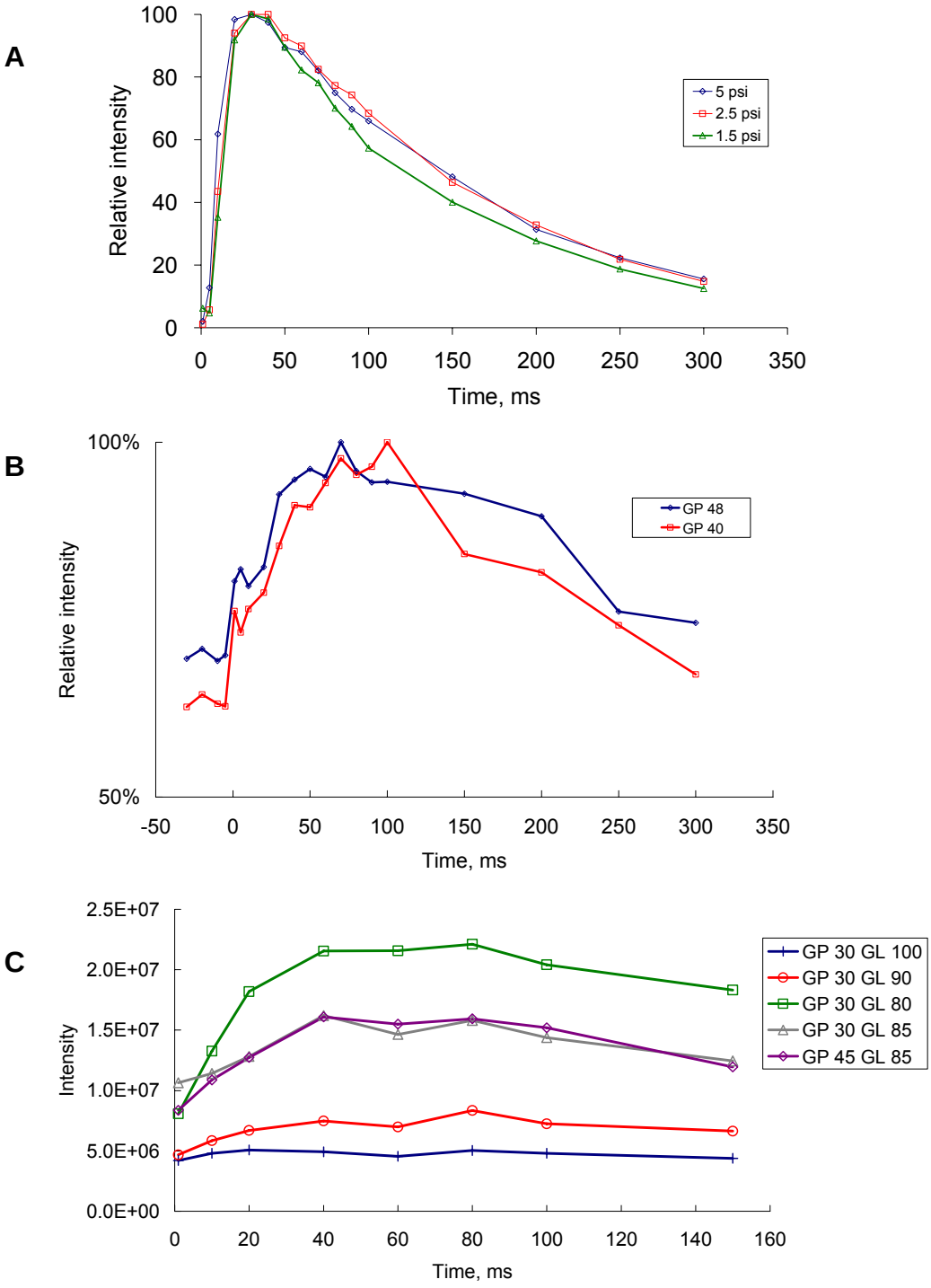

Figure 3-8. Preliminary data for gas pulse optimization, showing intensity of N_2^+ (*m/z* 28) formed by charge exchange with Ar^+ as a function of delay time. The pressure for the common (C_{in}) inlet was varied by controlling the head pressure or setting of the GP leak valve. A) NO closed and varying head pressure B) NO open and varying GP supply (head pressure 2.5 psi) C) NO and C with variable leak gauges. GP = setting for the supply restriction, GL= setting for the leak restriction (head pressure 10 psi)

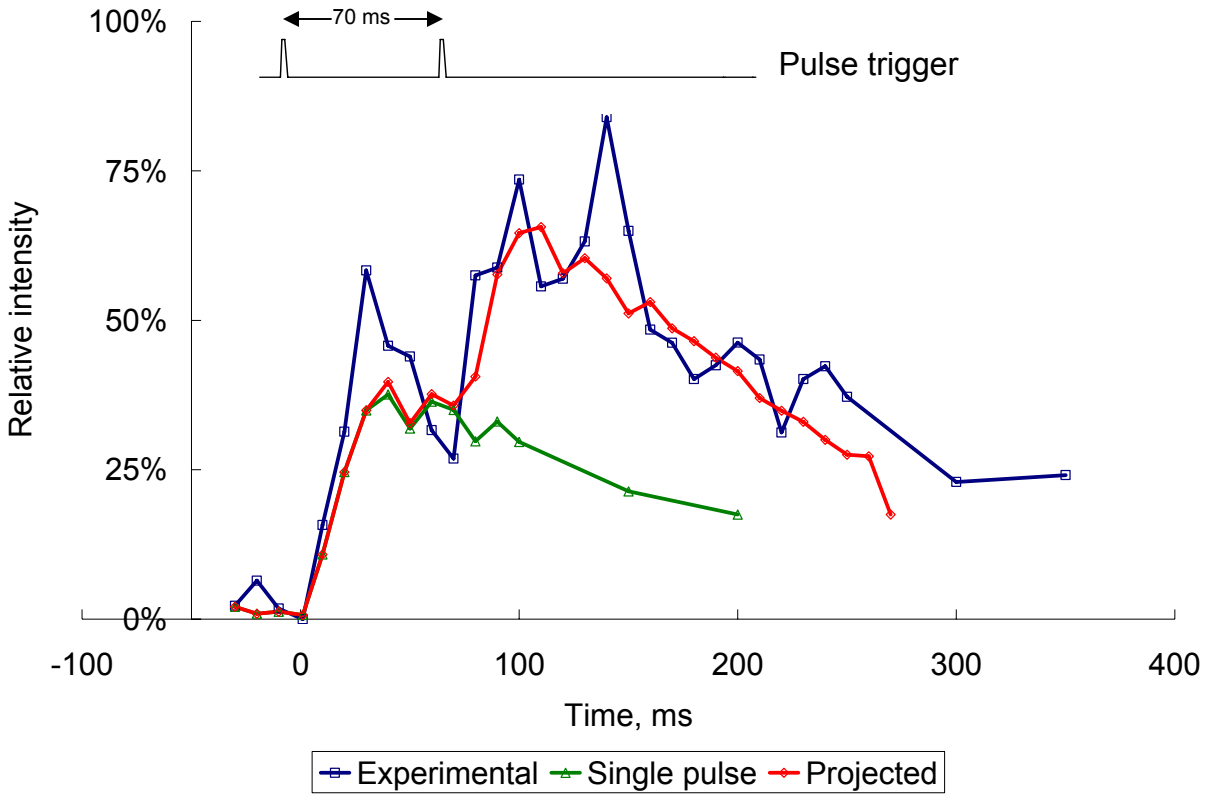

Figure 3-9. Gas profile of the multi-pulse experiment, measured by monitoring the CF_3^+ ion with buffer gas pulsed into the ion trap. Experimental data for a single pulse were taken and used to create the projected two-pulse data and plotted with the experimental two-pulse data. The pulsed valve was triggered twice with the second pulse 70 ms after the first. The experimental data for the two-pulse delivery of buffer gas followed a trend that is similar with the projected profile, indicating reproducibility of the pulsed gas profile. Shown above the figure is the pulse trigger timing that was sent to the pulse valve.

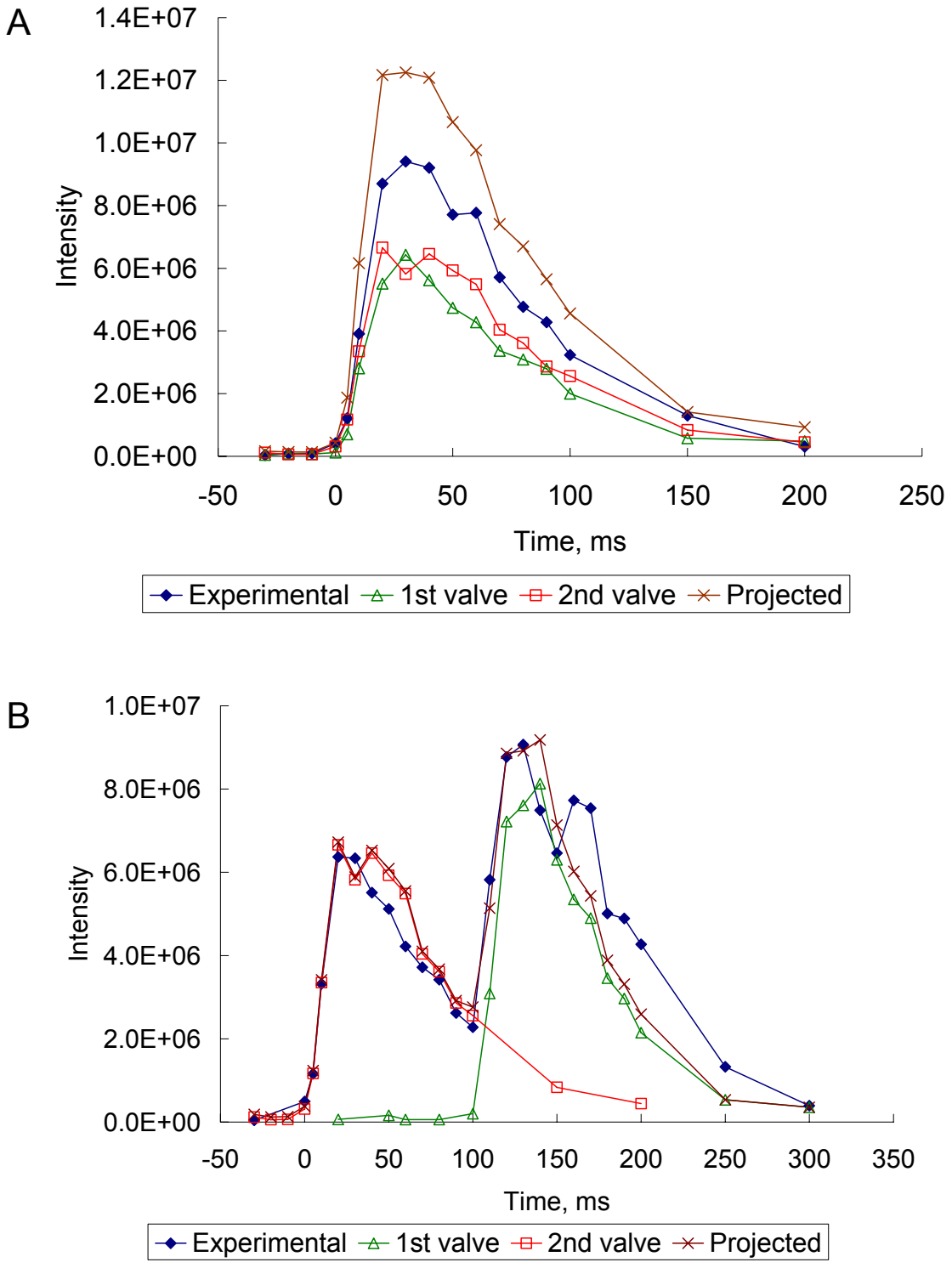

Figure 3-10. Gas profile of 2 pulsed valves operated synchronously as measured by monitoring the CF_3^+ ion intensity as function of delay time. The first valve's supply head pressure was set to 2.5 psi. The second valve's supply settings were set to GP= 40 and GL=200 with a head pressure of 10 psi. A) Both valves were opened at time 0. B) The 1st valve had a delay time of 100 ms in relation to the 2nd valve.

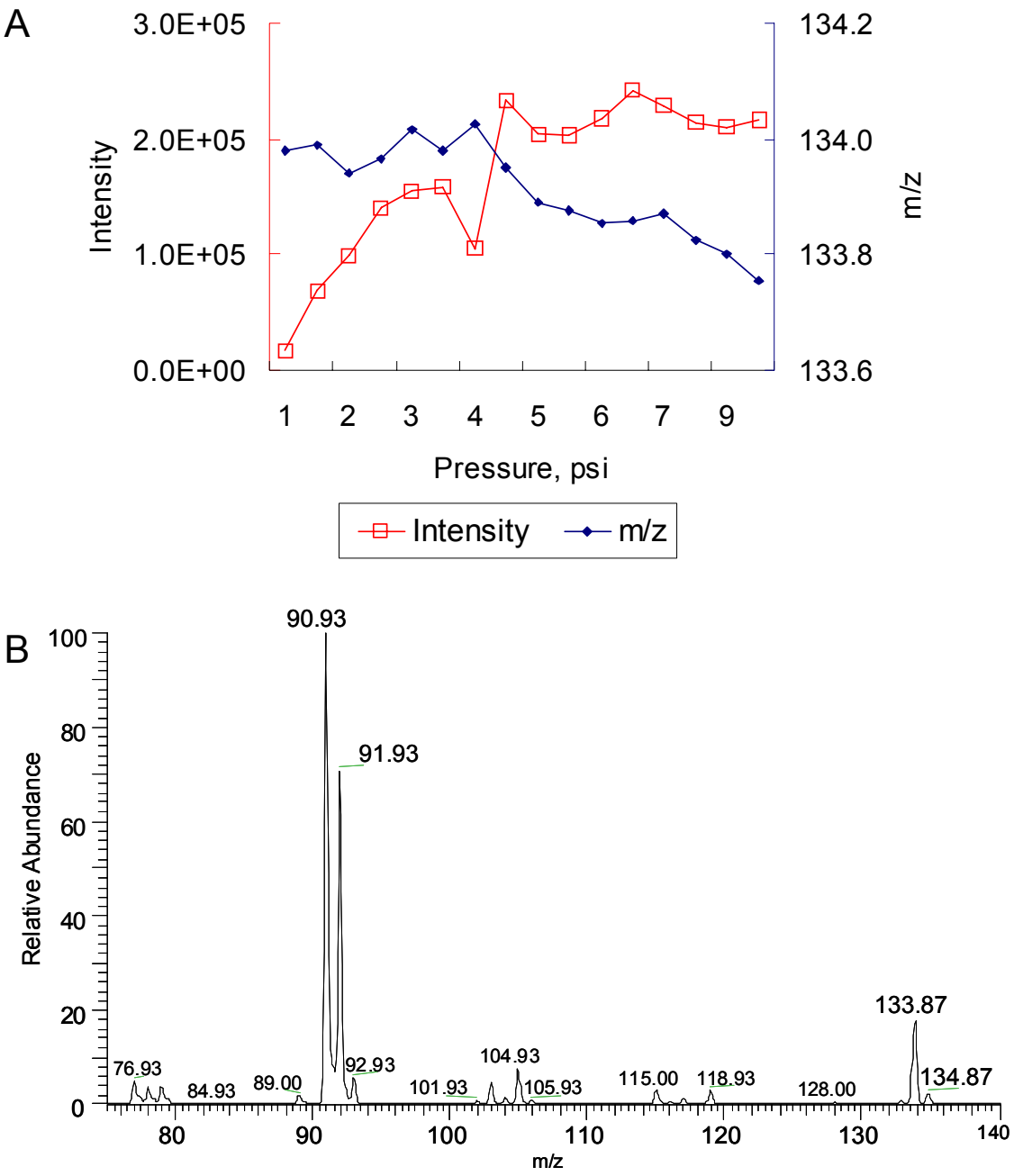

Figure 3-11. Static buffer gas experimental results.A) Effects of static buffer gas pressure on signal intensity and mass assignment of the M^+ ion of n-butylbenzene (*m/z* 134). The mass placement shifted downwards as the static pressure was increased. B) Full scan MS of n-butylbenzene at 2.5 psi buffer gas head pressure.

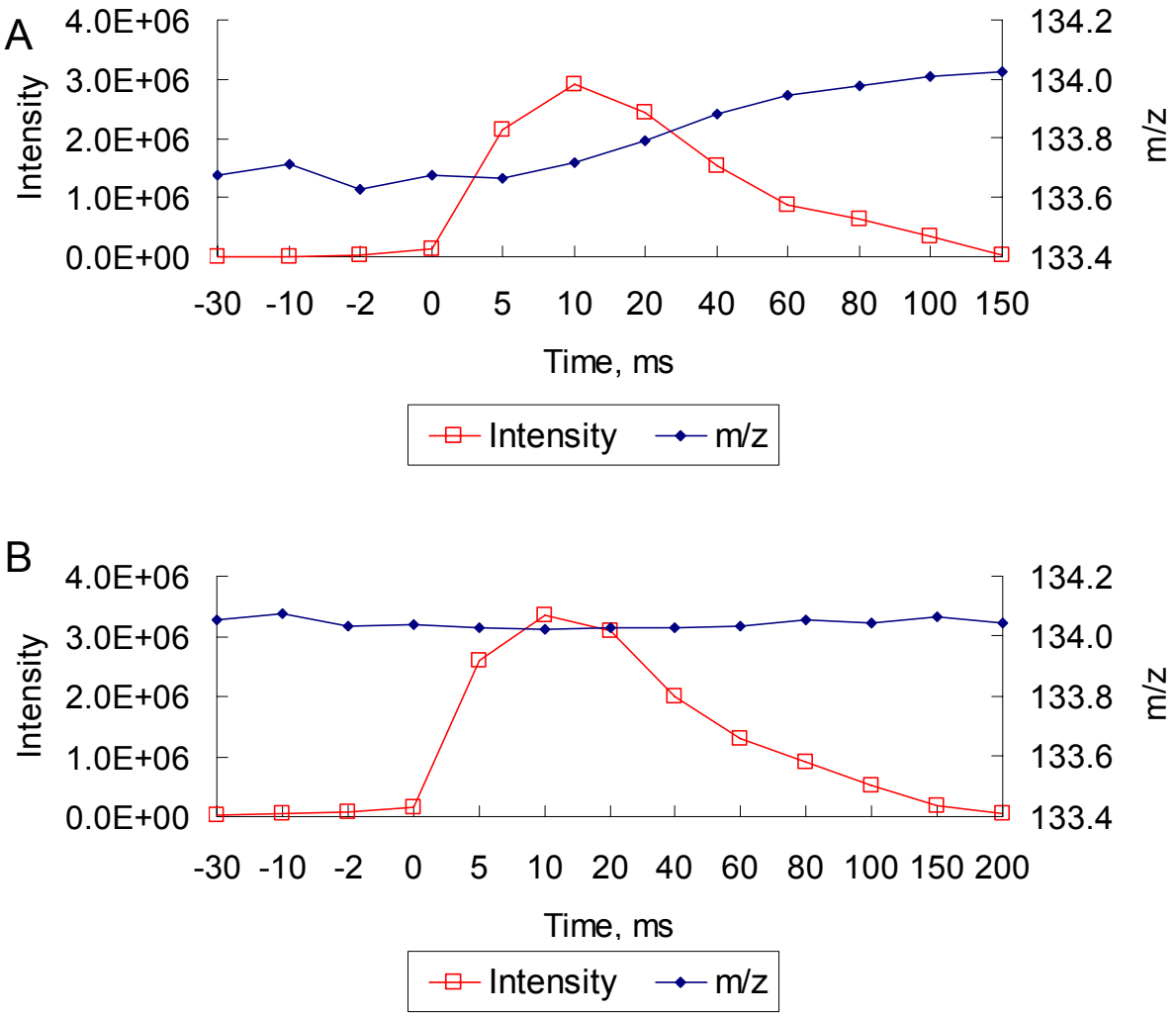

Figure 3-12. Experiments using pulsed buffer gas introduction and its effect on analysis of fragile ions. The intensity and mass assignment of the M+ ion (*m/z* 134) of n-butylbenzene is plotted vs delay time: A) Cooling time was 1 ms and post scan time was 1000 ms B) Cooling time was 1000 ms and post scan time was 1 ms.

CHAPTER 4
CONCLUSION AND FUTURE WORKS

The quadrupole ion trap (QIT) was developed by Paul in the 1950's using the Mathieu equation to describe the stability of an ion's trajectory. This equation was the basis for the mass-selective instability method, which transformed the QIT into a successful mass spectrometer. Currently, all commercial QITs have a stretched axial (z_0) configuration, which deviates from the theoretical z_0 by 11%. This modification was made to superimpose higher order fields, which counteract the effects of field imperfections caused by the endcap holes and truncation of the practical trap. Truncation is needed to limit the size of the device and avoid a voltage arc between the RF ring and grounded electrodes. The endcap holes are needed to admit ions into and eject them from the trap. Furthermore, the use of buffer gas, which helps trap and cool injected ions by reducing ion kinetic energy, focuses the ions into the trap center and away from the field imperfections. However, the increase in the z_0 distance superimposes higher order fields and consequently causes nonlinear resonance effects. Previous SIMION studies from our lab have shown that microscreening the endcap holes reduces field imperfections in the vicinity of the holes.

The goal of this research was to experimentally evaluate the microscreening of the endcap holes that would correct for the field imperfections brought about by the features of the practical trap. Using the PFTBA fragment ion CF_3^+ at *m/z* 69 as a monitor ion, mass spectra were taken with and without buffer gas using stretched endcap spacing and standard endcaps. Without buffer gas ions tend to have larger excursions from the trap center, and therefore are more likely to experience field imperfections near the trap end caps. With non-linear resonance, an ion's stability is no longer dependent on its *m/z* value, as the ions of a specific m/z can have multiple parameter values at which they are ejected, resulting in ghost peaks of that particular ion. The

intensity of the ghost peak of *m/z* 69 that appeared at *m/z* 67 was decreased by reducing the endcap spacing from stretched (10%) to theoretical (0%) dimensions. This peak intensity was reduced even further when coupled with the use of microscreened endcaps. The intensity of the ghost peaks at *m/z* 67 and 64.5 is even lower with the use of microscreened endcaps than with standard endcaps, even under buffer gas conditions.

The practical solution employed by Finnigan from a commercial standpoint is sufficient for most applications. For some applications, however, the use of buffer gas is a problem (e.g. space exploration where carrying He is unappealing, or in cases where ion-molecule reactions with impurities such as water in the buffer gas are problematic.) In such cases, using the QIT with the z_0 = 7.85 mm spacing would be problematic as the spectra it produces will be complicated with ghost peaks due to nonlinear resonance.

Using mesh inserts was a practical method of evaluating the solution of repairing field imperfections in the vicinity of the endcap holes. However, field imperfections contributed by the microscreened endcaps were also encountered, as peaks not present with standard endcaps appeared with microscreened endcaps. Wear and tear of the modified endcaps from repeated interchanges of the inserts may be the cause. Thus, this method may not be used as a permanent solution. An alternative, but not practical answer to this problem is to manufacture endcaps with incorporated microscreened holes. This method will avoid the possibility of performance degradation due to repeated interchanges.

This research can be applied to the 2-D linear ion trap. The X-rods, where slits are located through which ions are ejected, are also stretched by the manufacturer in the same manner to compensate for field imperfections in the vicinity of the slits. The slits are only 0.25 mm wide, which is significantly smaller that that of the 3-D trap. A future study would be to evaluate the

performance of the linear ion trap without buffer gas to determine the prevalent nonlinear resonance existing within this type of ion trap and then to evaluate microscreening if it would improve the performance in the same way as in the 3-D ion trap.

Buffer gas has always been used since the commercialization of the QIT mass spectrometer. The current He buffer gas pressure of 1 mTorr is a compromise between signal intensity and mass resolution. Adequate buffer gas pressure is needed to reduce the kinetic energy of externally created ions through collisional cooling with buffer gas. On the other hand, having too high buffer gas pressure leads to loss of mass resolution. Single pulsed valve experiments have shown key points in the analytical scan function where the presence of buffer gas is important and where it should be reduced. However, buffer gas pressure control with single valves is limited because it only offers two states, closed and open with constant pressure behind the valve.

The concept of tailoring buffer gas pressure with the use of multiple pulsed valves was presented with goal of achieving more control over the flow of buffer gas. With tailored buffer gas pressure, the possibility of optimizing a buffer gas pressure level for injection and trapping, while allowing another pressure level to be set for CID events without the detrimental effects in detection can be achieved. Data have shown that different gas profiles can be created.

Using the QIT as a pressure monitor, the produced gas pulse was profiled to be 100 ms FWHM. The scan function can be extended to accommodate the wide gas peak width but it is not be practical for most applications. There are several approaches that may shorten the gas peak width. Increasing the conductance out of the trap is one method. Currently, there are only four conductance holes in the endcap. Holes can be drilled in the endcap spacers to increase the conductance. Another way is to decrease the distance of the valve from the trap while increasing

the connecting tube diameter. This approach will shorten the rise time of the gas peak. Another consideration to shorten the gas peak width is to use an array of micromachined valves, which have faster response times than the solenoid valves used in this work. These valves can be manufactured smaller in size, which would be advantageous in placing an array of valves closer to the ion trap.

LIST OF REFERENCES

1. Paul, W.; Steinwedel, H. Apparatus for separating charged particles of different specific charges. US 2,939,952, Jun 7, 1960.

2. Wuerker, R. F.; Shelton, H.; Langmuir, R. V. Electrodynamic Containment of Charged Particles. *Journal of Applied Physics* **1959,** *30*, 342-349.

3. Dawson, P. H.; Whetten, N. R. Ion Storage in Three-Dimensional, Rotationally Symmetric, Quadrupole Fields. I. Theoretical Treatment. *Journal of Vacuum Science and Technology* **1968,** *5*, 1-10.

4. Dawson, P. H.; Whetten, N. R. Ion Storage in Three-Dimensional, Rotationally Symmetric, Quadrupole Fields. II. A Sensitive Mass Spectrometer. *Journal of Vacuum Science and Technology* **1968,** *5*, 11-18.

5. Mather, R. E.; Lawson, G.; Todd, J. F. J.; Bakker, J. M. B. Quadrupole Ion Storage Trap (Quistor) As A Low-Pressure Chemical Ionization Source for A Magnetic-Sector Mass-Spectrometer. *International Journal of Mass Spectrometry and Ion Processes* **1978,** *28*, 347-364.

6. Lawson, G.; Bonner, R. F.; Todd, J. F. J. The quadrupole ion store (quistor) as a novel source for a mass spectrometer. *Journal of Physics E: Scientific Instruments* **1973,** 357-362.

7. Stafford, G. C.; Kelley, P. E.; Stephens, D. R. Method of mass analyzing a sample by use of a quadrupole ion trap. US 4,540,884, Sep 10, 1985.

8. Stafford, G. C.; Kelley, P. E.; Syka, J. E. P.; Reynolds, W. E.; Todd, J. F. J. Recent Improvements in and Analytical Applications of Advanced Ion Trap Technology. *International Journal of Mass Spectrometry and Ion Processes* **1984,** *60*, 85-98.

9. Louris, J. N.; Stafford, G. C.; Syka, J. E. P.; Taylor, D. The Paul ion trap mass selective instability scan: trap geometry, scan speed, and resolution. In *Proceedings of the 40th ASMS Conference on Mass Spectrometry and Allied Topics*; 1992; p 139.

10. Guidugli, F.; Traldi, P. A Phenomenological Description of A Black-Hole for Collisionally Induced Decomposition Products in Ion-Trap Mass-Spectrometry. *Rapid Communications in Mass Spectrometry* **1991,** *5*, 343-348.

11. Vachet, R. W.; Asam, M. R.; Glish, G. L. Secondary interactions affecting the dissociation patterns of arginine-containing peptide ions. *Journal of the American Chemical Society* **1996,** *118*, 6252-6256.

12. Vachet, R. W.; Glish, G. L. New method to study the effects of peptide sequence on the dissociation energetics of peptide ions. *Journal of the American Society for Mass Spectrometry* **1998,** *9*, 175-177.

13. Wen, B.; Ma, L.; Nelson, S. D.; Zhu, M. High-througput screening and characterization of reative metabolites using polarity switching of hybrid triplequadrapole linear ion trap mass spectrometry. *Analytical Chemistry* **2008,** *80*, 1788-1799.

14. Koulman, A.; Tapper, B. A.; Fraser, K.; Cao, M. S.; Lane, G. A.; Rasmussen, S. High-throughput direct-infusion ion trap mass spectrometry: a new method for metabolomics. *Rapid Communications in Mass Spectrometry* **2007,** *21*, 421-428.

15. Landgraf, R. R.; Garrett, T. J.; Calcutt, N. A.; Stacpoole, P. W.; Yost, R. A. MALDI-linear ion trap microprobe MS/MS studies of the effects of dichloroacetate on lipid content of nerve tissue. *Analytical Chemistry* **2007,** *79*, 8170-8175.

16. Garrett, T. J.; Prieto-Conaway, M. C.; Kovtoun, V.; Bui, H.; Izgarian, N.; Stafford, G.; Yost, R. A. Imaging of small molecules in tissue sections with a new intermediate-pressure MALDI linear ion trap mass spectrometer. *International Journal of Mass Spectrometry* **2007,** *260*, 166-176.

17. Schwartz, J. C.; Senko, M. W.; Syka, J. E. P. A two-dimensional quadrupole ion trap mass spectrometer. *Journal of the American Society for Mass Spectrometry* **2002,** *13*, 659-669.

18. March, R. E. An introduction to quadrupole ion trap mass spectrometry. *Journal of Mass Spectrometry* **1997,** *32*, 351-369.

19. Stafford, G. C. Ion trap mass spectrometry: a personal perspective. *Journal of the American Society for Mass Spectrometry* **2002,** *13*, 589-596.

20. March, R. E. Quadrupole ion trap mass spectrometry: Theory, simulation, recent developments and applications. *Rapid Communications in Mass Spectrometry* **1998,** *12*, 1543-1554.

21. Huston, C. K. Manipulation of Ion Trap Parameters to Maximize Compound-Specific Information in Gas-Chromatographic Mass-Spectrometric Analyses. *Journal of Chromatography* **1992,** *606*, 203-209.

22. Kaiser, R. E.; Cooks, R. G.; Stafford, G. C.; Syka, J. E. P.; Hemberger, P. H. Operation of A Quadrupole Ion Trap Mass-Spectrometer to Achieve High Mass Charge Ratios. *International Journal of Mass Spectrometry and Ion Processes* **1991,** *106*, 79-115.

23. Murphy, J. P. Fundamental studies of the quadrupole ion trap mass spectrometer: compound dependent mass shifts and space charge. University of Florida, 2002.

24. Yates, N. A. Methods for gas chromatography/tandem mass spectrometry on the quadrupole ion trap. Chemistry University of Florida, 1994.

25. Syka, J. E. P. Commercialization of the quadrupole ion trap. In *Fundamentals of Ion Trap Mass Spectrometry*, CRC Press: Boca Raton, FL, 1995; Vol. 1, pp 169-205.

26. Plass, W. R.; Li, H. Y.; Cooks, R. G. Theory, simulation and measurement of chemical mass shifts in RF quadrupole ion traps. *International Journal of Mass Spectrometry* **2003,** *228*, 237-267.

27. Franzen, J.; Gabling, RH.; Schubert, M.; Wang, Y. Nonlinear ion traps. In *Fundamentals of Ion Trap Mass Spectrometry*, CRC Press: Boca Raton, FL, 1995; Vol. 1, pp 49-167.

28. Quarmby, S. T.; Yost, R. A. Fundamental studies of ion injection and trapping of electrosprayed ions on a quadrupole ion trap. *International Journal of Mass Spectrometry* **1999,** *191*, 81-102.

29. Williams, J. D.; Cox, K. A.; Cooks, R. G.; Mcluckey, S. A.; Hart, K. J.; Goeringer, D. E. Resonance ejection ion trap mass spectrometry and nonlinear field contributions - the effect of scan direction on mass resolution. *Analytical Chemistry* **1994,** *66*, 725-729.

30. Cameron, D.; Hemberger, P. H. Ionization and matrix gas effects observed in high pressure analysis with an ion trap mass spectrometer. In *Proceedings of the 38th ASMS Conference on Mass Spectrometry and Allied Topics*; Tucson, AZ, 1990; pp 61-62.

31. Franzen, J. The non-linear ion trap. Part 4. Mass selective instability scan with multipole superposition. *International Journal of Mass Spectrometry and Ion Processes* **1993,** *125*, 165-170.

32. Dawson, P. H.; Whetten, N. R. Non-linear resonances in quadrupole mass spectrometers due to imperfect fields I. The quadrupole ion trap. *Journal of Mass Spectrometry* **1969,** *2*, 45-59.

33. Beaty, E. C. Calculated electrostatic properties of ion traps. *Physical Review A* **1986,** *33*, 3645-3656.

34. Wang, Y.; Franzen, J.; Wanczek, K. P. The nonlinear resonance ion trap. 2. A general theoretical analysis. *International Journal of Mass Spectrometry and Ion Processes* **1993,** *124*, 125-144.

35. Eades, D. M.; Yost, R. A. Black canyons for ions stored in an ion trap mass spectrometer. *Rapid Communications in Mass Spectrometry* **1992,** *6*, 573-578.

36. Eades, D. M.; Johnson, J. V.; Yost, R. A. Nonlinear resonance effects during ion storage in a quadrupole ion trap. *Journal of the American Society for Mass Spectrometry* **1993,** *4*, 917-929.

37. Alheit, R.; Kleineidam, S.; Vedel, F.; Vedel, M.; Werth, G. Higher order non-linear resonances in a Paul trap. *International Journal of Mass Spectrometry and Ion Processes* **1996,** *154*, 155-169.

38. Mo, W. J.; Langford, M. L.; Todd, J. F. J. Investigation of ghost peaks caused by nonlinear fields in the ion trap mass spectrometer. *Rapid Communications in Mass Spectrometry* **1995,** *9*, 107-113.

39. Kocher, F.; Favre, A.; Gonnet, F.; Tabet, J. C. Study of ghost peaks resulting from space charge and non-linear fields in an ion trap mass spectrometer. *Journal of Mass Spectrometry* **1998,** *33*, 921-935.

40. Hilton, C. K.; Yost, R. A. High resolution modeling of the entrance and exit apertures in a quadrupole ion trap using SIMION 7.0. In *Proceedings of the 51st ASMS Conference on Mass Spectrometry and Allied Topics*; Montreal, Canada, 2003.

41. Ottens, A. K. Analysis of lightweight gases by quadrupole ion trap mass spectrometry for the safety of the American Space Shuttle program. University of Florida, 2003.

42. Coopersmith, B. I.; Yost, R. A. Internal Pulsed Valve Sample Introduction on A Quadrupole Ion-Trap Mass-Spectrometer. *Journal of the American Society for Mass Spectrometry* **1995,** *6*, 976-980.

43. Doroshenko, V. M.; Cotter, R. J. Pulsed gas introduction for increasing peptide CID efficiency in a MALDI quadrupole ion trap mass spectrometer. *Analytical Chemistry* **1996,** *68*, 463-472.

44. Williams, T. L.; Stephenson, J. L.; Yost, R. A. The effects of pulsed introduction of buffer gas on ion storage and detection efficiencies in a quadrupole ion trap. *Journal of the American Society for Mass Spectrometry* **1997,** *8*, 532-538.

45. Emary, W. B.; Kaiser, R. E.; Kenttamaa, H. I.; Cooks, R. G. Pulsed Gas Introduction Into Quadrupole Ion Traps. *Journal of the American Society for Mass Spectrometry* **1990,** *1*, 308-311.

46. Louris, J. N.; Amy, J. W.; Ridley, T. Y.; Cooks, R. G. Injection of Ions Into A Quadrupole Ion Trap Mass-Spectrometer. *International Journal of Mass Spectrometry and Ion Processes* **1989,** *88*, 97-111.

47. Fischer, E. Die Dreidimensionale Stabilisierung Von Ladungstragern in Einem Vierpolfeld. *Zeitschrift fur Physik* **1959,** *156*, 1-26.

48. Todd, J. F. J.; Waldren, R. M.; Freer, D. A.; Turner, R. B. The quadrupole ion store (QUISTOR). Part X. Space charge and ion stability. B. On the theoretical distribution and density of stored charge in RF quadrupole fields. *International Journal or Mass Spectrometry and Ion Physics* **1980,** *35*, 107-150.

49. Quarmby, S. T. Fundamental Studies of Ion Injection and Trapping of Electrosprayed Ions on a Quadrupole Ion Trap Mass Spectrometer. University of Florida, 1997.

50. Brodbelt, J. S. Effects of Collisional Cooling on Ion Detection. In *Fundamentals of Ion Trap Mass Spectrometry*, March, R. E., Todd, J. F. J., Eds.; CRC Press: Boca Raton, FL, 1995; Vol. 1, pp 209-220.

51. Murphy, J. P.; Yost, R. A. Origin of mass shifts in the quadrupole ion trap: dissociation of fragile ions observed with a hybrid ion trap/mass filter instrument. *Rapid Communications in Mass Spectrometry* **2000,** *14*, 270-273.

52. McClellan, J. E.; Murphy, J. P.; Mulholland, J. J.; Yost, R. A. Effects of fragile ions on mass resolution and on isolation for tandem mass spectrometry in the quadrupole ion trap mass spectrometer. *Analytical Chemistry* **2002,** *74*, 402-412.

53. Li, H. Y.; Plass, W. R.; Patterson, G. E.; Cooks, R. G. Chemical mass shifts in resonance ejection experiments in the quadrupole ion trap. *Journal of Mass Spectrometry* **2002,** *37*, 1051-1058.

54. Morand, K. L.; Cox, K. A.; Cooks, R. G. Efficient Trapping and Collision-Induced Dissociation of High-Mass Cluster Ions Using Mixed Target Gases in the Quadrupole Ion Trap. *Rapid Communications in Mass Spectrometry* **1992,** *6*, 520-523.

55. Danell, R. M.; Danell, A. S.; Glish, G. L.; Vachet, R. W. The use of static pressures of heavy gases within a quadrupole ion trap. *Journal of the American Society for Mass Spectrometry* **2003,** *14*, 1099-1109.

56. Louris, J. N.; Cooks, R. G.; Syka, J. E. P.; Kelley, P. E.; Stafford, G. C.; Todd, J. F. J. Instrumentation, Applications, and Energy Deposition in Quadrupole Ion-Trap Tandem Mass-Spectrometry. *Analytical Chemistry* **1987,** *59*, 1677-1685.

57. Bauerle, G. F.; Brodbelt, J. S. Evaluation of Steric and Substituent Effects in Phenols by Competitive Reactions of Dimethyl Ether Ions in A Quadrupole Ion-Trap. *Journal of the American Society for Mass Spectrometry* **1995,** *6*, 627-633.

58. Vedel, F.; Vedel, M.; Brodbelt, J. S. Ion/Molecule Reactions. In *Fundamentals of Ion Trap Mass Spectrometry*, CRC Press: Boca Raton, FL, 1995; Vol. 1, pp 345-399.

59. Einhorn, J.; Kenttamaa, H. I.; Cooks, R. G. Information on the Location of Carbon-Carbon Double-Bonds in C6-C23 Linear Alkenes from Carbon Addition-Reactions in A Quadrupole Ion Trap Equipped with A Pulsed Sample-Inlet System. *Journal of the American Society for Mass Spectrometry* **1991,** *2*, 305-313.

60. Guckenberger, G. B. Chemical Ionization and Ion Molecule Reactions in the Quadrupole Ion Trap Mass Spectrometer with Ion Injection. University of Florida, 1999.

61. Papanastasiou, D.; Ding, L.; Raptakis, E.; Brookhouse, I.; Cunningham, J.; Robinson, M. Dynamic pressure measurements during pulsed gas injection in a quadrupole ion trap. *Vacuum* **2006,** *81*, 446-452.

62. Schwartz, J. C.; Syka, J. E. P.; Jardine, I. High-Resolution on A Quadrupole Ion Trap Mass-Spectrometer. *Journal of the American Society for Mass Spectrometry* **1991,** *2*, 198-204.

BIOGRAPHICAL SKETCH

Dodge Lo Baluya was born in Iloilo, Philippines, in 1977. He grew up in Iloilo City, with his two brothers and sister, Brian, Nestor Jr., and Roxanne; his mother, Nila; and his father Nestor Sr.. Being of chinese descent, he went to a chinese school for his elementary education.

Starting high school, Dodge transferred schools to Iloilo National High School-Special Science Class. There he was exposed more to education that was science- and math-oriented. There he learned more about the basics of conducting research, and computer technology. He had opportunities to compete in science fairs and quizzes, and learned to appreciate chemistry.

Dodge enrolled at the Ateneo de Manila University, one of the top universities in the Philippines, and joined a double majors program that allowed him to pursue bachelor's degrees in chemistry and computer engineering. This unique program allowed him to hone his skills in computer programming and electronics while studying more about chemistry. His interest in chemical instrumentation showed when he developed a computer interface for a potentiometric stripping analysis instrument for his final project. After graduation, he taught general chemistry in the same university while studying for the Philippine chemist licensure exam.

Since computer jobs were in high demand that time, Dodge landed a programming job in Japan that involved web development and software inventory. After working for 18 months, he decided that chemistry was a better career path for him. Thus, he enrolled at the University of Florida in 2003 to obtain his doctorate degree. He performed research in analytical chemistry under the direction of Dr. Richard Yost and used his areas of knowledge into instrument development. He also had the opportunities to teach general chemistry, and work as a graduate assistant in a mass spectrometry facility under Dr. David Powell.

Dodge's career brought him from the Philippines to Tokyo, Japan, and many places here in the US such as Tennessee, Texas, Indiana, Washington, Colorado and Florida. He plans to pursue his passion for chemistry and instrumentation and see more of the world.